AD-A190 076 STUDY OF MICROCOMPUTER-BASED REAL-TIME PROGRAMMABLE OPTICAL SIGNAL PROCES..(U) PENNSYLVANIA STATE UNIV UNIVERSITY PARK DEPT OF ELECTRICAL EN.. F T YU

1/2

UNCLASSIFIED 10 NOV 87 AFOSR-TR-87-1002 AFOSR-86-0264 F/G 12/6 NL

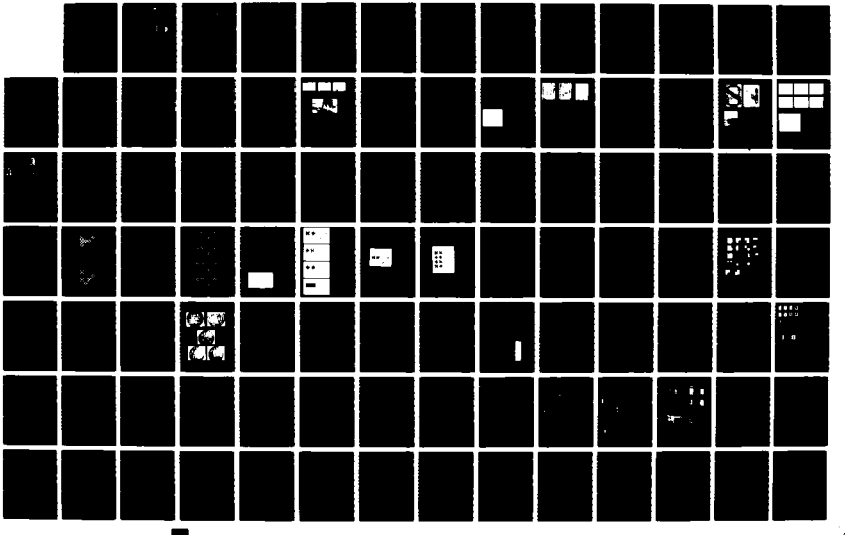

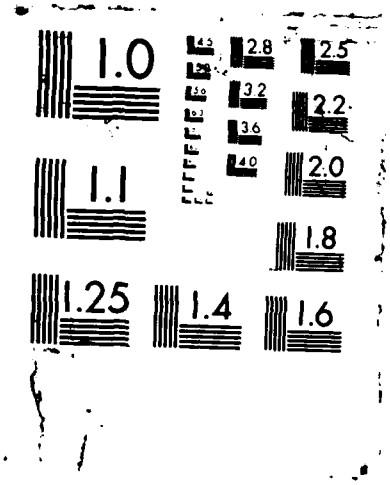
1.0
1.1
1.25
1.4
1.6
1.8
2.0
2.2
2.5
2.8
3.2
3.6
4.0

AFOSR-TR- 87-1802

DTIC FILE COPY (2)

Study of a Microcomputer-Based Real-Time Programmable Optical Signal Processor and Application

AD-A190 076

by

Francis T. S. Yu
(Principal Investigator)

Department of Electrical Engineering
The Pennsylvania State University
University Park, PA 16802

DTIC
ELECTE
JAN 1 2 1988
S D
cD

Prepared for:

AFOSR/NE

Building 410
Bolling Air Force Base
Washington, D.C. 20332

Attention: Dr. C. Lee Giles

AFOSR Final Report on
Grant AFOSR-86-0264

Period Covered (August 1, 1986 - September 30, 1987)

Date: November 18, 1987

DISTRIBUTION STATEMENT A
Approved for public release
Distribution Unlimited

87 12 29 309

Unclassified
SECURITY CLASSIFICATION OF THIS PAGE

REPORT DOCUMENTATION PAGE

1a. REPORT SECURITY CLASSIFICATION Unclassified	1b. RESTRICTIVE MARKINGS
2a. SECURITY CLASSIFICATION AUTHORITY	3. DISTRIBUTION / AVAILABILITY OF REPORT Unlimited Approved for public release; distribution unlimited.
2b. DECLASSIFICATION / DOWNGRADING SCHEDULE	
4. PERFORMING ORGANIZATION REPORT NUMBER(S)	5. MONITORING ORGANIZATION REPORT NUMBER(S) AFOSR-TR. 87-1802
6a. NAME OF PERFORMING ORGANIZATION Dept. of Elect. Engineering The Pennsylvania State Univ. 6b. OFFICE SYMBOL (If applicable)	7a. NAME OF MONITORING ORGANIZATION Dr. Lee Giles AFOSR
6c. ADDRESS (City, State, and ZIP Code) University Park, PA 16802	7b. ADDRESS (City, State, and ZIP Code) Building 410 Bolling Air Force Base Washington, D.C. 20332
8a. NAME OF FUNDING / SPONSORING ORGANIZATION AFOSR/NE 8b. OFFICE SYMBOL (If applicable)	9. PROCUREMENT INSTRUMENT IDENTIFICATION NUMBER AFOSR-86-0264
8c. ADDRESS (City, State, and ZIP Code) Building 410 Bolling Air Force Base Washington, D.C. 20332	10 SOURCE OF FUNDING NUMBERS PROGRAM ELEMENT NO. 61102F; PROJECT NO. 2305; TASK NO. B1; WORK UNIT ACCESSION NO.

11. TITLE (Include Security Classification)
STUDY OF A MICROCOMPUTER-BASED REAL-TIME PROGRAMMABLE OPTICAL SIGNAL PROCESSOR AND APPLICATION

12. PERSONAL AUTHOR(S)
Yu, Francis T.S.

13a. TYPE OF REPORT	13b. TIME COVERED	14. DATE OF REPORT (Year, Month, Day)	15. PAGE COUNT
Final Report	FROM 8/1/86 TO 9/30/87	November 18, 1987	125

16. SUPPLEMENTARY NOTATION

17. COSATI CODES			18. SUBJECT TERMS (Continue on reverse if necessary and identify by block number)
FIELD	GROUP	SUB-GROUP	MICROCOMPUTER BASED REAL-TIME PROGRAMMABLE OPTICAL SIGNAL PROCESSOR AND APPLICATION.

19. ABSTRACT (Continue on reverse if necessary and identify by block number)

Optical signal processor has been shown to perform a myriad of complicated processing operations. It is primarily due to the profound diffraction phenomena of coherent light. The essential merits, of an optical signal processor must be the capability of processing the signal in complex amplitude, parallelism, large capacity, high speed and wavelength diversity. There are several processing operations that have been shown more efficient with optical techniques. The operations are: Fourier transformation, convolution and correlation operations, spectrum analysis, and others. However, optical signal processors are still very inflexible as compared with the electronic computers. The major advantages of an electronic computer must be the flexibility, programmability, easy accessability, and many others. The question is that, can we exploit the efficient operation of the optics and the flexibility of the electronic computer to come up with a more realistic, but not futuristic, electro-optical (OE) architecture to meet our computational needs? The answer to this question is yes. It is the subject of (cont.)

20. DISTRIBUTION / AVAILABILITY OF ABSTRACT	21 ABSTRACT SECURITY CLASSIFICATION
☒ UNCLASSIFIED/UNLIMITED ☐ SAME AS RPT. ☐ DTIC USERS	Unclassified
22a. NAME OF RESPONSIBLE INDIVIDUAL Dr. Lee Giles	22b. TELEPHONE (Include Area Code) (202) 767-4984
	22c. OFFICE SYMBOL AFOSR

DD FORM 1473, 84 MAR 83 APR edition may be used until exhausted. All other editions are obsolete.

SECURITY CLASSIFICATION OF THIS PAGE
Unclassified

87 12 23 [illegible]

AFOSR-TR- 87-1809

this report to illustrate a microcomputer-based optical processor that can exploit these advantages. In the following, we shall highlight some of the major results accomplished with this research supported by AFOSR Grant-86-0264, which covers the period from August 1, 1986 to September 30, 1987.

We have developed a microcomputer-based optical processor for linear transformation. The technique uses the systolic array processing method, such that various types of linear transformations can be carried out with the programmable optical system.

We have, in this research, developed and experimentally demonstrated that Boolean logic operations can be performed with a microcomputer-based optical architecture. The technique uses magneto-optic spatial light modulators (MOSLMs) for logic gates.

We have also, in this phase of research, studied the effect of a microchannel spatial light modulator (MSLM) under partially coherent illumination. A variety of optical image processing operations can be carried out with the MSLM device. Several image processing results have been experimentally illustrated.

Concurrently, we have also developed a multichannel optical correlator. This correlator is capable of performing N x N parallel correlations, which has a processing capacity of more than 400 times over the conventional optical correlator.

In this research, we have also accomplished a research on Boolean logic gates using MSLM and liquid crystal televisions (LCTVs). The MSLM is used as an adder, an inverter, a subtractor, or a buffer, while the LCTVs are used as input data generators. The sixteen Boolean functions can be performed rather easily with the hybrid optical architecture.

We have also illustrated a technique of performing binary adder with a microcomputer-based optical processor. We stress that, the optical binary adder is a basic part of the central processing unit in a digital-optical computer. An experimental result shows that a 4-bit half-addition can be implemented, and the technique can be extended to perform the addition on larger arrays of numbers by simply changing the subroutines of the microcomputer.

In this period of research, we have developed several techniques to perform matrix multiplication. We have used outer products, systolic-outer product, systolic-inner product techniques for multiple-matrix operation. Bilinear transformation can also be carried out with this microcomputer-based optical architecture (MOA). The essential merits of the MOA must be the high accuracy and high speed performance.

Remarks, the net effects of this study is to emphasize that, by exploiting the efficient operation of optics and the programmability of electronic computer, it is our belief that the microcomputer-based optical architecture would be the logical approach toward the real-time programmable optical processing and computing. However, much remains to be done in the development of electro-optical devices before the hybrid optical processing can become a widespread practical reality. It is, therefore, hoping that this study would stimulate the interested researchers with imaginative approaches toward the hybrid optical computing applications.

Study of a Microcomputer-Based Real-Time Programmable Optical Signal Processor and Application

by

Francis T. S. Yu
(Principal Investigator)

Department of Electrical Engineering
The Pennsylvania State University
University Park, PA 16802

Prepared for:

AFOSR/NE

Building 410
Bolling Air Force Base
Washington, D.C. 20332

Attention: Dr. C. Lee Giles

AFOSR Final Report on
Grant AFOSR-86-0264

DTIC
COPY
INSPECTED
6

Period Covered (August 1, 1986 - September 30, 1987)

Date: November 18, 1987

Accesion For
NTIS CRA&I
DTIC TAB
Unannounced
Justification
By
Distribution /
Availability Codes
Dist
A-1

DTIC
COPY
INSPECTED
6

Table of Contents

1. Introduction

We have, in this period of research from August 1, 1986 to September 30, 1987, completed the major tasks in the area on "Study of a Microcomputer Based Real-Time Programmable Optical Signal Processor and Application." The research done is very consistent with our proposed program to the Air Force Office of Scientific Research Grant AFOSR-86-0264. Several of research findings have either been published or in the process to be published in open literatures. Several of the results have also be presented in various scientific conferences and meetings (e.g., Optical Society Meeting, SPIE, and ICO). Sample copies of these papers are included in this report, in the subsequent sections, to provide a concise documentation of our research accomplishment in this study. In the following section, we shall highlight the overall research done, that covers the entire period of this funding research. A list of publications resulting from this support is included at the end of this report.

2. Summary and Overview

2.1 Optical Linear Transformation (Section 6)

We have, in this period, developed a microcomputer-based optical linear transformation processing technique. The technique utilizes a systolic array processing method to perform various types of linear transformations, such as discrete Fourier transformation, discrete Hilbert transformation, discrete chirp-Z transformation and many others. By partially parallel addressing two magneto-optic spatial light modulators (MOSLM), this proposed system would offer high speed and parallel processing capability of optics and programmability of microcomputer.

2.2 Real-Time Signal Detection using LCTV (Section 4)

In this research, we have shown that a color liquid crystal television (LCTV) can be used for color pattern recognition. The grid structure of the display panel together with a specially designed color filter provides spatially isolated polychromatic spectra to enable polychromatic signal detection.

We have found a serious drawback of the color LCTV which is the lack of space invariance, even after it has been immersed in a liquid gate. This drawback is primarily due to the inherent color filter in the liquid crystal display and the phase modulation by liquid crystal molecules. A quantitative investigation of space variance of the LCTV, especially the color LCTV, is currently being studied.

We have used a multiple matched filtering technique to improve the correlation signal. However, in practice the diffraction efficiencies vary for different matched spatial filters. The Horner efficiency in a multiple matched filtering correlated output was observed to be approximately 30(=N) times higher than the single matched filtering correlation using a color LCTV. With the aid of a hard-clipping signal. With further improvements, the color LCTV can be useful for color-sensitive robotic vision and other automatic color pattern recognition applications.

2.3 Implementation of Symbolic Substitution (Section 5)

Symbolic substitution is essentially a combination of recognition and substitution phase. Although symbolic substitution is not restricted to space invariant operations, it is indeed based on the space invariant connectivity of optics. A method of optical associative memories as applied to implement a symbolic substitution logic is proposed in this study. The merits of the proposed implementation are that it can (1)

handle very large (SBP) data, (2) perform any substitution in one simple step, and (3) perform multiple instruction, multiple data (MIMD) operation using a multiplexed hologram. The price is the use of more than 1 pixel (e.g., 9 pixels) to encode a bit. A thresholding process may be required before the data are transferred to the next operation.

We have also, in this study, experimentally demonstrated a one-step holographic associative memory as applied to symbolic substitution. The linearity of multiple holographic filtering is abolished in practice. The results of parallel half-addition are illustrated. We note that parallel half-addition is an example of multiple-instruction-multiple-data (MIMD) operation.

2.4 Optical Parallel Logic Operation (Section 6)

We have, in this research, experimentally demonstrated that the sixteen Boolean logic operations can be performed with the microcomputer based optical signal processor using magneto-optic spatial light modulators (MOSLMs). The parallel logic, which includes flip-flop, half adder, full adder, binary image subtraction and cellular processing, have also been demonstrated. The advantages of using the MOSLM devices are: (1) electronically-addressability and microcomputer-programmability, (2) fast switching time (≈50μs), (3) capability of storing an input pattern with-out power supplied, and (4) low power consumption. Many new architectures of hybrid optical processing and computing may be implemented using MOSLMs based on the proposed technique.

2.5 Microchannel Spatial Light Modulator Processing (Section 7)

In this period of research, we have investigated the signal processing capability using a microchannel spatial light modulator (MCSLM) under partially coherent light. We have shown that the MCSLM provides an

effective means of performing optical processing operations in color under white-light illumination. The external crystal plate in conjunction with the electro-optic crystal in the MSLM plays an important role in the system by performing color filtering, and allocating some colors to the background and others to the object. A variety of operations can be carried out. Image subtraction and edge enhancement have been demonstrated. Color selection and/or reversal can be obtained by rotating the external crystal plate.

The system or its expanded version can potentially be valued for night vision, medical imaging, and interferometric applications.

2.6 Multichannel Optical Correlation (Section 8)

We have, in this research program, developed a multichannel optical correlator for mass image correlation. This correlator utilizes reference beams with different directions in construction the (MSFs). Since the output correlation diffraction is based upon the direction of the spatial carrier frequency, the correlation distribution from each MSF will appear at different diffracted locations. Thus, N x N channels can be synthesized by employing a phase mask to diffract the reference beam into N x N directions. Thus a parallel optical correlator, which has a processing capacity of more than 400 times over the conventional signal channel, can be constructed. Since the correlation outputs are diffracted in different locations, the output signal-to-noise (SNR) is independent of the number of channels. This technique is rather easy to implement since no mechanical scanner is used for the mass channel correlations, and it can apply to rapid optical mass pattern recognitions.

2.7 Boolean Logic Gates using MSLM and LCTVs (Section 9)

We have, in this research task, developed a microcomputer based optical system to perform binary Boolean logic, using a microchannel spatial light modulators (MSLM) and liquid crystal televisions (LCTVs). The logic states of the input and output data arrays are represented by light intensity. Combining the merits of the MSLM, LCTV's and a computer, the system offers the advantages of optical parallel-processing capability, programmability, and feedback consecutive-processing flexibility. We notice that the MSLM is used as an adder, an inverter, a subtractor, or a buffer. We used three liquid-crystal televisions with a computer as input interfacing devices. Through the use of its feedback loop, the system can consecutively execute a series of logic operations.

We conclude that, with advances in MSLM performance, the performance of this optical system is expected to improve, resulting in faster response, higher resolution, and less image distortion.

2.8 Optical Binary Adder (Section 10)

We note that the optical binary adder, in a digital optical computer, is a basic part of the central processing unit (CPU). We have, in this research program, developed a technique of implementing an optical half-adder and a full adder utilizing programmable liquid crystal televisions (LCTV). The concept of constructing an optical full adder is based upon the realization of an optical read-only-memory (OROM). We have experimentally demonstrated that a 4-bit half-addition can be implemented. The results reflect the general case for half-addition. Notice that the half-adder can be easily extended to perform the addition on larger arrays of numbers by changing the program in the control computer. There is no extra coding processing required in the half-adder, since the number is

automatically encoded by the LCTV into the directions of polarization. To extend a half-adder to a full adder, we introduced an OROM to realize carry transmission and overflow error detection.

2.9 Digital-Optical Matrix Multiplication (Section 11)

In this research task, we have developed a technique to perform multiple binary number multiplication in parallel. With reference to the basic approach, two optical architectures for multiple matrix multiplication are constructed. Since the matrices are in binary or mixed binary form and the processing is performed in parallel, these systems have the capability to perform high accuracy and high speed multiple matrix multiplication. Several preliminary experimental demonstrations have been carried out. The technique involves the hybrid optical system using real-time SLM's and are also studied. We note that the digital-optical architectures can also be applied to linear and bilinear transformations

2.10 Optical Perfect Shuffle (Section 12)

One of the inherent advantages of the optical computer is its noninteractive interconnecting capability. The optical perfect shuffle (PS) which forms the basis of such an interconnection network is a useful concept in optical computer architecture. In this phase of research, we have shown that an optical perfect shuffle can be easily performed by coherent or partially coherent spatial filtering. We have experimentally demonstrated two sets of input data (e.g., English letters) can be shuffled with a conventional optical filtering technique. The input data can be easily generated by a microcomputer and then written onto programmable spatial light modulators.

2.11 Hybrid Optical Computing (Section 13)

We have, in this research program, investigated several optical computing architectures with a microcomputer based optical processor. The basic philosophy of the approach must be exploiting the efficient operation of optics and the programmability of electronic computer. It is our belief that the hybrid optical architecture is the logical approach toward modern optical computing.

SECTION 3

Optical Linear Transformation

Copy available to DTIC does not permit fully legible reproduction

A Hybrid Optical System for Linear Transformation Processing

F. T. S. Yu, M. F. Cao and T. W. Lu

Electrical Engineering Department
The Pennsylvania State University, University Park, PA 16802

Abstract

A microcomputer-based optical linear transformation processing system is proposed. The technique utilizes a systolic array processing method to perform various types of linear transformations, such as discrete Fourier transformation, discrete Hilbert transformation, discrete chirp-Z transformation and many others. By partially parallel addressing two magneto-optic spatial light modulators (MOSLM), this proposed system would offer high speed and parallel processing capability of optics and programmability of microcomputer.

1. Introduction

Optical signal processing was initially based upon the two-dimensional Fourier transformation achievable with a lens. However, this is not the only optical method to perform the Fourier transform. Mention must be made that a mask-LED based approach was subsequently proposed by Goodman[1] and Bromley, etc.[2] to compute a one dimensional (1D) discrete Fourier transform (DFT). By considering 1D DFT as a matrix-vector product, they developed an electro-optical processor (EOP) with a mask representing the transform matrix and an LED representing an input signal sequence.

In this paper, we would propose a systolic array processing technique utilizing two-cascaded magneto-optic spatial light modulators to perform the discrete linear transformation (DLT). We will show that this proposed system would offer the advantages of programmability, high accuracy and high speed parallel processing capability.

2. The Discrete Linear Transformation (DLT)

2.1. Definition

It is well known that a discrete linear system, as shown in Figure 1, can be characterized by the response $h_{m,n}$ to an impulse at the input. The input-output relationship of such a system can be summarized by the following equation:

$$g_m = \sum_{n=1}^{N} f_n h_{m,n}, \quad m = 1, 2, \ldots, M. \tag{1}$$

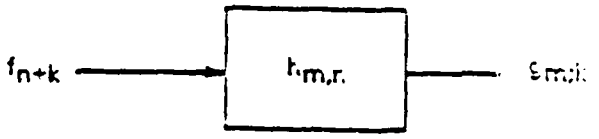

Figure 1. Input and output functions of discrete linear transformation (DLT).

In other words, the output sequence $\{g_m\}$ and input sequence $\{f_n\}$ can be considered as vectors, such that Eq. (1) can be expressed in matrix form,

$$\begin{bmatrix} g_0 \\ g_1 \\ \cdot \\ \cdot \\ \cdot \\ g_{M-1} \end{bmatrix} = \begin{bmatrix} h_{0,0} & h_{0,1} & h_{0,2} & \cdots & h_{0,N-1} \\ h_{1,0} & h_{1,1} & h_{1,2} & \cdots & \cdot \\ h_{2,0} & h_{2,1} & h_{2,2} & \cdots & \cdot \\ \cdot & \cdot & \cdot & & \cdot \\ \cdot & \cdot & \cdot & & \cdot \\ h_{M-1,0} & \cdots & \cdots & \cdots & h_{M-1,N-1} \end{bmatrix} \begin{bmatrix} f_1 \\ f_2 \\ \cdot \\ \cdot \\ \cdot \\ f_{N-1} \end{bmatrix} \tag{2}$$

Copy available to DTIC does not
permit fully legible reproduction

or abbreviated, as

$$[g_m] = [h_{m,n}]\,[f_n]. \tag{3}$$

The set of impulse response represented by $h_{m,n}$ is known as a transform matrix $[h_{m,n}]$. Thus different DLT would have different transform matrices. Let us now illustrate a few of frequently used DLTs:

2.1.1. Discrete Fourier Transform (DFT)

The DFT is defined by

$$F_m = \frac{1}{N}\sum_{n=0}^{N-1} f_n \exp\left[\frac{-i2\pi}{N}mn\right],\quad 0\le m\le N-1. \tag{4}$$

where

$$h_{m,n} = \exp\left[\frac{-i2\pi}{N}mn\right], \tag{5}$$

is also known as the transform kernel. In order to implement the DFT transformation in a electro-optical processor, we would represent the complex transform matrix in real elments. The corresponding real transform matrices can be written as

$$Re(h_{m,n}) = \cos\left[\frac{2\pi}{N}mn\right], \tag{6a}$$

and

$$Im(h_{m,n}) = \sin\left[\frac{2\pi}{N}mn\right], \tag{6b}$$

which are the well known discrete cosine transform (DCT) and discrete sine transformation (DST).

2.1.2. Discrete Hilbert Transform (DHT)

It is well known that the relationship between the real and imaginary parts of an analytic signal can be described by Hilbert transformation. The elements of a discrete Hilbert transform (DHT) matrix can be written as,

$$h_{m,n} = \begin{cases} \dfrac{2}{\pi}\cdot\dfrac{\sin^2[\pi(m-n)/2]}{(m-n)}, & m-n\neq 0, \\ 0, & m-n=0 \end{cases} \tag{7}$$

2.1.3. Discrete Chirp-Z Transform (DCZT)

Another frequently used linear transformation is Chirp-Z transform, which can be used to compute the DFT coefficients. The elements of the DCZT transform matrix can be written as

$$h_{m,n} = \exp\left[i\pi(m-n)^2/N\right]. \tag{8}$$

We note that this type of shift-invariant transformation, as well as other types of DLT can be implemented by an electro-optical processor with a systolic array processing technique.

2.2. DLT Implementation with Systolic Array Processing

Since the discrete linear transformation can be viewed as result from a matrix-vector multiplication, the systolic array processing architecture can be used for the implementation of DLT. Thus by combining the systolic array processing technique and the two's complement representation, a DLT can be performed with a digital optical processor. As compared with the analog optical processor, the technique that we will propose would have high accuracy and low error rate. And it is compatible with other digital processors.

2.2.1. Two's Complement Representation

Two's complement representation has been applied for improving the accuracy of matrix multiplication. This technique allows the handling of both positive and negative numbers. A detailed discussion of two's complement arithmetic can be found in the work of Booker, Bromley and Clayton.[3] Let us now briefly describe the concept of two's complement arithmetic.

Since the size of optical processor is fixed, the two's complement representation used in digtal optical processor should be modified. For example, the decimal numbers -3.25 and +13,375 would have a traditional two's complement representation such as

Decimal Representation	Traditional Two's Complement Representation
-3.25	100.11 +_sign bit
+13.375	01101.011 +_sign bit

The left-most bit is a sign bit, which is needed for two's complement representation. For fixed size processor, it requires the input numbers be represented by the same number of bits. For a 12 bit processor, the examples discussed above should be represented by a 12 bit representation such as

Decimal Representation	Optical Two's Complement Representation
-3.25	111111100.110
+13.375	000001101.011

In our proposed system, mixed binary representation is employed. The advantages of utilizing the mixed binary representation is to avoid the carry bit in optical processing, which make the implementaion much simpler.

2.2.2. Systolic Array Processing

We note that systolic array processing is suitable for performing matrix-vector multiplication.[11] In our proposed system, we would utilize the systolic array technique to perform various discrete linear transformations.

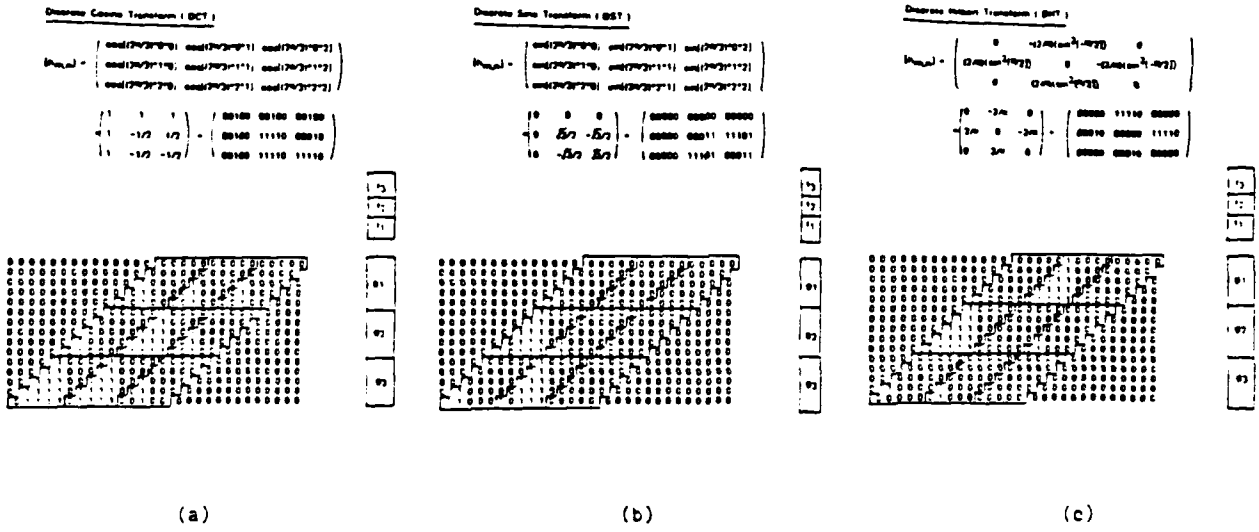

(a) (b) (c)

Figure 2. Examples of DLT implementation using systolic array processing.
(a) discrete cosine transformation (DCT).
(b) discrete sine transformation (DST).
(c) discrete Hilbert transformation (DHT).

Several examples of DLT using the systolic array processing technique are illustrated in Figure 2. In Figure 2(a), a discrete cosine transform (DCT) matrix is encoded in two's complement form and multiplied with input vector (signal) using systolic array method. A discrete sine transformation (DST) carried out by systolic array method is also shown in Figure 2(b). Thus by combining DCT and DST of Figure 2(a) and (b), a discrete Fourier transform can be obtained. Moreover, the systolic array formats for discrete Hilbert transform (DHT) is also shown in Figure 2(c).

Copy available to DTIC does not permit fully legible reproduction

3. Electro-Optical DLT Processor Design

The proposed microcomputer-based digital optical DLT processing system is illustrated in Figure 3. From this figure, we see that two cascaded magneto-optic spatial light modulators (MOSLM) are utilized to perform systolic array engagement section and a CCD array detector is used for time-integration.

Since MOSLM can be addressed in partial parallel mode, the whole frame pattern on MOSLM can be switched very fast (e.g., 50 μs for a 512 x 512 MOSLM).[5,6] By proper design of a high speed memory subsystem and an interface circuit, a relatively slow microcomputer can be used to control the parallel operation for large data, which would result in higher operation speed. At the same time, the flexiblity of man-machine interaction of microcomputer is still retained. In order to generate the systolic array pattern of transform matrix rapidly, these patterns are stored in a high speed read only memory (ROM), while the input signal sequence is converted by a high speed analog to digital converter (if input is analog signal) and then is formated by a high speed parallel-serial buffer. The time-integration operation is done by a CCD detector, and a high speed serial-parallel deformater is therefore needed. By controlling the microcomputer, various DLT systolic patterns can be selected, for which the related DLT can be performed. Software design for this proposed DLT processor is illustrated by a flow chart in Figure 4.

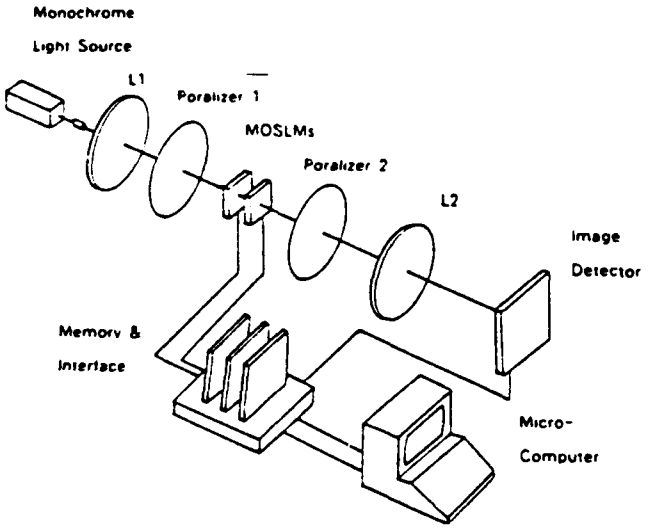

Figure 3. A microcomputer-based optical DLT processor.

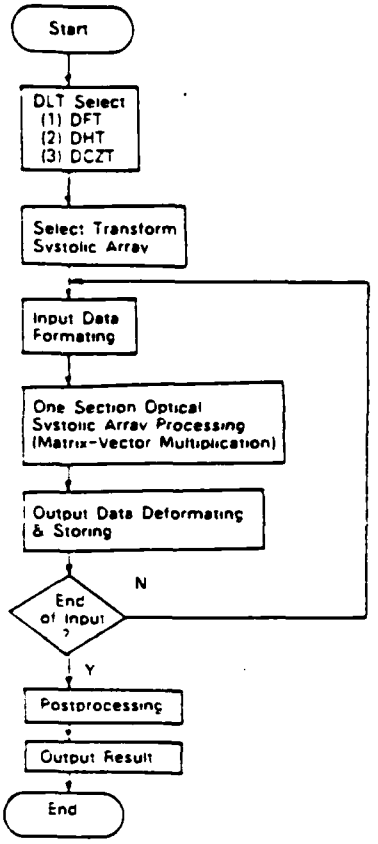

Figure 4. Flow chart of main program.

4. Experimental Demonstration

In order to verify the proposed technique, an experimental system is constructed. For experimental demonstration, some DLT systolic patterns are generated onto the spatial light modulators, and an optical RAM (OPRAM) detector is used with an Apple IIe computer to perform engagement processing. Several DLT systolic patterns are illustrated in Figure 5 and an experimental set up is depicted in Figure 6.

Copy available to DTIC does not permit fully legible reproduction

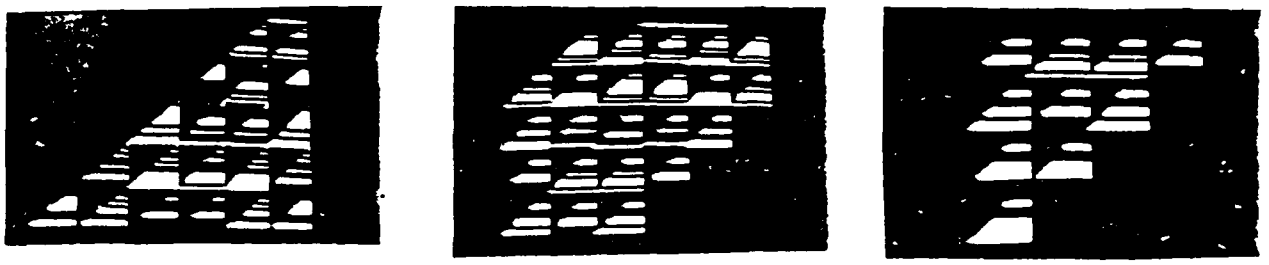

(a) (b) (c)

Figure 5. Part of systolic array patterns generated by microcomputer
(a) for DFT transform matrix (cosine part).
(b) for DHT transform matrix.
(c) for DCZT transform matrix (cosine part).

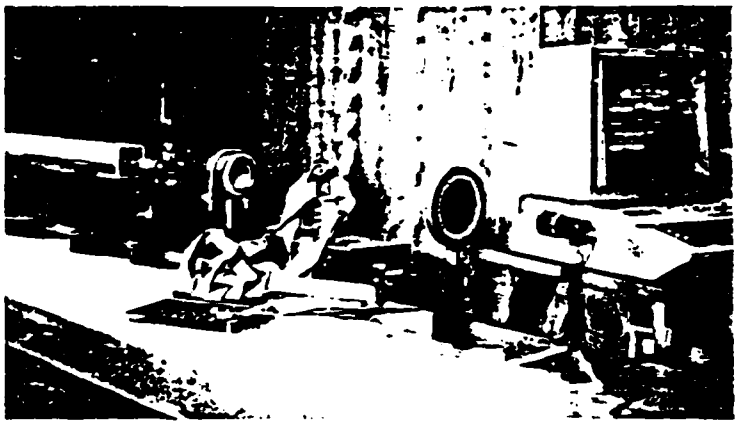

Figure 6. An experimental set-up.

5. Conclusion

We have demonstrated the capabilities of a microcomputer-based optical signal processor in performing various types of DLT operations. By utilizing systolic array engagement architecture and two's complement mixed binary representation, this proposed system would offer the advantages of high accuracy, high speed, and programmability. Anotner advantage of this system must be the capability to process two dimensional DLT, which will be discussed in detail in our forthcoming papers.

6. Acknowledgement

We wish to acknowledge the support of U.S. Air Force Office of Scientific Research grant AFOSR-86-0264.

7. References

[1] J. W. Goodman, A. R. Dias, and L. M. Woody, "Fully parallel, high-speed incoherent optical method for performing discrete Fourier transforms." Optics Letters, 2(1), 1-3 (1978)

[2] R. H. Patterson, K. Bromley, M. A. Monahan, J. J. Symanski, "Charge-coupled device (CCD) based electrooptic processor." Proc. SPIE 352, 76-81 (1982)

[3] R. P. Bocker, K. Bromley, S. R. Clayton, "A digital optical architecture for performing matrix algebra." Proc. SPIE 431, 194-200 (1983)

[4] S. Cartwright, S. C. Gustafson, "Convolver-based optical systolic processing architectures." Opt. Eng. 24(1), 59-64 (1985)

[5] W. E. Ross, D. Psaltis, and R. H Anderson, "Two-dimensional magneto-optic spatial light modulator for signal pocessing." Opt. Eng. 22(4), 485-490 (1983)

[6] F. T. S. Yu, M. F. Cao, and J. E. Ludman, "Microcomputer-based programmable optical signal processor." Opt. Eng. 25(7), 846-852 (1986)

SECTION 4

Real-Time Signal Detection using LCTV

Real-time polychromatic signal detection using a color liquid crystal television

Francis T. S. Yu, FELLOW SPIE
Suganda Jutamulia, MEMBER SPIE
Tsongneng W. Lin, MEMBER SPIE
The Pennsylvania State University
Electrical Engineering Department
University Park, Pennsylvania 16802

Abstract. A novel low-cost color liquid crystal television is applied in a real-time color pattern recognition system. In this system, a target is identified on the basis of both shape and spectral content. A multiple matched filtering technique is also proposed to improve the detected correlation signal. Experimental results of the bichromatic signal detection are presented.

Subject terms: optical information processing; color pattern recognition; multiple matched filtering; real-time device; liquid crystal television.

Optical Engineering 26(5), 453-460 (May 1987).

CONTENTS

1. INTRODUCTION

The recent appearance of a low-cost (~$100) black-and-white liquid crystal television (LCTV) has attracted a great deal of attention to explore its usefulness for real-time optical signal processing.[1-7] It is undoubted that a color LCTV (~$300) can be applied to real-time optical processing as well. In optical signal processing, polychromatic signal detection is significant because all natural objects are colored. It would be desirable to have a detecting system capable of discriminating different colors in addition to different shapes. This kind of detecting system would be a step closer to artificial intelligence resembling a human recognition system. In this paper we present the application of color LCTV to real-time polychromatic signal detection.

Color pattern recognition has been performed using a transmission-type as well as a reflection-type matched spatial filter (MSF) by Case[8] and by Ishii and Murata,[9] respectively. Their techniques used color-sensitive optical filters that were in essence multiplexed volume holograms as proposed by Shi.[10] The utilization of a prism in a polychromatic coherent optical correlator for color pattern recognition was described by Braunecker and Bryngdahl.[11] We have studied polychromatic signal detection utilizing a diffraction grating,[12] which can also be performed in real time using an expensive liquid crystal light valve (LCLV).[13,14] In this method, a color signal transparency is placed in contact with a one-dimensional sinusoidal diffraction grating at the input plane of a polychromatic coherent optical processor. It is always possible to design a diffraction grating such that the first-order spectra of the red, green, and blue (R, G, B) wavelengths are adequately separated. If a set of color-sensitive MSFs is properly inserted in the Fourier plane, a color correlation signal can be detected at the output plane of the processor.

2. GENERAL CONCEPT

We previously noted that a color LCTV can be applied to real-time optical signal processing. With proper modification, a disassembled color LCTV is suitable for the diffraction method in polychromatic signal detection. Because the display panel of an LCTV consists of a tricolor (red, green, blue) pixel structure, the Fourier transform of a pattern displayed on the LCTV will be diffracted into many orders. Therefore, a diffraction grating is no longer needed. However, separations of the polychromatic spectra cannot be determined freely.

The structure of the display panel of a color LCTV is illustrated in Fig. 1(a). The corresponding polychromatic spectral distribution is shown schematically in Fig. 1(b). Note that the first-order spectra of different colors may overlap. However, assuming that the four first-order spectra have the same intensity, isolated polychromatic spectra can be obtained by superimposing some specific color filters at the Fourier plane, as shown in Fig. 1(c). Thus, a polychromatic signal can be detected by three primary MSFs. The three primary color autocorrelation spots would then all be at the same position on the output plane since they depend only on the angle of the reference beam in the MSF synthesis.

Figure 2 is a photograph of the Fourier transform of the display panel illuminated by red laser light. It was observed

Invited Paper IP-101 received Sept. 17, 1986; revised manuscript received Dec. 29, 1986; accepted for publication Jan. 12, 1987; received by Managing Editor Feb. 9, 1987.
© 1987 Society of Photo-Optical Instrumentation Engineers.

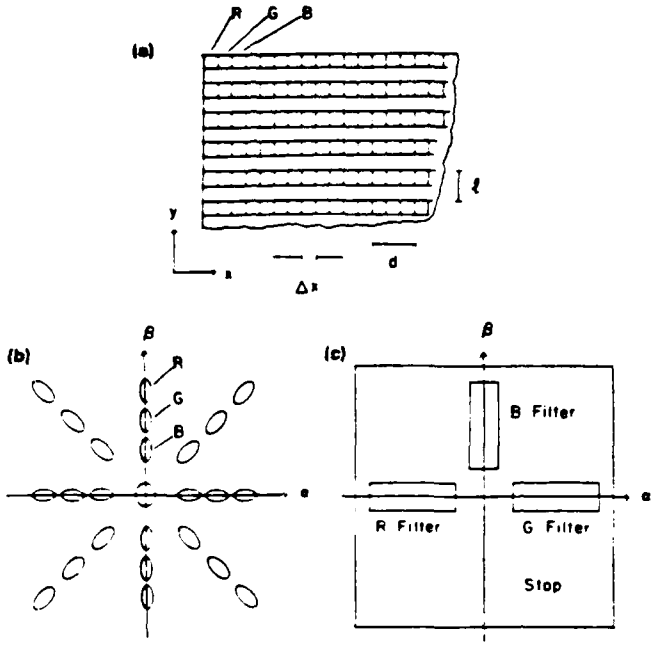

Fig. 1. (a) Structure of color LCTV display panel. (b) Schematic diagram of polychromatic spectral distribution at Fourier transform plane. (c) Color filters at Fourier transform plane.

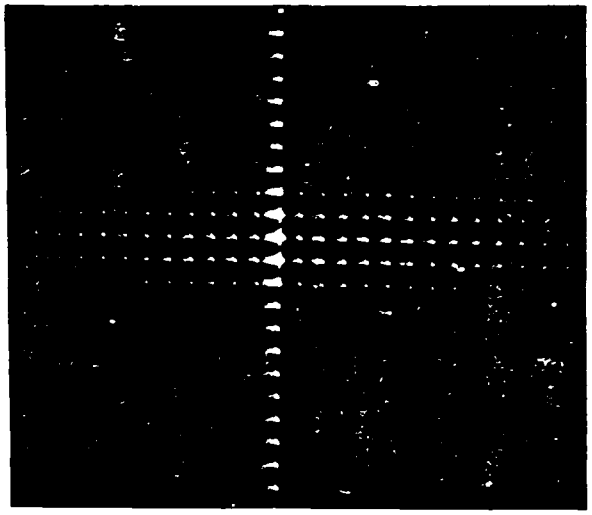

Fig. 2. Fourier transform of the display panel illuminated by red laser light.

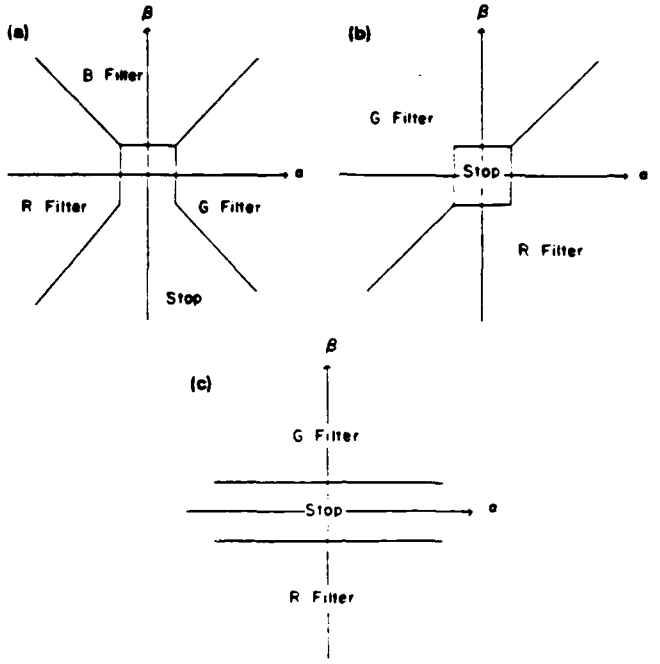

Fig. 3. Color filters at Fourier transform plane proposed for multiple matched filtering method: (a) polychromatic correlation, (b) bichromatic correlation. (c) Color filters actually used for bichromatic correlation based on multiple matched filtering method.

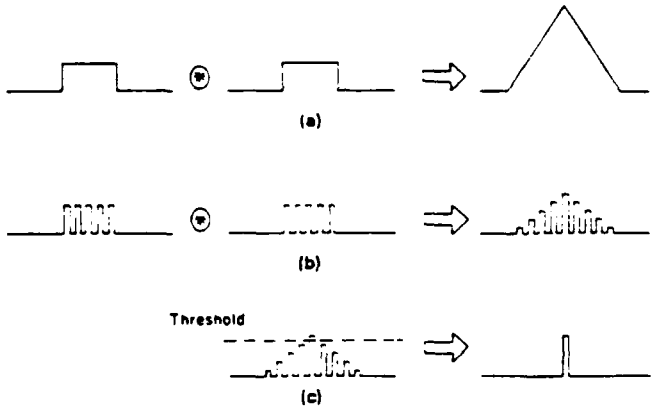

Fig. 4. (a) Autocorrelation of a window function. (b) Autocorrelation of a sampled window function. (c) Hard-clipping process.

that the intensity of the zero-order spectrum was much stronger than that of the higher diffraction orders. The zero-order spectrum was utilized in the monochromatic signal detection using a black-and-white LCTV.[2,3,6] In theory, the basic concept illustrated in Fig. 1(c) will provide polychromatic signal detection. In practice, however, the first-order spectra may be too weak. This is a significant difference between the inherent grating structure of the LCTV and the sinusoidal diffraction grating used in Ref. 8, which concentrates the diffracted light into the first-order spectra.

3. MULTIPLE MATCHED FILTERING METHOD

To enhance the correlated output signal, a multiple matched filtering technique is proposed. In this technique, many spectra are utilized simultaneously instead of only one, as shown in Fig. 3(a). The Fourier plane is divided into four quadrants covered by red, green, and blue filters and an opaque stop. In this arrangement, a higher than normal Horner efficiency,[15] which is the ratio of autocorrelation output power and input power, can be expected. For the sake of simplicity, a bichromatic correlation (red and green) will be performed to verify the proposed technique. To utilize diffracted light efficiently, a configuration of color filters as shown in Fig. 3(b) may be used at the Fourier plane. However, the configuration shown in Fig. 3(c) is preferred because it approximates the one in Fig. 3(a), i.e., only one axis is covered by each color filter.

We now consider the correlation signal of the multiple matched filtering technique. Figure 4(a) shows the autocorrelation of a window function, and Fig. 4(b) shows the autocorrelation of a sampled window function. Comparing these autocorrelations, we see that (1) the autocorrelation in (b) is

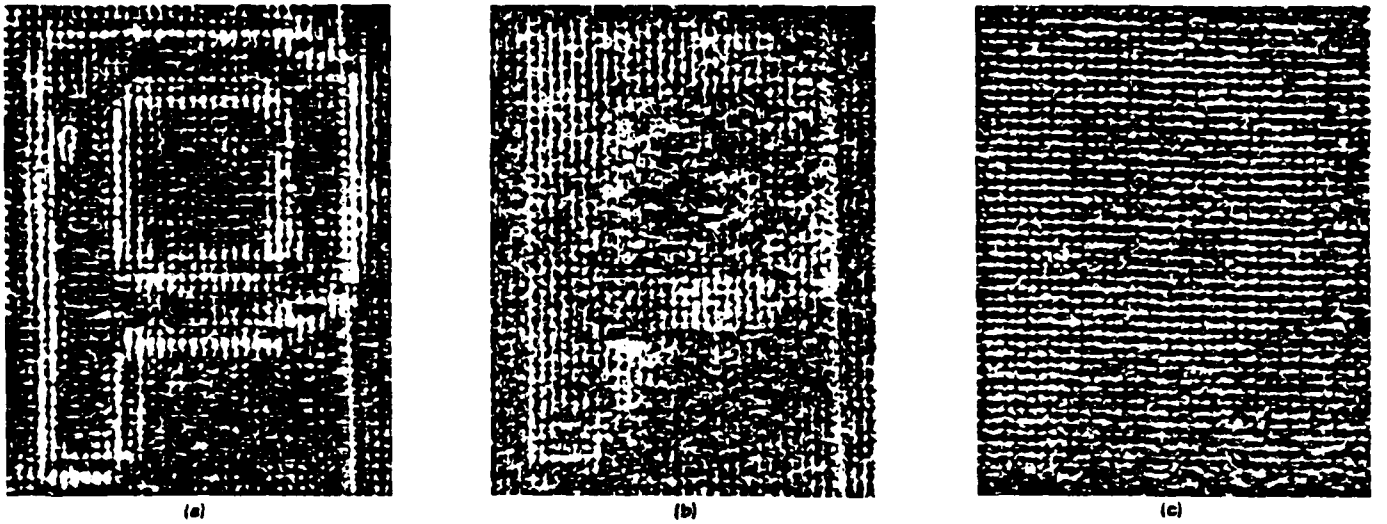

Fig. 5. Impulse responses of synthesized MSFs of letter P with (a) high frequency content, (b) medium frequency content, and (c) low frequency content.

also sampled; (2) the width of the envelope in (b) is the same as that in (a); and (3) the peak height of the envelope in (b) is half that in (a).

Since the input signal displayed on the LCTV is a sampled pattern due to the inherent grating structure, multiple spectra are produced at the Fourier plane. If only one spectrum is matched with an MSF, it is essentially a correlation similar to that shown in Fig. 4(a), with a very low peak height. If all of the spectra are matched with the proper MSFs, we would have a correlation peak similar to that in Fig. 4(b) but with a higher peak height. Approximately N matched spectra split the correlation spot into N subpeaks. The most important feature is that the height of the main peak increases by N^2 while the width of the envelope of the correlation signal remains unchanged. To improve the detectability of the correlation signal, a hard-clipping process can be done using an image digitizer to depress all subpeaks except the main one, as shown schematically in Fig. 4(c). A similar hard-clipping technique has proved effective in other applications.[16] An alternative process also can be done to integrate subpeaks so that an averaged spot is obtained. We note that this averaged spot is approximately the same size as a single matched filtering correlation spot.

In addition, the multiple matched filtering technique makes it possible to match the entire frequency content of the object. Because of the limitation of the dynamic range in a photographic process, an MSF is usually synthesized for a narrow frequency band. By multiple matched filtering, each MSF contributes a different frequency content. Thus, it takes us a step closer to complete frequency matched filtering. For illustration, Fig. 5 depicts a series of impulse responses of the synthesized MSFs of a letter P.

4. MATHEMATICAL DESCRIPTION

A mathematical description may be required to support the physical concept described above. Figure 6 is a schematic of the proposed optical setup. Suppose that the color display of the LCTV is constructed as in Fig. 1(a). The complex light amplitude distribution behind the input plane can be described as

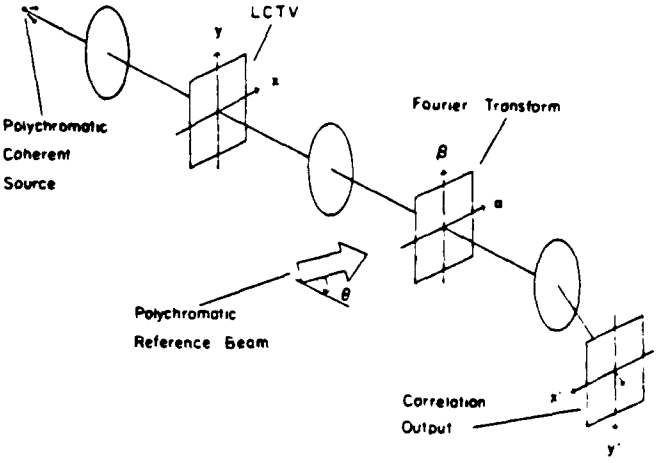

Fig. 6. Schematic diagram of optical setup for polychromatic signal detection.

$$s(x,y;\lambda) = s_r(x,y)\exp[i\phi(x,y)]t_r(x,y) + s_g(x,y)\exp[i\phi(x,y)]t_g(x,y) + s_b(x,y)\exp[i\phi(x,y)]t_b(x,y)\,, \tag{1}$$

where s_r, s_g, and s_b are the red, green, and blue complex amplitude transmittances of the input pattern; $t_r(x, y)$, $t_g(x, y)$, and $t_b(x, y)$ are the red, green, and blue sampling functions; and $\phi(x, y)$ represents the inherent phase variation of the liquid crystal that cannot be compensated by a liquid gate. The sampling functions are

$$t_r(x,y) = \sum_m \sum_n C_{mn}\exp\left[-i\left(\frac{mx}{d} + \frac{ny}{\ell}\right)\right],$$

$$t_g(x,y) = \sum_m \sum_n C_{mn}\exp\left\{-i\left[\frac{m(x-\Delta x)}{d} + \frac{ny}{\ell}\right]\right\}, \tag{2}$$

$$t_b(x,y) = \sum_m \sum_n C_{mn}\exp\left\{-i\left[\frac{m(x-2\Delta x)}{d} + \frac{ny}{\ell}\right]\right\},$$

where C_{mn} denotes Fourier coefficient; m and n are integers; d and ℓ are the periods of the grating in the x and y directions, respectively; and $\Delta x = 2\pi d/3$ is the width of a color pixel shown in Fig. 1(a).

If $\phi(x, y)$ is a slowly varying function compared with $s_r(x, y)$, $s_g(x, y)$, and $s_b(x, y)$, then $\phi(x,y)$ is approximately uniform and can be neglected in the analysis. The system is then a space-invariant processor. In fact, for the LCTV used, $\phi(x, y)$ cannot be approximated as unity, and the system suffers from space variance. For simplicity, Eq. (1) is rewritten as

$$s(x,y;\lambda) = \sum_{k=r,g,b} s_k'(x,y) t_k(x,y) , \tag{3}$$

where

$$s_k'(x,y) = s_k(x,y)\exp[i\phi(x,y)] . \tag{4}$$

Keep in mind that the electronic signal modulates both the amplitude and phase of the complex amplitude function $s_k(x, y)$ but does not alter the inherent phase function $\phi(x, y)$. Since the input plane is illuminated by collimated polychromatic coherent plane waves of red, green, and blue wavelengths, the complex light distributions at the back focal plane of the achromatic transform lens are

$$s(\alpha,\beta;\lambda) = \sum_{k=r,g,b} S_k'(\alpha,\beta) * T_k(\alpha,\beta) , \tag{5}$$

where * stands for the *convolution operation*, $S_k'(\alpha,\beta)$ is a Fourier transform of $s_k'(x,y)$, and the $T_k(\alpha,\beta)$ are

$$T_r(\alpha,\beta) = \sum_m \sum_n C_{mn}\delta\left(\alpha \pm \frac{f\lambda_r m}{2\pi d}, \beta \pm \frac{f\lambda_r n}{2\pi \ell}\right) ,$$

$$T_g(\alpha,\beta) = \sum_m \sum_n C_{mn}\delta\left(\alpha \pm \frac{f\lambda_g m}{2\pi d}, \beta \pm \frac{f\lambda_g n}{2\pi \ell}\right) \times \exp\left(-i\frac{m\Delta x}{d}\right), \tag{6}$$

$$T_b(\alpha,\beta) = \sum_m \sum_n C_{mn}\delta\left(\alpha \pm \frac{f\lambda_b m}{2\pi d}, \beta \pm \frac{f\lambda_b n}{2\pi \ell}\right) \times \exp\left(-i\frac{2m\Delta x}{d}\right),$$

where $\delta(\xi,\eta)$ is a Dirac delta function and f and λ are the achromatic focal length and wavelength, respectively.

If the color filter is constructed as shown in Fig. 3(a), color spectra are isolated spatially at the Fourier transform plane. Thus, multiple MSFs can be synthesized for all three wavelengths with a sufficiently expanded collimated polychromatic reference beam.

We now discuss the correlation due to a single wavelength, using as an example the red light. Since in the synthesis of MSFs the complex light field at the red section on the Fourier plane is

$$E_r(\alpha,\beta) = \exp\left(\frac{-i\theta\beta}{\lambda_r}\right) + S_r'(\alpha,\beta) * T_r(\alpha,\beta) ,$$

$$= \sum_m \sum_n \left[C_{mn} S_r'\left(\alpha \pm \frac{f\lambda_r m}{2\pi d}, \beta \pm \frac{f\lambda_r n}{2\pi \ell}\right) + \frac{1}{N}\exp\left(\frac{-i\theta\beta}{\lambda_r}\right)\right], \tag{7}$$

where N is the number of spectra ($N \equiv \max\{mn\}$) and θ is a small reference angle. The recorded complex MSFs then can be written as

$$H_r(\alpha,\beta) = \left|E_r(\alpha,\beta)\right|^2$$

$$= \sum_m \sum_n \left\{ \left[\left| C_{mn} S_r'\left(\alpha \pm \frac{f\lambda_r m}{2\pi d}, \beta \pm \frac{f\lambda_r n}{2\pi \ell}\right)\right|^2 + \left|\frac{1}{N}\right|^2 \right] + \frac{C_{mn}}{N} S_r'\left(\alpha \pm \frac{f\lambda_r m}{2\pi d}, \beta \pm \frac{f\lambda_r n}{2\pi \ell}\right)\exp\left(\frac{i\theta\beta}{\lambda_r}\right) + \frac{C_{mn}}{N} S_r'^*\left(\alpha \pm \frac{f\lambda_r m}{2\pi d}, \beta \pm \frac{f\lambda_r n}{2\pi \ell}\right)\exp\left(\frac{-i\theta\beta}{\lambda_r}\right)\right\} , \tag{8}$$

where the superscript * denotes the complex conjugate. For simplicity, we have ignored the proportional constant. If these complex MSFs are inserted in the Fourier transform *plane and illuminated* by the object beam, the field immediately behind the MSFs is

$$U_r(\alpha,\beta) = \left[\sum_m \sum_n C_{mn} S_r'\left(\alpha \pm \frac{f\lambda_r m}{2\pi d}, \beta \pm \frac{f\lambda_r n}{2\pi \ell}\right)\right] H_r(\alpha,\beta) . \tag{9}$$

The field at the output plane is the inverse Fourier transform of Eq. (9), which consists of zero-order, convolution, and correlation terms corresponding to the first, second, and third terms of Eq. (8). Since we are interested only in correlation output, we ignore the first and second terms. Therefore, the red correlation output can be expressed as

$$g_r(x,y) = FT^{-1}\left\{ \sum_m \sum_n C_{mn} S_r'\left(\alpha \pm \frac{f\lambda_r m}{2\pi d}, \beta \pm \frac{f\lambda_r n}{2\pi \ell}\right) \times \sum_m \sum_n \frac{C_{mn}}{N} S_r'^*\left(\alpha \pm \frac{f\lambda_r m}{2\pi d}, \beta \pm \frac{f\lambda_r n}{2\pi \ell}\right) \times \exp\left(\frac{-i\theta\beta}{\lambda_r}\right)\right\} , \tag{10}$$

where $FT^{-1}\{\ \}$ represents inverse Fourier transformation. Since $S_r'[\alpha \pm (f\lambda_r m/2\pi d), \beta \pm (f\lambda_r n/2\pi \ell)]$ are not overlapped for different (m, n), Eq. (10) becomes

$$g_r(x,y) = \sum_m \sum_n \left[|C_{mn}|^2 FT^{-1}\left\{ S_r'\left(\alpha \pm \frac{f\lambda_r m}{2\pi d}, \beta \pm \frac{f\lambda_r n}{2\pi \ell}\right) \times S_r'^*\left(\alpha \pm \frac{f\lambda_r m}{2\pi d}, \beta \pm \frac{f\lambda_r n}{2\pi \ell}\right)\frac{\exp(-i\theta\beta/\lambda_r)}{N}\right\}\right] . \tag{11}$$

By taking the inverse Fourier transform, we have

$$g_r(x,y) = \sum_m \sum_n C_{mn} s_r(x,y) \exp\left[-i\left(\frac{mx}{d} + \frac{ny}{\ell}\right)\right] \otimes \frac{C_{mn}}{N} s_r^*(x,y-\theta f)\exp\left\{i\left[\frac{mx}{d} + \frac{n}{\ell}(y-\theta f)\right]\right\}, \quad (12)$$

where $\otimes$ denotes correlation. From this equation, we see that the red correlation signal of the sampled input is diffracted in the neighborhood of $(0,\theta f)$ at the output plane of the polychromatic coherent processor. It is not difficult to see that green and blue correlation signals are also diffracted in the neighborhood of $(0,\theta f)$. In other words, the color correlation signals are superimposed to form the actual color of the input.

We now discuss the correlation output for the single matched filtering and multiple matched filtering techniques. For simplicity, the $t_k(x,y)$, where $k = r,g,b$, are assumed to be normalized comb functions. In reference to Eq. (2), C_{mn} denotes the Fourier coefficient of the sampling functions; thus, it can be approximated as unity ($C_{mn} \approx 1$) in the following analysis.

4.1. Single matched filtering

If only one order of the spectra of each color is used for matched filtering—for example, we may choose $(-1,0)$ order for red, $(0,1)$ order for green, and $(1,0)$ order for blue—then the polychromatic correlation signal would be

$$|g(x,y)|^2 = \frac{1}{N^2} \sum_{k=r,g,b} |s_k(x,y) \otimes s_k^*(x,y-\theta f)|^2, \quad (13)$$

where $C_{-1,0} = C_{0,1} = C_{1,0} = 1$ and where the unimportant phase factor has been neglected. Therefore, a perfect correlation between two unsampled color patterns can be obtained. The correlation peak height is

$$(PH)_s = \frac{1}{N^2} \max\left\{ \sum_{k=r,g,b} |s_k(x,y) \otimes s_k^*(x,y-\theta f)|^2 \right\}, \quad (14)$$

where max { } denotes the operation of taking a maximum.

4.2. Multiple matched filtering

The pixel structure of the LCTV diffracts light energy into many orders, as shown in Fig. 2. That makes the single matched filtering correlation signal expressed in Eq. (13) difficult to detect in practice. A multiple matched filtering method to overcome this difficulty was proposed conceptually in Sec. 3. The red correlation is expressed in Eq. (12) and can be further written as

$$g_r(x,y) = \frac{1}{N}\left[s_r(x,y) \otimes s_r^*(x,y-\theta f)\right] \times \sum_m \sum_n |C_{mn}|^2 \exp\left\{-i\left[\frac{mx}{d} + \frac{n}{\ell}(y+\theta f)\right]\right\}. \quad (15)$$

Assuming that all diffracted spectra are used and that $|C_{mn}|^2 \approx C_{mn} \approx 1$, Eq. (15) can be interpreted as an approximation of the sampled correlation coutput when compared with Eq. (2). This equation also shows that the final correlation signal $g_r(x, y)$ is a coherent superposition from all of the individual MSFs. Each MSF contributes an individual correlation signal common in amplitude but different in phase. Therefore, the final correlation signal would have an envelope function,

$$\left[s_r(x,y) \otimes s_r^*(x,y-\theta f)\right], \quad (16)$$

covering subpeaks resulting from the constructive interference among contributions from different MSFs. The constructive interference occurs when

$$\sum_m \sum_n |C_{mn}|^2 \exp\left\{-i\left[\frac{mx}{d} + \frac{n}{\ell}(y+\theta f)\right]\right\}$$

in Eq. (15) is equal to N. The main correlation peak height of the multiple matched filtering can be expressed as

$$(PH)_M = \max\left\{ \sum_{k=r,g,b} |s_k(x,y) \otimes s_k^*(x,y-\theta f)|^2 \right\}. \quad (17)$$

Substitution of Eq. (14) into Eq. (17) yields

$$(PH)_M = N^2 (PH)_S, \quad (18)$$

where $(PH)_M$ and $(PH)_S$ are the correlation peak heights of multiple and single matched filterings, respectively. The important features of the multiple matched filtering method are (1) the main correlation peak height is increased; (2) the width of the envelope is the same as for the single matched filtering correlation signal; and (3) subpeaks are created, which probably raise false alarms. Although subpeaks are covered by the envelope function in expression (16), they are separated, as illustrated schematically in Fig. 4. An example of experimental observation is also shown in Fig. 9(a). A proper electronic postprocessing system can be introduced to eliminate false alarms. An image digitizer can be applied to detect the correlation signal, where a threshold is set to hard clip the signal and to select only one main correlation peak for a correlated pattern.

5. EXPERIMENTS

Experiments were conducted using the optical setup shown schematically in Fig. 6. A disassembled color LCTV (Radio Shack catalog No. 16-154) was applied as a real-time input screen. To eliminate the variation introduced by the surfaces of the cover glasses,the LCTV was immersed in a liquid gate filled with mineral oil. The poor-quality plastic polarizers on the LCTV were replaced by two higher-quality polarizers in front of and behind the liquid gate. HeNe laser generated red coherent light was combined with Ar laser generated green coherent light by a beam splitter as the polychromatic coherent light source.

The LCTV is equipped with a video input jack, which allows an image to be written electronically with a microcomputer or optically with a TV camera. An Apple IIE microcomputer was used to write a color input pattern with the low-resolution mode. Figures 7(a) and 7(b) show black-and-white pictures of a color pattern generated on a TV monitor and on the LCTV, respectively, where a red letter P was superimposed on a green letter S and the overlapping areas were yellow to simulate a multicolored object. The multiple MSFs were synthesized using the setup shown in Fig. 6. The Fourier transform plane was covered with color filters arranged as shown in Fig. 3(c), i.e., the green MSFs were in the upper

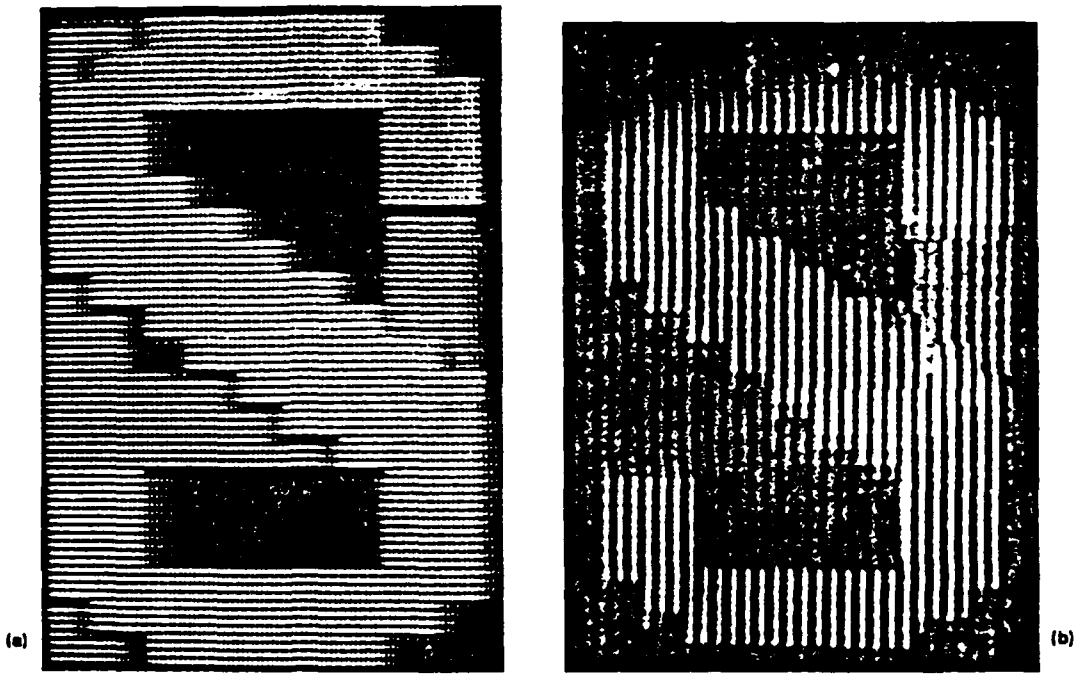

Fig. 7. Black-and-white pictures of color pattern generated on (a) TV monitor and (b) LCTV display. (A red letter P was superimposed on a green letter S, with yellow overlapping areas to simulate a color object.)

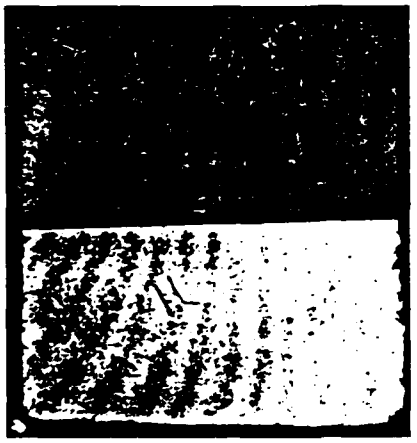

Fig. 8. Synthesized MSFs of the object in Fig. 7(b). Upper part was used for green light and lower part for red light. (There were actually 10 spectra in the vertical line and 20 spectra in the horizontal line for each section. Distance between two adjacent spectra in the red section is about 0.7 mm.)

part and the red MSFs were in the lower part. To achieve the optimum performance of the MSFs, the red and green portions of the filters were exposed under different exposures due to the spectral characteristics of the photographic plate. However, the exposed MSFs were developed in a single process. Figure 8 is a photograph of the synthesized MSFs of the color pattern shown in Fig. 7(b).

To verify the proposed method, two experimental results are demonstrated. Figure 9 shows the results using a single laser to illustrate the method of multiple matched filtering. Figure 10 shows the result using two lasers to illustrate bichromatic correlation. First, using a HeNe laser, a red letter P was used as an input to correlate with the MSFs shown in Fig. 8. Successively, a red letter S and a dark screen were tested. The experimental results are presented in Fig. 9. Figures 9(a), 9(b), and 9(c) are the correlations obtained without hard clipping when the tested input was a red P, a red S, and a dark screen. Figures 9(d), 9(e) and 9(f) are the correlation peaks after a photographically hard-clipping process. The autocorrelation of the color pattern shown in Fig. 7(b) is presented in Fig. 10. In this figure, a black-and-white picture of the yellow color correlation signal (i.e., the superposition of red and green) is presented. Similarly, a hard-clipping technique could also be used to obtain a cleaner correlation peak.

6. DISCUSSION AND CONCLUSION

A color LCTV is suitable for polychromatic coherent processing since the display panel is composed of three primary color pixels. We have shown that a color LCTV can be used for color pattern recognition. The grid structure of the display panel together with a specially designed color filter provides spatially isolated polychromatic spectra to enable polychromatic signal detection.

A serious drawback of the color LCTV is the lack of space invariance, even after it has been immersed in a liquid gate. This drawback may be partially due to the inherent color filter in the liquid crystal display and the phase modulation by liquid crystal molecules. A quantitative investigation of space variance of the LCTV, especially the color LCTV, is currently under intensive study and will be reported in the near future.

We have proposed a multiple matched filtering technique to improve the correlation signal. However, in practice the diffraction efficiencies vary for different MSFs, and thus Eq. (18) is not valid. The Horner efficiency in a multiple matched filtering correlated output was observed to be approximately $30\ (\approx N)$ times higher than the single matched filtering correlation using a color LCTV. With the aid of a hard-clipping

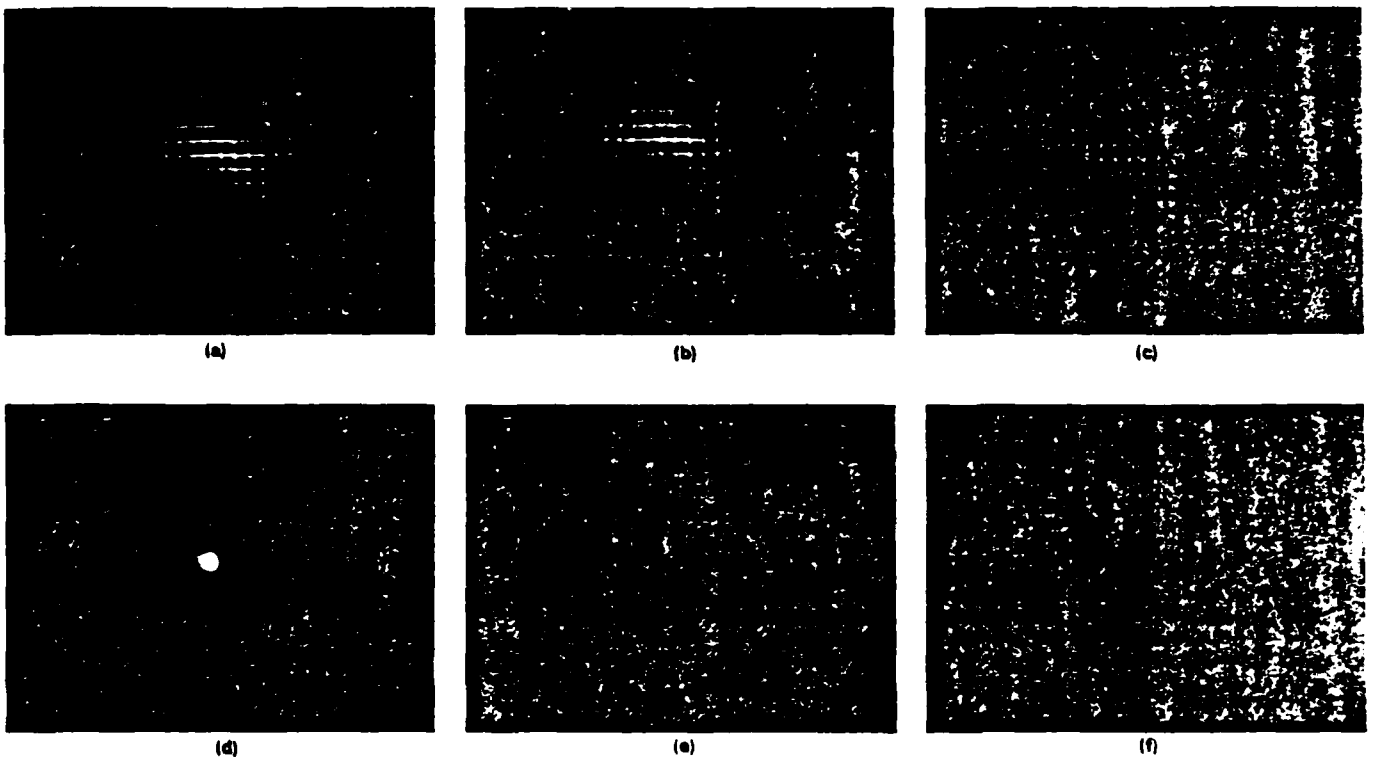

Fig. 9. Correlations without hard clipping of (a) red letter P and red letter P, (b) red letter P and red letter S, and (c) red letter P and dark screen [distance between two adjacent points in (a), (b), and (c) is about 340 μm]. (d) Enlarged hard-clipping result of (a); (e) hard-clipping result of (b); and (f) hard-clipping result of (c).

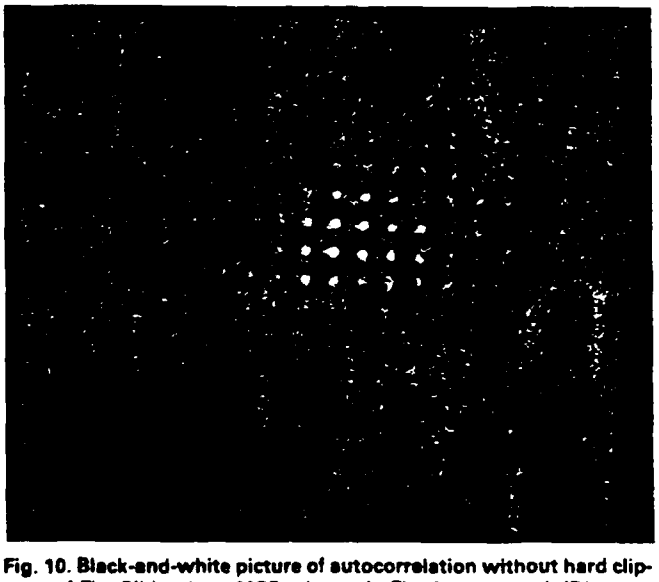

Fig. 10. Black-and-white picture of autocorrelation without hard clipping of Fig. 7(b), where MSFs shown in Fig. 8 were used. (Distance between two adjacent points is about 340 μm.)

technique, the multiple matched filtering correlated output presents a higher signal-to-noise ratio while the false alarm is simultaneously depressed. We also have demonstrated polychromatic signal detection using the color LCTV. By implementing a hard-clipping postprocessing system, a fully real-time color pattern recognition system can be constructed.

We would like to stress that the color LCTV is a low-cost spatial light modulator capable of processing polychromatic signals. With further improvements the color LCTV should be useful for color-sensitive robotic vision and other automatic color pattern recognition as applied to real-time reconnaissance, guidance, and surveillance.

7. ACKNOWLEDGMENT

We acknowledge the support of the U.S. Air Force Office of Scientific Research under grant No. AFOSR-86-0264.

8. REFERENCES

1. J. A. McEwan, A. D. Fisher, P. D. Rolsma, and J. N. Lee, "Optical-processing characteristics of a low-cost liquid crystal display device," J. Opt. Soc. Am. A2(13), 8 (1985).
2. H. K. Liu, J. A. Davis, and R. A. Lilly, "Optical-data-processing properties of a liquid-crystal television spatial light modulator," Opt. Lett. 10, 635 (1985).
3. D. A. Gregory, "Real-time pattern recognition using a modified liquid crystal television in a coherent optical correlator," Appl. Opt. 25, 467 (1986).
4. M. Young, "Low-cost LCD video display for optical processing," Appl. Opt. 25, 1024 (1986).
5. A. M. Tai, "Low-cost LCD spatial light modulator with high optical quality," Appl. Opt. 25, 1380 (1986).
6. D. Casasent and S. F. Xia, "Phase correction of light modulators," Opt. Lett. 11, 398 (1986).
7. F. T. S. Yu, S. Jutamulia, and X. L. Huang, "Experimental application of low-cost liquid crystal TV to white-light optical signal processing," Appl. Opt. 25, 3324 (1986).
8. S. K. Case, "Pattern recognition with wavelength-multiplexed filters," Appl. Opt. 18, 1890 (1979).
9. Y. Ishii and K. Murata, "Color-coded character-recognition experiment with wavelength-triplexed, reflection-type holographic filters," Opt. Lett. 7, 230 (1982).
10. N. K. Shi, "Color-sensitive spatial filters," Opt. Lett. 3, 85 (1978).
11. B. Braunecker and O. Bryngdahl, "Multiplex optical processing—combination of polychromatic light and a dispersive element," Opt. Commun. 40, 332 (1982).
12. F. T. S. Yu and T. H. Chao, "Color signal correlation detection by matched spatial filtering," Appl. Phys. B:32, 1 (1983).

13. F. T. S. Yu and B. Javidi, "Experiments on real-time polychromatic signal detection by matched spatial filtering," Opt. Commun. 56, 384 (1986).
14. F. T. S Yu and X. Lu, "Large-capacity real-time spatial-spectral scanning optical correlator," Appl. Opt. 25, 812 (1986).
15. H. J. Caulfield, "Role of the Homer efficiency in the optimization of spatial filters for optical pattern recognition," Appl. Opt. 21, 4391 (1982).
16. See, for example, H. Bartelt and A. W. Lohmann, "Polar tomography," Opt. Commun. 57, 380 (1986).

Francis T. S. Yu received his BSEE degree from Mapua Institute of Technology, Manila, Philippines, and his MS and Ph.D. degrees in electrical engineering from the University of Michigan. From 1958 to 1965 he was a teaching fellow, instructor, and lecturer in the Electrical Engineering Department and a research associate with the Communication Sciences Laboratory at the University of Michigan. From 1966 to 1980 he was on the faculty of the Electrical and Computer Engineering Department at Wayne State University. He was a visiting professor in electrical and computer engineering at the University of Michigan during 1978-1979. Dr. Yu is now a professor in the Electrical Engineering Department at The Pennsylvania State University. He has been a consultant to several industrial and government laboratories. He is an active researcher in the fields of optical signal processing, holography, optics, and information theory and has published numerous technical papers in these areas. He was a recipient of the 1983 Faculty Scholar Medal for Outstanding Achievement in Physical Sciences and Engineering and the 1984 Outstanding Researcher in College of Engineering at Penn State and was named Evan Pugh Professor of Electrical Engineering there in 1985. He is the author of *Introduction to Diffraction, Information Processing and Holography; Optics and Information Theory; Optical Information Processing;* and *White-Light Optical Processing*. Dr. Yu is a Fellow of OSA, SPIE, and IEEE.

Suganda Jutamulia was born in Indonesia in 1954. He received his BS degree in physics from Institut Teknologi Bandung in 1977 and his MS degree in optoelectronics from Universitas Indonesia in 1980. He received the Ph.D. degree in electronic engineering from the Hokkaido University, Japan, in 1985. His current research interests are information processing, holography, pattern recognition, and optical computing. Dr. Jutamulia has more than 25 technical publications. He is currently conducting postdoctoral research at The Pennsylvania State University. He is a member of OSA, SPIE, and the Japan Society of Applied Physics.

Tsongneng W. Lin was born in Taiwan in 1954. He received the BS degree from the National College of Education, Taiwan, in 1976 and the MS degree in physics from the University of Southern Mississippi in 1981. He will receive the Ph.D. degree in electrical engineering from The Pennsylvania State University this year. Lin is presently an assistant professor in the Department of General Engineering at The Pennsylvania State University, DuBois Campus. His research interests include information processing, holography, pattern recognition, and image processing. He is a member of OSA and SPIE.

SECTION 5

Implementation of Symbolic Substitution

Reprinted from Applied Optics, Vol. 26, page 2293, June 15, 1987
Copyright © 1987 by the Optical Society of America and reprinted by permission of the copyright owner.

Implementation of symbolic substitution logic using optical associative memories

Francis T. S. Yu and Suganda Jutamulia

Pennsylvania State University, Electrical Engineering Department, University Park, Pennsylvania 16802.
Received 24 December 1986.
0003-6935/87/122293-02$02.00/0.
© 1987 Optical Society of America.

Symbolic substitution was first proposed by Huang[1] as a means of utilizing the parallelism of optics to perform digital computing. In this method, specific logic patterns are substituted into new logic patterns in parallel according to a given transformation rule. The operation and possible implementation of the symbolic substitution are recently reported by Brenner *et al.*[2] and Brenner.[3] It has been demonstrated that symbolic substitution can be applied to Boolean logic, binary arithmetic, Turing machine, artificial intelligence, etc.[1,2]

Unlike the Boolean logic, symbolic substitution recognizes not only a combination of bits but also the relative location of these bits. The output is not just a single bit but rather a combination of bits positioned in a particular manner. The schematic diagram of symbolic substitution is depicted in Fig. 1(a). The transformation of specific logic pattern in the process of symbolic substitution is carried out by a series of operations: split–shift–combine–NOR–mask–split–shift–combine–mask.

Symbolic sutstitution is essentially a combination of recognition and substitution phase. In addition, although symbolic substitution is not restricted to space invariant operations, it is indeed based on the space invariant connectivity of optics. Therefore, a method of optical associative memories[4] may be alternatively applied to implement a symbolic substitution logic system. In the method of optical associative memories, logical 1 and logical 0 are encoded in certain spatial patterns instead of bright and dark[2] or polarization direction.[3] For example, the logic patterns shown in Fig. 1(a) may be encoded into the patterns shown in Fig. 1(b), where logical 1 and logical 0 are encoded into a cross and a ring, respectively. This has the advantage of distinguishing logical 0 and a void space having no information.

A method is first proposed using a matched spatial filter (MSF) to recognize input patterns. The autocorrelation spots (assumed to be delta functions) are convoluted with a desired output pattern so that each correlated input pattern produces an output pattern. The proposed optical setup is schematically depicted in Fig. 2. The MSF1 and MSF2 are Fourier transform holograms of input and output patterns, respectively. The drawback of this method may be the low diffraction efficiency, although a phase-only hologram may be used. In general, cross-correlation noise appears. To depress the output pattern come from cross-correlation,

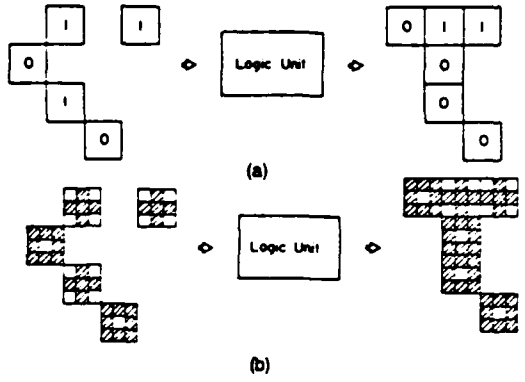

Fig. 1. Schematic diagram of symbolic substitution: (a) An input logic pattern is substituted into another logic pattern. (b) Logical 1 and logical 0 are encoded into a cross and ring, respectively.

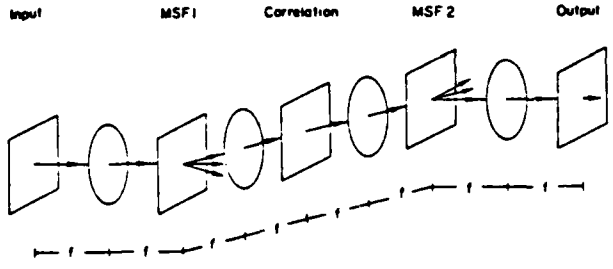

Fig. 2. Optical setup using two matched spatial filters to implement symbolic substitution logic.

however, a thresholding process may be applied at the correlation or output plane.

The second proposed method is making use of a specially designed computer-generated hologram (CGH). By using a computer-generated hologram, an input image is converted into another associative image. If the input pattern is denoted by a function $i(x,y)$, and the associative output pattern is $o(x,y)$, the mathematical relation can be expressed as

$$I(u,v)P(u,v) = O(u,v), \tag{1}$$

where $P(u,v)$ stands for the filter function, $I(u,v)$ and $O(u,v)$ are Fourier transforms of $i(x,y)$ and $o(x,y)$, respectively.

A carrier frequency may be added to encode the complex value of $P(u,v)$ and give diffracted output. This technique is possible to implement optically. A more sophisticated two-way code translation has been demonstrated by Lohmann and Thum.[5] In two-way code translation, a holographic

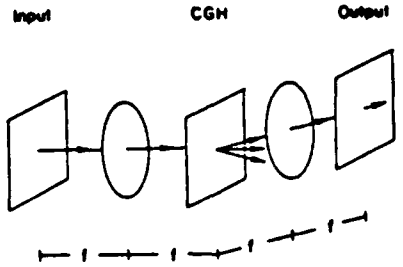

Fig. 3. Optical setup using computer-generated holographic associative memories to implement symbolic substitution logic.

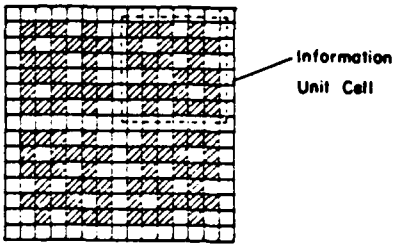

Fig. 4 Example of information unit cell with 4 bits.

filter converts one specific image into a second associative image, and it can also convert the second image into the first image. Mathematically, the filter function must satisfy simultaneously Eq. (1) and the following Eq. (2):

$$O(u,v)P^*(u,v) = I(u,v). \tag{2}$$

For the implementation of symbolic substitution, only a *filter function satisfying* Eq. (1) is required. Thus it is easier to realize rather than that of Lohmann and Thum.[5] In the computation of filter function $P(u,v)$, an approximation might be taken, because there will be no analytic solution for $P(u',v')$ when $I(u',v')$ is zero but $O(u',v')$ is not zero. To avoid this difficulty, an alternative method of optically made associative hologram[4] may be applied. The proposed optical setup of this second method is schematically depicted in Fig. 3. In the above described methods, each information unit cell must have a boundary to distinguish from neighboring cells as illustrated in Fig. 4.

On the basis of the configuration shown in Fig. 3, the use of a muliplexed hologram can realize the operation of multiple instruction multiple data (MIMD), which has been a major problem in optical computing. In reference to the recent analysis of Hong and Psaltis,[6] to obtain a recognizable output pattern (SNR $\geq$ 1), the storage capacity of a multiplexed holographic associative memory is limited by

$$M \leq (\mathrm{SBP})_H/(\mathrm{SBP})_P, \tag{3}$$

where M is the number of associations, $(\mathrm{SBP})_H$ and $(\mathrm{SBP})_P$ are the SBP of the hologram and an information unit, respectively. For a numerical example, if an information unit is encoded in thirty-six pixels as shown in Fig. 4 and a computer-controlled photoprinter with a moderate resolution of 10 $\times$ 10 μm is used to print the SGH, an area of 1 $\times$ 1 cm of the CGH can store 277 associative memories.

In conclusion, the merits of the proposed implementation are that it can (1) handle very large SBP data, (2) perform any substitution in one simple step, and (3) perform MIMD operation using a multiplexed hologram. The price is the use of more than 1 pixel (e.g., 9 pixels) to encode a bit. A thresholding process may be required before the data are transferred to the next operation.

We acknowledge the support of the U.S. Air Force Office of Scientific Research grant AFOSR-86-0264.

References

1. A. Huang, "Parallel Algorithms for Optical Digital Computers," in *Technical Digest, Tenth International Optical Computing Conference* (1983), pp. 13–17.
2. K.-H. Brenner, A. Huang, and N. Streibl, "Digital Optical Computing with Symbolic Substitution," Appl. Opt. 25, 3054 (1986).
3. K.-H. Brenner, "New Implementation of Symbolic Substitution Logic," Appl. Opt. 25, 3061 (1986).
4. D. Gabor, "Associative Holographic Memories," IBM J. Res. Dev. 13, 156 (1969).
5. A. W. Lohmann and C. Thum, "Two-Way Code Translation by Computer-Generated Holographic Filters," Opt. Commun. 46, 74 (1983).
6. J. Hong and D. Psaltis, "Storage Capacity of Holographic Associative Memories," Opt. Lett. 11, 812 (1986).

Experimental Application of One-Step Holographic Associative Memories to Symbolic Substitution

Francis T. S. Yu, Fellow SPIE

Chenhua Zhang

Suganda Jutamulia, Member SPIE

Electrical Engineering Department

The Pennsylvania State University

University Park, Pennsylvania 16802

Abstract

An experimental procedure using one-step holographic associative memories to implement symbolic substitution is described. The linearity of multiple holographic filtering is abolished in practice. Experimental results of parallel half-addition are presented. It is seen that parallel half-addition is an example of multiple-instruction-multiple-data (MIMD) operation.

Subject terms: optical computing, symbolic substitution, associative memories, multiple-instruction-multiple-data

I. Introduction

Recently, we proposed two methods to optically implement symbolic substitution logic using holographic associative memories [1]. Symbolic substitution was originally proposed by Huang [2] as a means of utilizing the paralellism of optics to perform digital computing. Some possible implementations of symbolic substitution have been demonstrated by Brenner et al. [3], Brenner [4], Tsao et al. [5], and Casasent and Botha [6]. In our recent Letter [1], we proposed the implementation of symbolic substitution based on: (1) two step Vander Lugt filter, which is also applied by Paek and Psaltis [7], and pointed out by Casasent and Botha [6], and (2) one step holographic associative memories [8], which is also described in Ref. [7]. In this paper, we shall demonstrate the experimental verification of symbolic substitution using only one step holographic associative memories.

II. Background

Unlike the Boolean logic, symbolic substitution recognizes not only a combination of bits but also the relative location of these bits [2]. The output is not just a single bit but rather a combination of bits positioned in a particular manner. The schematic diagram of symbolic substitution logic is depicted in Fig. 1(a). Symbolic substitution is essentially a combination of recognition and substitution phase. Therefore, optical associative memories may be applied to construct a symbolic substitution logic system. In this system logical 1 and logical 0 are encoded in certain spatial patterns. For example, the logic patterns shown in Fig. 1(a) may be encoded into the patterns shown in Fig. 1(b). This has the advantage of distinguishing logical 0 and a void space having no information.

The basic experimental setup is depicted in Fig. 2. A joint Fourier transform hologram of an input and an output pattern is first recorded as shown in Fig. 2(a). The output pattern will be generated optically by illuminating the hologram with the input pattern in the same optical setup as shown in Fig. 2(b). To perform a Boolean operation, for instance, AND function, four associative memories are required, which correspond to four possible combinations of two inputs. This technique differs from the truth-table look-up optical processor [9,10] which basically applies interferometric subtraction technique.

III. BCB's Contradiction of Linearity

Botha, Casasent, and Barnard (BCB) pointed out that a contradiction would be present if a linear holographic filter was used to perform nonlinear logic operations [11]. To show this, the symbolic substitution for the AND function is considered. Denoting the four possible inputs as $I_1(0,0)$, $I_2(0,1)$, $I_3(1,0)$, and $I_4(1,1)$, the four AND outputs are $0_1 = 0_2 = 0_3 = 0$ and $0_4 = 1$. In symbolic substitution, specific spatial patterns are used to represent each argument in the inputs I_1 to I_4 and in the output. Considering the holographic filtering as a linear system, it is seen that

$$I_4 = I_2 + I_3 - I_1 \quad , \tag{1}$$

and the corresponding output must be

$$0_2 + 0_3 - 0_1 = 0 \quad , \tag{2}$$

which is contradictory to the logic output

$$0_4 = 1 \quad . \tag{3}$$

To overcome this problem, the linearity of the multiple holographic

filtering must be abolished. We actually conducted the experiment in the same spirit as that of Refs [6], [7] and [10], or the first method described in our previous Letter [1], that is a process of independent multi-channel correlations. In reality, a multi-holographic filtering is not an ideal linear system. In the example discussed above, four independent holographic associative memories are required, i.e., holographic filters to associate outputs 0_1, 0_2, 0_3, and 0_4 with inputs I_1, I_2, I_3, and I_4, respectively. Using a nonlinear thresholding device in the output plane and varying each filter bandwidth in the hologram synthesis, it can be expected that

$$0_2 + 0_3 - 0_1 \neq 0 \quad , \tag{4}$$

while individual outputs may still be approximated as .

$$0_1 \simeq 0$$

$$0_2 \simeq 0$$

$$0_3 \simeq 0$$

$$0_4 \simeq 1 \quad . \tag{5}$$

Note that 0 and 1 represent specific spatial patterns rather than numbers. We will be back to this discussion in the next section.

IV. Experiments

We used photographic film as input transparency in the experiment. Nine pixels were required to encode one bit as depicted in Fig. 1(b). The patterns representing 1 and 0 cannot be orthogonal, since the orthogonality will eliminate the association of two patterns. In other words, the two patterns must have overlapping spectra in the Fourier plane

in order to obtain good holographic image. We have implemented a half-adder, in which sum (XOR function) and carry (AND function) were performed simultaneously from the same data. This is an example of the realization of multiple-instruction-multiple-data (MIMD) architecture utilizing the parallelism of optics. Four combinations of input and the corresponding output combinations of sum and carry are illustrated in Fig. 3. To implement four associative memories in a single hologram, the spatial modulation technique [12] was applied. An additional cross Ronchi grating was superimposed with the input pattern to give multiple carrier frequencies as shown schematically in Fig. 4(a).

In the synthesis of holographic filters, a mask was employed in the Fourier plane such that each input combination occupies only one quadrant of the Fourier plane as depicted in Fig. 4(b). This multiple spectra configuration would enhance the dynamic range of holographic filter as pointed out elsewhere [13]. It is more important to notice that this multiple spectra configuration approaches the conditions expressed in Eqs. (4) and (5), since it is very common to obtain slightly different bandwidth for different associative memories. In the final stage, a video monitor system was applied in the system to detect and threshold the hologram-generated output.

A set of experimental result is illustrated in Fig. 5. The direct associations shown in Fig. 5 were obtained using only one uncovered quadrant of the hologram for each association. To perform parallel half-addition, the whole hologram was uncovered. An example of parallel half-addition, i.e., sum and carry are obtained in parallel, is demonstrated in Fig. 6. This picture was also taken from the video monitor after thresholding. Although cross correlation still exists, the dominant output is the correct logic pattern. It is seen that the BCB's contradiction of linearity may be overcome in practice. For comparison, Fig. 7 shows the output when four input

combinations are associated with only one memory (only one quadrant of the hologram). The input associated with the filter produced the dominant output pattern.

The absence of the BCB's contradiction of linearity can be explained in the following discussion. In the case that the input is I_4, a quarter of the input energy (assume 1/4 E) will be incident on the quadrant associated with I_4. The output O_4 will have a total intensity of $1/4\alpha$ E, where α is the energy diffraction efficiency of the hologram. A quarter of the input energy (1/4 E) will also be incident on the quadrant associated with I_2. Since $I_4 = I_2 + I_3 - I_1$, the output from this quadrant is O_2 plus the noise come from the crosstalks between I_3 and I_2, and I_1 and I_2. This leads to the fact that the output pattern O_2 will have a total intensity lower than $1/4\alpha$ E. The other two quadrants follow the same analysis. We may conclude that the output pattern $O_2 + O_3 - O_1$ generated from three quadrants always have lower intensity than that of the output pattern O_4 directly generated from the quadrant associated with I_4. Thus a thresholding process can be applied to hardclip the total output pattern and result in a clean pattern O_4.

V. Conclusion

We have demonstrated an experimental procedure to implement symbolic substitution logic using one step holographic associative memories. To alleviate the BCB's contradiction in practice, a spatial modulation technique was applied. The spatial modulation technique also gives more flexibility in the filter synthesis compared with the multiplexing technique, since the hologram has a limited dynamic range. An example of MIMD operation, i.e., parallel half-addition has been shown. Utilizing real-time spatial light modulators such as LCLV, LCTV, MOSLM, etc, a full-addition may be realized

by multi-step substitution [2]. If the cross correlation can be totally eliminated, the proposed one step technique may be superior to the pinhole sampling technique [7], since the one step holographic technique is fully space invariant.

VI. Acknowledgement

We acknowledge the support by U.S. Air Force Office of Scientific Research grant AFOSR-86-0264.

VII. References

1. F.T.S.Yu and S.Jutamulia, "Implementation of Symbolic Substitution Logic Using Optical Associative Memories," Appl. Opt. 26, 2293 (1987).

2. A.Huang, "Parallel Algorithms for Optical Digital Computers," in Tech. Digest, Tenth International Optical Conference (1983), pp. 13-17.

3. K.-H.Brenner, A.Huang, and N.Streibl, "Digital Optical Computing with Symbolic Substitution," Appl. Opt. 25, 3054 (1986).

4. K.-H.Brenner, "New Implementation of Symbolic Substitution Logic," Appl. Opt. 25, 3061 (1986).

5. M.T.Tsao, L.Wang, R.Jin, R.W.Sprague, G.Gigioli, H.-M.Kulcke, Y.D.Li, H.M.Chou, H.M.Gibbs, and N.Peyghambarian, "Symbolic Substituion Using ZnS Interference Filters," Opt. Eng. 26, 41 (1987).

6. D.Casasent and E.Botha, "Correlator-Based Optical Architecture for Symbolic Substitution," Opt. Commun. To be published.

7. E.G.Paek and D.Psaltis, "Optical Associative Memory Using Fourier Transform Holograms," Opt. Eng. 26, 428 (1987).

8. D.Gabor, "Associative Holographic Memories," IBM J. Res. Dev. 13, 156 (1969).

9. C.C.Guest and T.K.Gaylord, "Truth-Table Look-Up Optical Processing Utilizing Binary and Residue Arithmetic," Appl. Opt. 19, 1201 (1980).

10. C.C.Guest, M.M.Mirsalehi, and T.K.Gaylord, "EXCLUSIVE OR Processing (Binary Image Subtraction) Using Thick Fourier Holograms," Appl. Opt. 23, 3444 (1984).

11. E.Botha, D.Casasent, and E.Barnard, "Optical Symbolic Substitution Using Multi-Channel Correlators," Appl. Opt. To be published.

12. Chenhua Zhang, "Some Applications of Spatial Modulation to Optical Information Processing," Acta Optica Sinica, 2, 406 (1982).

13. F.T.S.Yu, S.Jutamulia, and T.W.Lin, "Real-time Polychromatic Signal Detection Using a Color Liquid Crystal Television," Opt. Eng. 26, 453 (1987).

Figure Captions

Fig. 1. (a) Schematic diagram of symbolic substitution logic.
(b) Logical 1 and logical 0 are encoded into certain spatial patterns.

Fig. 2. (a) Recording of joint Fourier transform hologram of an input and an output pattern. (b) Reconstruction of output from an associated input pattern. Input pattern is also observed in the output plane due to the dc term of hologram.

Fig. 3. Combinations of inputs and the resulted carry and sum.

Fig. 4. (a) Input pattern is superimposed with cross Ronchi grating in spatial modulation technique. (b) Hologram indicates that multiple spectra occupy four quadrants of Fourier plane.

Fig. 5. Experimental results showing direct associations.

Fig. 6. Experimental result of 1+1 half-addition.

Fig. 7. Experimental result showing the associations between four inputs with a filter of 0+0. Only one dominant output pattern was observed as it was expected (carry=0, sum=0).

Fig 1 (a)

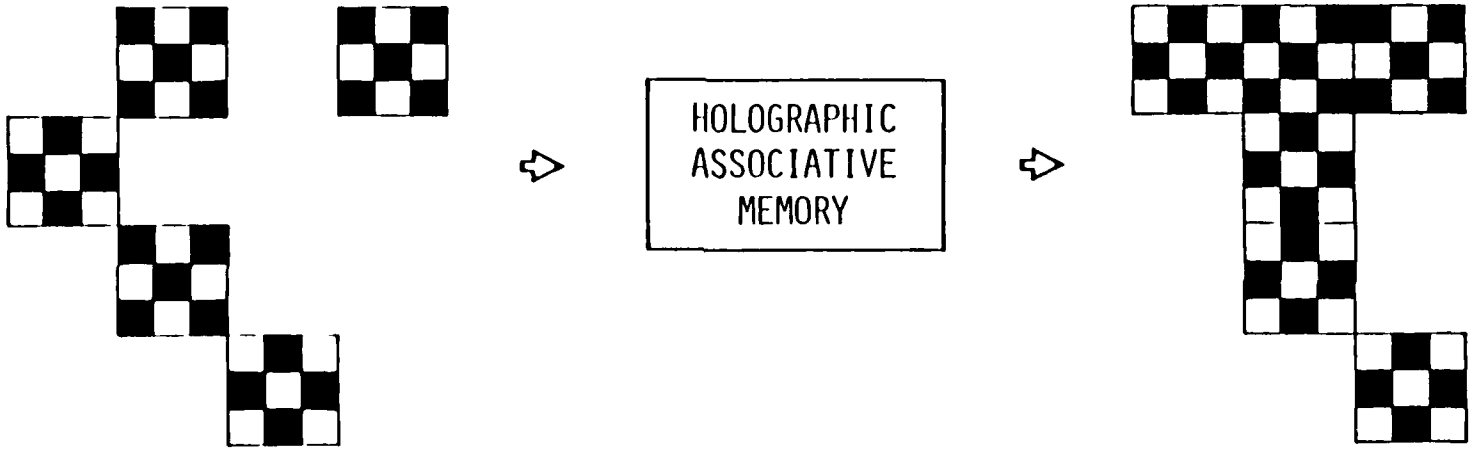

Fig 1. (b)

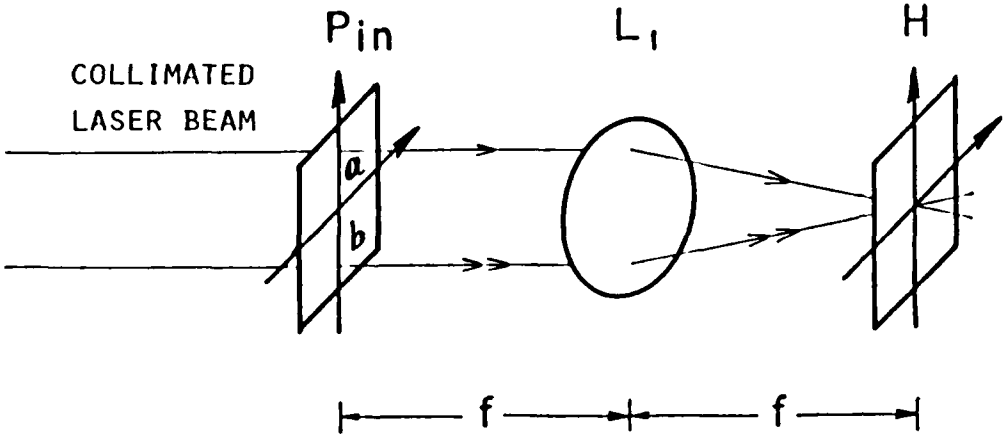

(a) FILTER RECORDING

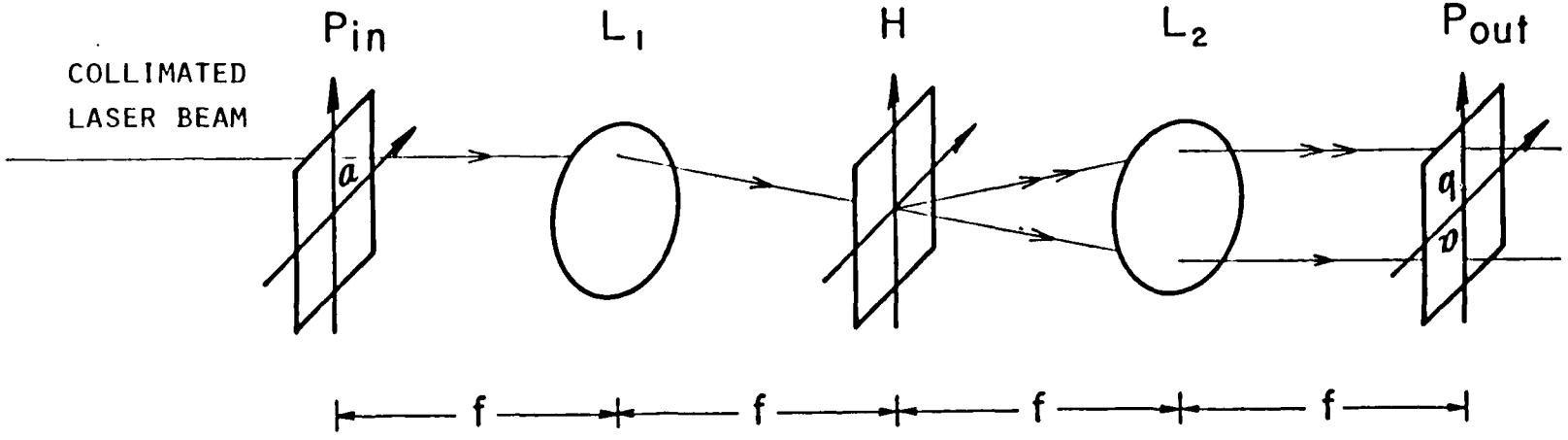

(b) COMPUTING

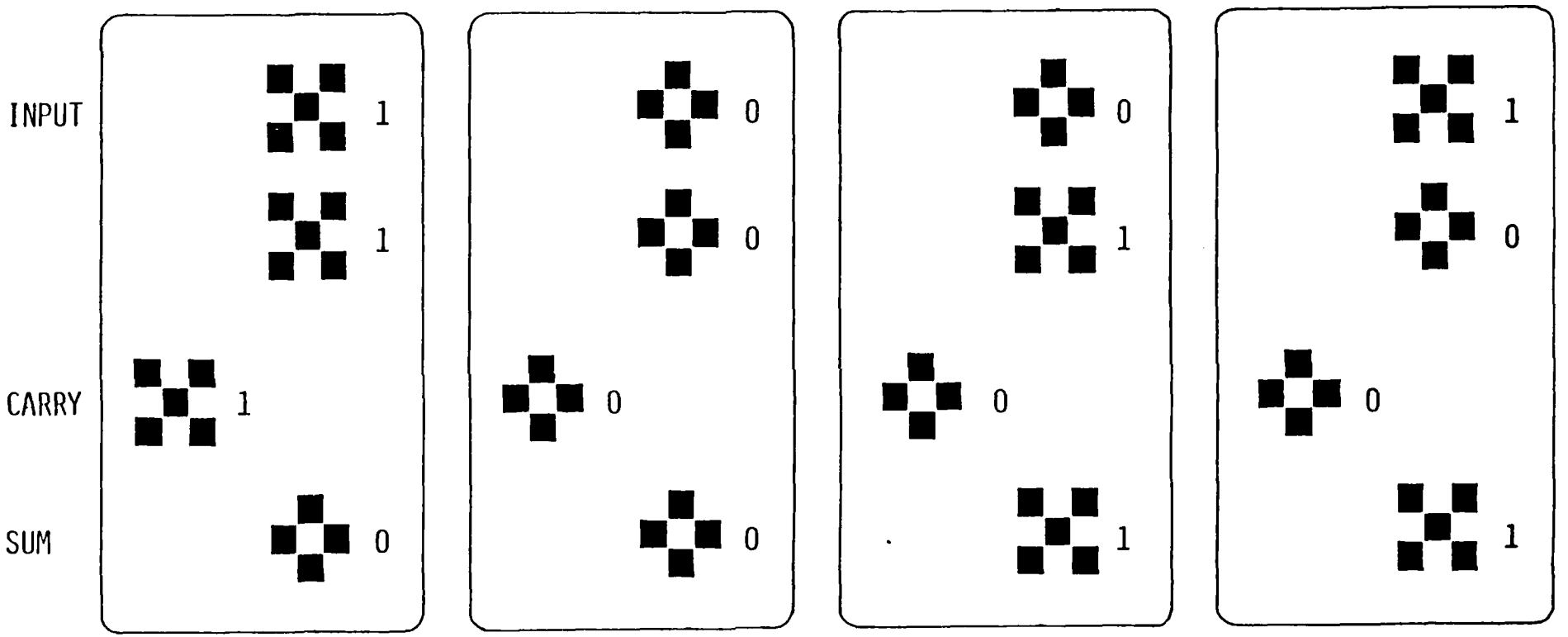

FIG. 3

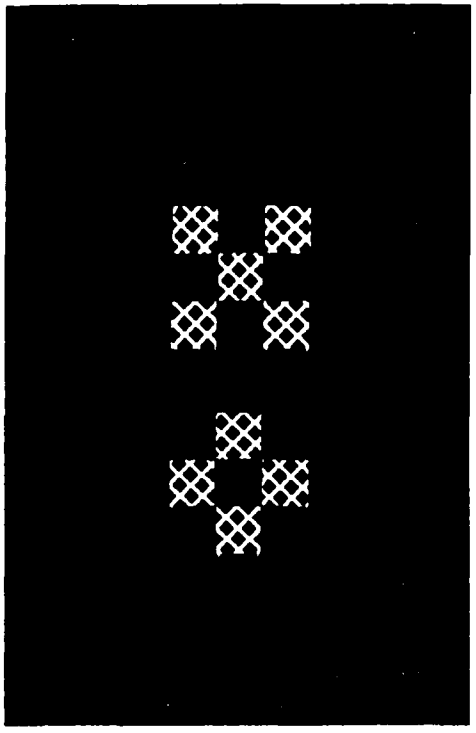

(a)

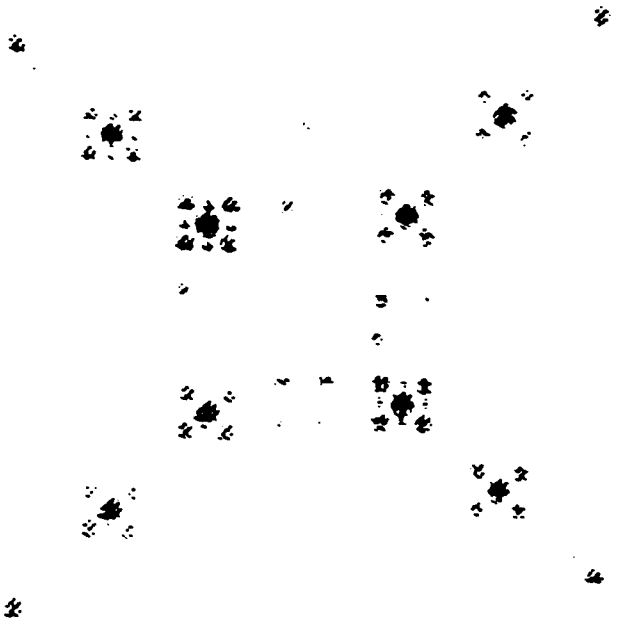

(b)

FIG 4- (a) & (b)

UP

FIG 5

UP ←

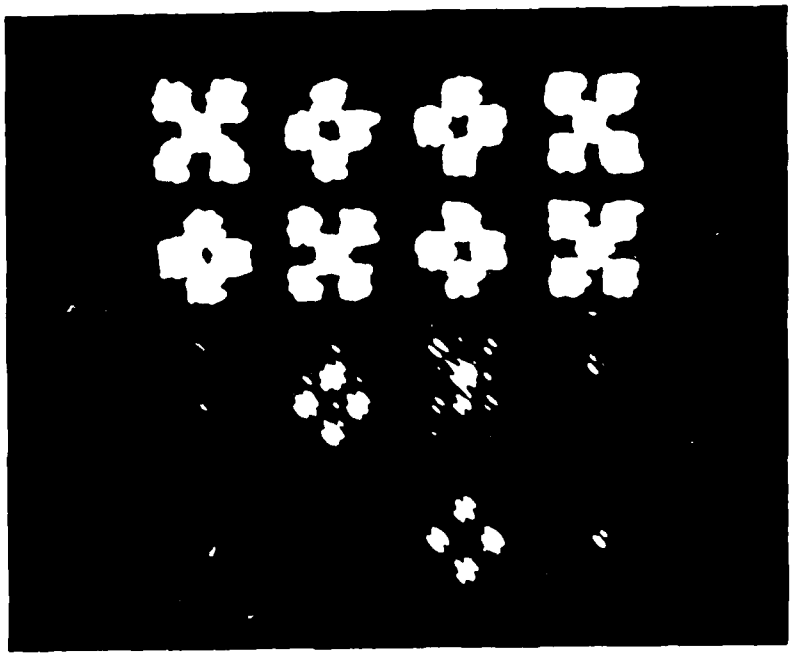

UP

SECTION 6

Optical Parallel Logic Operation

Volume 63, number 4 OPTICS COMMUNICATIONS 15 August 1987

OPTICAL PARALLEL LOGIC BASED ON MAGNETO-OPTIC SPATIAL LIGHT MODULATOR

Francis T.S. YU, Suganda JUTAMULIA and Taiwei LU
Electrical Engineering Department, The Pennsylvania State University, University Park, PA 16802, USA

Received 24 March 1987

The implementation of sixteen optical parallel boolean logic gates using two magneto-optic spatial light modulators are described. The experimental results are also presented.

1. Introduction

Optical and electro-optical switches have been extensively studied for applications such as optical computing, opto-digital circuit, and optical communication networks. Complementary to the rapidly emerging photonic devices [1], many optical parallel logic gates have been successfully implemented using current technology. The optical parallel logic operations have been performed using PROM devices [2,3], twisted nematic liquid crystal devices [4], liquid crystal light valves [5], shadowgrams [6], and spatial filtering technique [7]. Recently we have demonstrated a new implementation of optical parallel logic gates using two cascaded inexpensive commercially available liquid crystal televisions [8]. Khan and Nejib [9] presented a theoretical description of optical logic gates employing liquid crystal switches. Optical parallel logic gates can also be implemented using magneto-optic spatial light modulators (MOSLMs) in a similar manner as that proposed by Khan and Nejib. This paper demonstrates the implementation of optical parallel logic based on MOSLM.

2. Magneto-optic spatial light modulator

The MOSLM is a transmission-type electro-optic spatial light modulator [10]. When polarized light passes through the MOSLM, its plane of polarization is altered due to the Faraday effect in the MOSLM. Currently available MOSLMs have 48×48 or 128×128 randomly accessible pixels. The pattern on the MOSLM can be generated by a microcomputer or by a CCD camera. When the magnetization of a pixel is in the positive direction, the polarization of the incident light will be rotated by an angle α, and the polarization will be rotated by $-\alpha$ for negative magnetization. These two states are the stable states of the device. Ideally, $\alpha=45^\circ$, and using an analyzer with a 45° orientation, a high contrast output would be obtained. Currently available devices, however, are only capable of a few degrees of polarization rotation.

3. Theory

In boolean algebra, there are sixteen logic functions for two inputs A and B. Table 1 shows in regular order all sixteen possible functions for positive logic. For simplicity, only the case of positive logic is discussed in this paper. The analysis can be modified straightforwardly for the case of negative logic.

Fig. 1 shows the multiplicative configuration to perform F1, F2, F4, F6, F8 and F9. Two MOSLMs are arranged in tandem. The three polarizers are placed, resp., in front of MOSLM1, between the two MOSLMs and behind MOSLM2. A collimated beam is required to preserve a one-to-one pixel relationship. Recalling that the Faraday rotation effect is

0 030-4018/87/$03.50 © Elsevier Science Publishers B.V.
(North-Holland Physics Publishing Division)

Table 1
Sixteen possible functions of two binary variables for positive logic

Input		Output															
A	B	F0	F1	F2	F3	F4	F5	F6	F7	F8	F9	F10	F11	F12	F13	F14	F15
0	0	0	0	0	0	0	0	0	0	1	1	1	1	1	1	1	1
0	1	0	0	0	0	1	1	1	1	0	0	0	0	1	1	1	1
1	0	0	0	1	1	0	0	1	1	0	0	1	1	0	0	1	1
1	1	0	1	0	1	0	1	0	1	0	1	0	1	0	1	0	1
Function name		0	AND	$A\bar{B}$	A	$\bar{A}B$	B	XOR	OR	NOR	XNOR	$\bar{B}$	$A+\bar{B}$	$\bar{A}$	$\bar{A}+B$	NAND	1

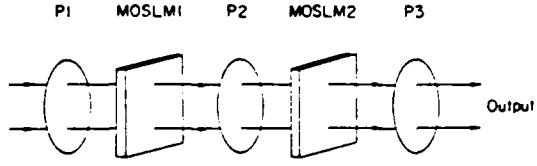

Fig. 1. Multiplicative configuration of optical parallel logic gates. P1, P2, P3: polarizers.

independent of the sense in which the beam traverses the magnetic field lines, logic operations can be performed by setting polarizes P2 and P3 at certain orientations. To perform XOR (=F6) polarizer P2 is removed. It is noticed that XNOR can be only performed using this configuration if $\alpha \approx 45^\circ$ [8].

To perform F7, F11, F13 and F14, an additive configuration shown in fig. 2 is applied. The two

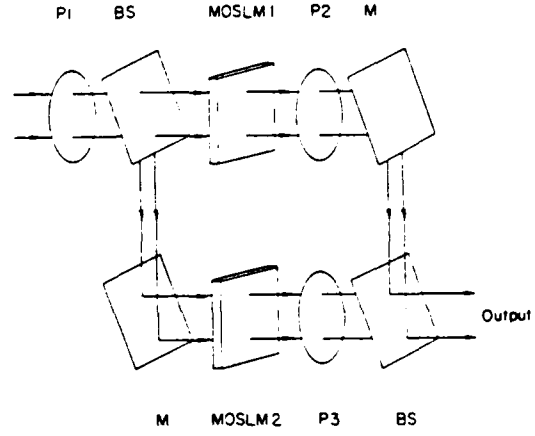

Fig. 2. Additive configuration of optical parallel logic gates. M: mirror; BS: beam splitter; P1, P2, P3: polarizers.

MOSLMs are arranged in parallel. The polarizers P2 and P3 are placed behind MOSLM1 and MOSLM2, respectively. The images of two MOSLMs are incoherently superimposed by means of a beam splitter. Because α is actually small ($\approx 9^\circ$), function 1 (=F15) and function 0 (=F0) can be approximated by setting the analyzer at the orientations of 0° and 90°, respectively. Therefore F0, F3, F5, F10, F12 and F15 can be performed using the configuration shown either in fig. 1 or fig. 2.

4. Experiment

A polarization rotation of $\alpha \approx 9^\circ$ has been observed in the experiment. Malus law states that the intensity of the transmitted light through a polarizer placed at an angle with the analyzer varies as the square of the cosine of the angle. If the maximum transmittance after the analyzer is denoted by T and the bias denoted by B, the intensity ratio of the bright (logical 1) and dark (logical 0) portions will be

$$R_1 = \frac{T-B}{T\cos^2 18^\circ + B} = \frac{T-B}{0.91T-B}, \quad (1)$$

when the analyzer is oriented at 9°, and

$$R_2 = \frac{T\sin^2 18^\circ + B}{B} = \frac{0.1T-B}{B}, \quad (2)$$

when the analyzer is oriented at $(-9+90)^\circ = 81^\circ$. Note that eq. (1) gives logical 1 the highest possible transmittance. On the other hand, eq. (2) gives to logical 0 the lowest possible transmittance.

The combinations of polarizers to perform all the sixteen logic operations are summarized in table 2.

Table 2
Combinations of polarizers to implement logic gates ($\alpha = 9°$)

Function	Configuration	P1	P2	P3	Comment
F0	fig. 1	0°	90°	0°	
F1	fig. 1	0°	81°	162°	
F2	fig. 1	0°	−81°	0°	
F3	fig. 1	0°	81°	81°	
F4	fig. 1	0°	81°	0°	
F5	fig. 1	0°	0°	81°	
F6	fig. 1	0°	no polarizer	0°	
F7	fig. 2	0°	81°	81°	
F8	fig. 1	0°	−81°	−162°	
F9	fig. 1	0°	no polarizer	18°	shown in fig. 4(a)
				−18°	shown in fig. 4(b)
F10	fig. 1	0°	0°	−81°	
F11	fig. 2	0°	81°	−81°	
F12	fig. 1	0°	−81°	81°	
F13	fig. 2	0°	−81°	81°	
F14	fig. 2	0°	−81°	−81°	
F15	fig. 1	0°	0°	0°	

Table 2 is applied to the case of lowest possible logical 0, i.e., eq. (2). The experimental results are shown in fig. 3. An intermediate level is produced due to the bias term of the low contrast binary patterns. The transmittance of the activated MOSLM consists of a and b, where $a > b > 0$. The product of two patterns will include three transmittances, i.e., a^2, ab, b^2, where $a^2 > ab > b^2 > 0$. To eliminate the intermediate level ab in F1, F2, F4 and F8, a hardclipping may be conducted such that $ab \approx b^2$. The addition of two patterns will also result in three levels, i.e., $2a$, $a+b$, $2b$, where $2a > a+b > 2b > 0$. To eliminate the intermediate level $a+b$ in F7, F11, F13 and F14, a hardclipping of $a+b \approx 2a$ may be conducted.

A good XNOR could not be performed in the experiment. This problem is explained in the following. Without the polarizer P2, the combinations of (1,0) and (0,1) will result in no polarization rotation. A combination of (1,1) produces a final polarization angle of 18°. A combination of (0,0) produces −18°. When the polarizer P3 is set at 0°, the combinations of (1,0) and (0,1) will be bright and the combinations of (1,1) and (0,0) will be dark. According to the Malus law, the combinations of (1,1) and (0,0) have the same irradiance. An XOR operation thus can be obtained. There are three approximations to an XNOR operation. Neglecting the bias, transmittances may be calculated as follows:

(a) Polarizer P3 is set at 18°
transmittance of $(1,0) = (\cos 18°)^2 = 0.91$
$(0,1) = (\cos 18°)^2 = 0.91$
$(1,1) = (\cos 0°)^2 = 1$
$(0,0) = (\cos 32°)^2 = 0.72$

(b) Polarizer P3 is set at −18°
transmittance of $(1,0) = (\cos 18°)^2 = 0.91$
$(0,1) = (\cos 18°)^2 = 0.91$
$(1,1) = (\cos 32°)^2 = 0.72$
$(0,0) = (\cos 0°)^2 = 1$

(c) Polarizer P3 is set at 90°
transmittance of $(1,0) = (\cos 90°)^2 = 0$
$(0,1) = (\cos 90°)^2 = 0$
$(1,1) = (\cos 72°)^2 = 0.10$
$(0,0) = (\cos 72°)^2 = 0.10$

In reality, when P3 was set at 90°, an approximation of F0 instead of F9 was obtained. This result was similar to F0 shown in fig. 3. The experimental results of 18° and −18° oriented polarizers are shown in fig. 4. It is clearly shown that these configurations

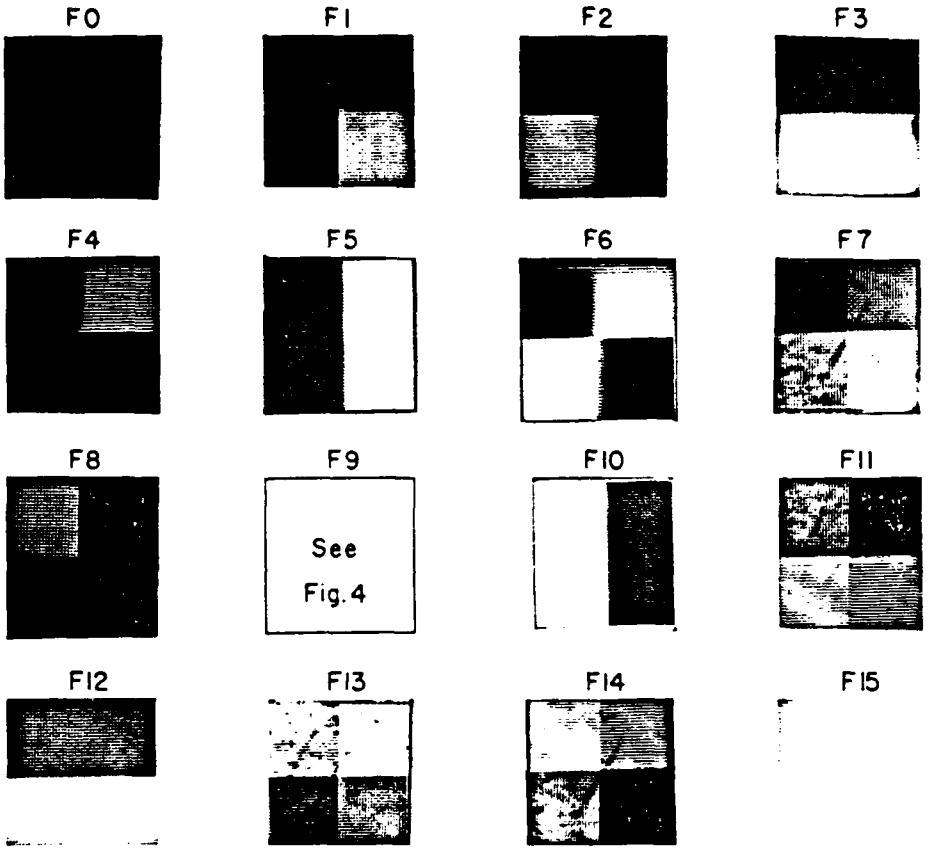

Fig. 3. Experimental results of optical parallel logic operations.

Fig. 4. Approximations of XNOR. Polarizer P3 is set at (a) 18° and (b) −18°.

cannot be used as a XNOR gate, because the transmittance of (1,0) and (0,1) is always in between that of (1,1) and (0,0). Alternatively, $\bar{A}$ instead of A may be input to MOSLM to perform XNOR operation, since an XNOR of A and B is equivalent to XOR and $\bar{A}$ and B.

5. Concluding remarks

We have demonstrated the sixteen boolean logical operations by means of two MOSLMs. The applications of optical parallel logic including flip-flop, half adder, full adder, binary image subtraction and cellular processing, have been discussed in detail in the literature [2–9]. The advantages of the MOSLM are: (1) electronically-addressability and microcomputer-programmability, (2) fast switching time (≈ 50 μs), (3) capability of storing an input pattern without power supplied, and (4) low power consumption. Many new architectures of hybrid optical processing and computing may be implemented using MOSLMs based on the proposed technique.

Acknowledgements

We acknowledge the support by U.S. Air Force Office of Scientific Research grant AFOSR-86-0264, and the generosity of Semetex Corporation to provide us the SIGHT-MOD.

References

[1] S.D. Smith, Appl. Optics 25 (1986) 1551.
[2] B. Horwitz and F. Corbett, Opt. Eng. 17 (1978) 353.
[3] T. Minemoto, K. Okamoto and Kei Miyamoto, Appl. Optics 24 (1985) 2055.
[4] R.A. Athale and S.H. Lee, Opt. Eng. 18 (1979) 513.
[5] M.T. Fatehi, K.C. Wasmundt and S.A. Collins, Jr., Appl. Optics 20 (1981) 2250.
[6] J. Tanida and Y. Ichioka, J. Opt. Soc. Am. 73 (1983) 800.
[7] J. Weigelt, Opt. Eng. 26 (1983) 28.
[8] F.T.S. Yu, S. Jutamulia, J.S. Jin and D.A. Gregory, Appl. Optics, submitted for publication.
[9] A.H. Khan and U.R. Nejib, Appl. Optics 26 (1987) 270.
[10] W.E. Ross, D. Psaltis and R.H. Anderson, Opt. Eng. 22 (1983) 485.

SECTION 7

Microchannel Spatial Light Modulator Processing

Volume 63, number 6 OPTICS COMMUNICATIONS 15 September 1987

MICROCHANNEL SPATIAL LIGHT MODULATOR WITH WHITE LIGHT PROCESSING

F.T.S. YU, X.J. LU
Electrical Engineering Department, The Pennsylvania State University, University Park, PA 16802, USA

Y. SUZUKI
Hamamatsu Photonics KK, Hamamatsu City, Japan

and

M. WU
Hamamatsu Corporation, Bridgewater, NJ 08807, USA

Received 29 January 1987

The color characteristics of a microchannel spatial light modulator (MSLM) under white-light read out illumination is examined, and a system for performing color optical processing operations using an electro-optic crystal plate along with the MSLM is presented. Experimental results for edge enhancement and image subtraction operations are demonstrated.

1. Introduction

The microchannel spatial light modulator (MSLM) is a real-time optical processing device with high optical sensitivity and high framing speed. The architecture, fundamental operating characteristics and inherent space-domain image processing operations of the device have been reported in the literature [1,2]. It is a rather versatile device in that a wide variety of operations can be performed such as edge enhancement, image subtraction, contrast reversal, analog thresholding and hard clipping. In this paper we consider the operation of the MSLM in a white-light system and examine the color characteristics of the system for various image processing operations.

2. MSLM principles of operation

The MSLM consists of a photocathode and a microchannel plate (MCP) in proximity focus with an electro-optic crystal, all inside a sealed vacuum tube [3]. The electro-optic crystal has a dielectric mirror over the surface facing the MCP and photocathode side. During operation (as in the system shown in fig. 1), an input write-in light incident on the photocathode generates free electrons which are multiplied by the MCP and proximity focused onto the surface of the dielectric mirror. This spatially varying charge distribution represents the input image. A grid inside the MSLM controls the writing, erasing, and modulation level of this surface charge distribution. The charge produces a spatially varying electric field across the crystal longitudinally which in turn spatially modulates the birefringence of the electro-optic crystal.

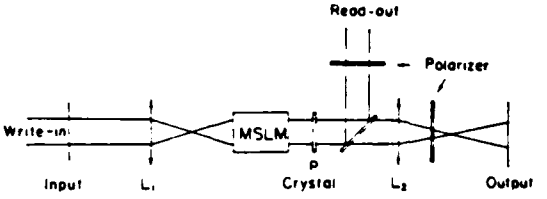

Fig. 1. Optical system with MSLM and electro-optic crystal plate.

The read-out light passes through the electro-optic

0 030-4018/87/$03.50 © Elsevier Science Publishers B.V.
(North-Holland Physics Publishing Division)

crystal plate and is reflected back through the plate by the dielectric mirror, effectively making a double pass through the plate. The output light is thus spatially phase-modulated. Considering the polarization components of the light within the crystal, we note that the components along the birefringence axes of the crystal (X, Y) are phase-shifted by different amounts due to different indices of refraction. The relative phase retardation, δ, is defined as the difference in phase shifts for the polarization components along the crystallographic X and Y axes and is given by

$$\delta = (2\pi/\lambda)(n_1 - n_2)2d\,. \tag{1}$$

Here λ is the wavelength of the read-out light, d is the thickness of the crystal in the MSLM ($2d$ is used in eq. (1) because a double pass is made), n_1 and n_2 are the indices of refraction along the X and Y axes.

The electro-optical crystal in the MSLM analyzed in this paper is a 300 μm thick $LiNbO_3$ single crystal cut so that the normal to the plate lies in the $(-Y, Z)$ plane of the crystal and makes an angle of 55° with the Z axis. This crystal cut optimizes the electro optic coefficient for the crystal plate in longitudinal mode.

Now consider the system shown in fig. 1, ignoring the crystal P outside the MSLM for now. If the input polarizer in the read-out light is vertically oriented, the X' and Y' axes of the crystal in the MSLM are 45° from vertical (we take the X' and Y' axes here since we are using an optimally cut crystal), and the output polarizer (analyzer) is horizontal, a high contrast image can be produced at the output plane when a coherent source is used for the read-out light [4]. The intensity distribution is given by

$$I = K\sin^2(\delta/2)\,, \tag{2}$$

where K is a proportionality constant (which depends on the charge distribution and hence on the input write-in image), and δ is the relative phase retardation.

An equivalent representation of the read-out mode of the MSLM is illustrated in fig. 2(a). The output may be taken as the relative phase retardation of π and represents the retardation due to the crystal plate without an input image (i.e. background). The doublepass through the plate on read-out gives $\delta = 2\pi$.

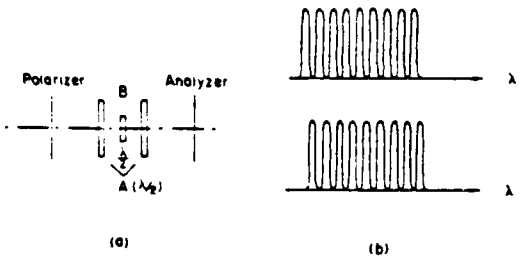

Fig. 2. Properties of system without the crystal plate under white light readout illumination. (a) An equivalent transmittance representation. (b) Shown at top intensity as a function of wavelength for image and background shown at bottom.

Plate B represents the change in δ due to the write-in image.

3. White light operation

Assume that the charge distribution and the resulting indices of refraction are adjusted (via the grid in the MSLM) so that for some read-out wavelength, λ_0, and at some bright area of the input image the relative phase retardation equals π. It is apparent from eq. (2) that the output intensity at the point will be a maximum resulting in a high contrast between the background and the image at the output plane. At some other wavelength, however, we see from eq. (1) that in general $\delta \neq \pi$ and the output intensity of the image (and hence the contrast) is reduced.

Note from eq. (2) that a change in δ of π results in a contrast reversal and from eq. (1) that δ varies with λ. The change in δ due to a change in read-out

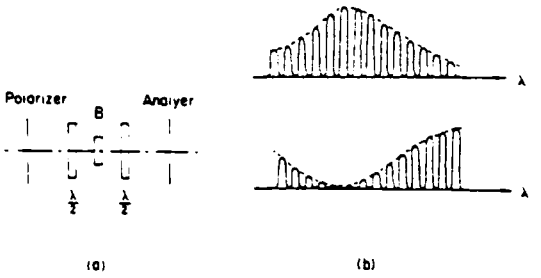

Fig. 3. System with crystal plate. (a) Equivalent representation. (b) Intensity as a function of wavelength for image shown at top and background shown at bottom.

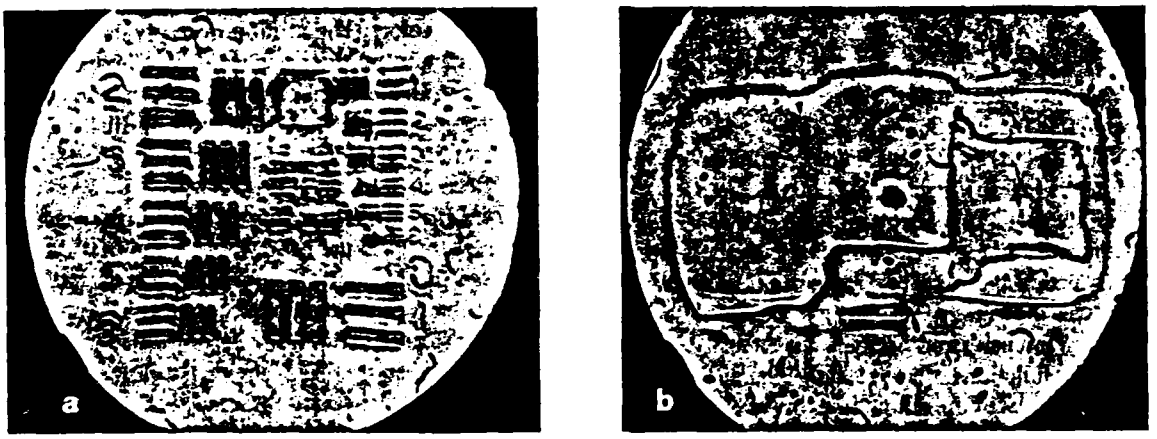

Fig. 4. Color image processing results. (a) Image of resolution chart. (b) Edge enhancement.

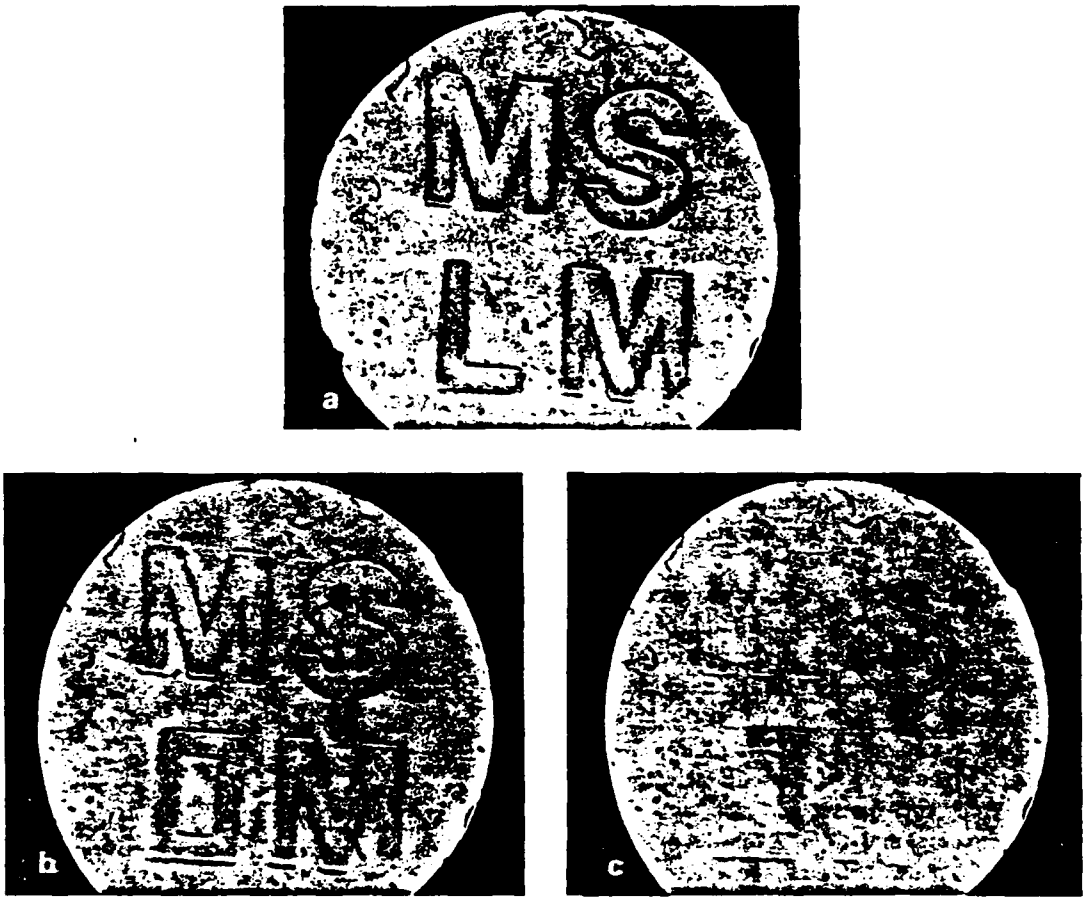

Fig. 5. Color image subtraction. (a), (b) Input color objects. (c) Subtracted results.

wavelength, $\Delta\lambda$, is obtained from eq. (1) to be

$$\Delta\delta = 4\pi d(n_1 - n_2)\Delta\lambda/\lambda_0^2 , \quad (3)$$

where we have assumed that the variation of $n_1 - n_2$ is negligible for $\Delta\lambda \ll \lambda_0$.

Evaluating $\Delta\lambda$ with reasonable estimates of the parameters ($d = 0.30$ mm, $n_1 - n_2 = 0.03$, $\lambda_0 = 6 \times 10^{-7}$ m), we see that λ changes by π radians for $\Delta\lambda \approx \lambda_0/30$. This means that phase retardation changes very quickly with wavelength and many contrast reversals occur over the range of visible light. Fig. 2(b) shows the image intensity and background intensity distributions as functions of wavelength. The net result is that the contrast of the output image is very low when white light is used.

In order to make the output image under white light illumination more visible, another crystal plate, P, similar to the one in the MSLM, is inserted in the read-out beam as shown in fig. 1. The principal section of the plate is parallel to that of the plate in the MSLM and the effect of the two is similar. The plate, P, is not spatially modulated and its contribution to δ changes relatively slowly over the white light spectrum. An equivalent representation of the read-out mode of the MSLM and the plate p is shown in fig. 3(a). The composite effect of the two plates is to act like a color filter. This is illustrated in fig. 3(b) where the image and background intensity distributions are shown as a function of λ. The image appears as one color at the output plane while the background appears as a different color, that is the well known polarization interference. The background and image colors can be modified by slightly rotating the plate transversely along the vertical axis, effectively changing the path length d that the readout beam travels within the plate.

The optical system shown in fig. 1 was used with the same white light source illuminating both the write-in and read-out. The effective aperture of the MSLM is 15 mm in diameter and the resolution is about 5 lines/mm.

Fig. 4(a) shows a color image of a resolution chart. Color images of the chart were produced with red strips on a green background and also with green strips on a red background. Color reversal is obtained when the crystal plate is rotated about 1.1° in the azimuthal direction (about the vertical axis). Alternatively, the voltage of the plate can be adjusted to reverse the colors. The minimum resolvable strip is about 0.12 mm on the resolution chart image.

An edge enhancement color image of the top views a small truck, fig. 4(b), is obtained by adjusting the voltage of the plate. The color of the edge changes as the plate is rotated.

For image subtraction the two write-in images are input separately to the MSLM. After the first image is written in, the controlling grid voltage is changed to give color reversal and the second image is entered. The writing time cycles must be controlled properly to get good results. Fig. 5 shows two images to be subtracted and the result obtained.

4. Concluding remarks

The microchannel spatial light modulator provides an effective means of performing optical processing operations in color under white-light illumination. The external crystal plate in conjunction with the electro-optic crystal in the MSLM plays an important role in the system by performing color filtering, and allocating some colors to the background and others to the object. A variety of operations can be caried out. Image subtraction and edge enhancement have been demonstrated. Color selection and/or reversal can be obtained by rotating the external crystal plate.

The system or its expanded version can potentially be valuable for night vision, medical imaging, and interferometric applications.

Acknowledgement

We acknowledge the support of the U.S. Air Force of Scientific Research Grant AFOSR-86-0264.

References

[1] C. Warde and J. Thackara, Opt. Eng. 22 (1983) 695.
[2] C. Warde and J. Thackara, Optics Lett. 7 (1982) 344.
[3] T. Hara, M.Sugiyama and Y. Suzuki, Advances in Electronics and Electron. Phys. 64 B (1985) 637.
[4] D. Casasent, in: Applied optics and optical engineering, eds. R. Kingslake and B. Thompson (Academic Press, New York, 1980) p. 150.

SECTION 8

Multichannel Optical Correlation

Volume 64, number 2 OPTICS COMMUNICATIONS 15 October 1987

A MULTICHANNEL OPTICAL CORRELATOR

Francis T.S. YU and Q.H. ZHOU
Electrical Engineering Department, The Pennsylvania State University, University Park, PA 16802, USA

Received 29 January 1987; revised manuscript received 10 June 1987

A multichannel parallel optical pattern recognition system is proposed. The synthesis of a large capacity matched filter is discussed. The technique uses a phase mask and telescopic arrangement for the mass filter construction. The processing capacity of the proposed optical correlator, which is over 400 times of a single channel system, is evaluated.

1. Introduction

Correlation detection has been widely adopted in the application of optical character and pattern recognition. Based on the concept of the optical matched filtering of Vander Lugt [1], various types of optical correlators have been proposed. Generally, these systems can be classified as either serial or parallel type. Matching spatial filters (MSFs) are addressed sequentially for a serial correlator [2,3], while two or more filters are addressed simultaneously [4–6] for a parallel type.

In the operation of parallel type correlators, Grummet [4] utilized an $N \times N$ array of holographic lenses. Liu and Duthie [5], and later Gregory and Liu [6] reported a real time correlator using a liquid crystal light valve (LCLV). In these systems the reference beams were fixed in one direction, such that all the cross-correlations and auto-correlations would be displayed at about the same region. If a correlation peak is observed, the input scene should contain one of the reference objects. However, it is difficult to determine which reference object is actually correlated with the input. These systems are therefore inadequate in distinguishing more than one object. Nevertheless, these systems can be applied to detect an object with finite orientations. Another drawback of this kind of systems occurs in the signal-to-noise ratio (SNR) which decreases as the number of the matched filters increases.

In this paper, we propose a parallel optical correlator, which separates the output correlation functions. This correlator utilizes reference beams with different directions in constructing the MSFs. Since the output correlation diffraction is based upon the direction of the spatial carrier frequency, the correlation distribution from each MSF will appear at different diffracted locations. Thus, $N \times N$ channels can be synthesized by employing a phase mask to diffract the reference beam into $N \times N$ directions. Because the correlation outputs are diffracted in different locations, SNR is independent of the number of channels.

2. System description

With reference to the multichannel optical correlator of fig. 1, a collimated laser beam is incident on a phase mask P to produce $N \times N$ equi-intensity beams in different directions. These diffracted beams would propagate through a conventional matched spatial filtering setup, as shown in the figure. Since the diffraction angles are assumed to be small, all of the diffracted beams would pass through the same optical elements. Thus, an $N \times N$ array of image spectra is produced in the Fourier transform plane. The separation between two adjacent spectra is $f_1\alpha$, where f_1 is the focal length of the Fourier transform lens L_1, and α the angle of the first-order diffraction. α is also the angle between two adjacent diffracted beams. S_1 is a selecting screen which allows only the desired

0 030-4018/87/$03.50 © Elsevier Science Publishers B.V.
(North-Holland Physics Publishing Division)

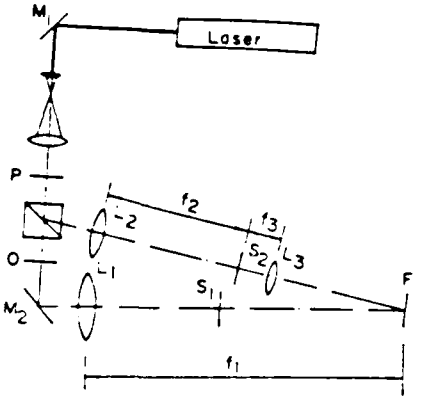

Fig. 1. Parallel optical correlation system. M, reflection mirror; P, phase mask; O, object scene, S, movable selecting screens; F: matched filter.

object spectrum to pass. In the correlation process, S_1 is removed from the system, and all the diffracted beams are projected onto the corresponding MSFs.

We note that the reference beams are focused by lens L_2. S_2 is another selecting screen used for reference beams, in the synthesizing of the MSFs. Thus we see that an $N\times N$ array of reference beams in different directions would be incident on the filter plane F. By choosing the proper focal lengths f_1, f_2 and f_3 respectively, all of the reference beams would coincide with the respective object spectra.

In multi-image correlation, the $N\times N$ object spectra are superimposed with the $N\times N$ MSFs. The correlation peak from each MSF corresponding to the direction of the diffracted reference beam can be identified. Thus an $N\times N$ channel parallel correlator can be synthesized.

3. System analysis

3.1. Phase mask

The design of a binary phase mask based on an interlacing π phase shift technique has been proposed by Dammann and Klotz [7]. By adjusting the width of the mask period, they were able to obtain an array of equi-intensity diffracted beams. By utilizing a half-tone screen technique, Liu [8] has also investigated an $N\times N$ array equi-intensity diffractions. Since our optical correlator diffracts the output correlations in various locations, the $N\times N$ array of diffracted beams are not necessarily required to be equal. However, different detection criteria should be imposed on different channels. In practice, the $N\times N$ beams may have equal intensity, but the correlations generally have different peak intensities. It is rather difficult to synthesize the $N\times N$ MSFs such that they all possess the same diffraction efficiency. It is, however, more essential to have an overall optimum efficiency rather than to have equi-intensity diffraction.

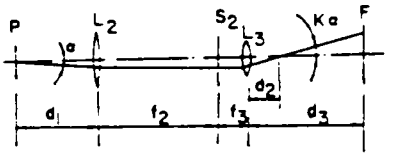

Fig. 2. Effect of reference beam due to the telescopic structure; K is the angular magnification.

3.2. Telescope structure for reference beam

In view of fig. 2, the arrangement of L_2 and L_3 is in fact a telescopic structure, which plays an important role in the proposed system. In this structure, the reference beams are directed to combine with the object spectra. Let us assume that the coherent length of the laser is adequately long; the reference beams can be made to superpose with the object spectra by simply adjusting the distance between the phase mask and the filter plane. To synthesize a mass spatial filter, the diffraction angle α should be made adequately small. If the angular separation of the reference beams were also α, the output correlations would overlap. However, the shortcoming can be alleviated if the angular separation is increased. With the aid of the telescopic structure, the angle is increased to $(f_2/f_3)\alpha$. Choosing f_2 sufficiently larger than f_3, the overlapping in output correlations can be avoided.

In practice, the intensity of the reference beam should be higher than that of the object beam to avoid the nonlinear effect of the matched filters. We note that with the telescopic structure the intensity in the reference beam would be increased by a factor of f_2/f_3. Furthermore the telescope structure also provides a suitable plane in choosing the desired reference beam.

3.3. Relations of system parameters

Since the diffraction angle from the phase mask is α, the separatioin of the object spectra at the filter plane is $f_1\alpha$. If an angular separation of the reference beam, $K\alpha$, is needed to avoid overlapping, then the angular magnification factor required for the telescopic structure should be $K=f_2/f_3$.

In view of fig. 2, the relation between d_2 and d_1 can be obtained with geometrical optics, i.e.,

$$d_2 = f_3 + f_3/K - d_1/K^2 , \quad (1)$$

where factor K should be sufficiently large, such that output correlation distributions could be separated. By neglecting $f_3/K - d_1/K^2$, as composed with f_3, eq. (1) can be reduced to

$$d_2 = f_3 . \quad (2)$$

Furthermore, to obtain the same angular separation $f_1\alpha$ of the reference beams, the distance from L_3 to the filter plane should be

$$d_3 = f_3(1 + f_1/f_2) . \quad (3)$$

3.4. Processing capacity

Suppose the width of input object transparency is W and the focal length of the Fourier transform lens is f_1. An angular separation of $2W/f_1$ for the adjacent reference beams would be required to separate the adjacent output correlation distributions. For example, if the maximal separation angle leaving the telescopic structure is about 60°, we would have a maximum of $\pi f_1/(6W)$ filters in one dimension. Further assume that $f_1 = 80$ cm and $W = 2$ cm. The maximum number of the matched filters in two dimensional representation would be over 400.

In order to avoid channel overlapping, the angular separation of the reference beam should be $2W/f_1$. If the distance between neighboring matched filters is u, the diffraction angle $\alpha = u/f_1$. The angular magnification K can be determined as

$$K = 2W/u . \quad (4)$$

For instance, if $W = 2$ cm and $u = 0.4$ cm, then $K = 10$. The fact that K is larger than unity demonstrates that a telescope structure is required to avoid overlapping.

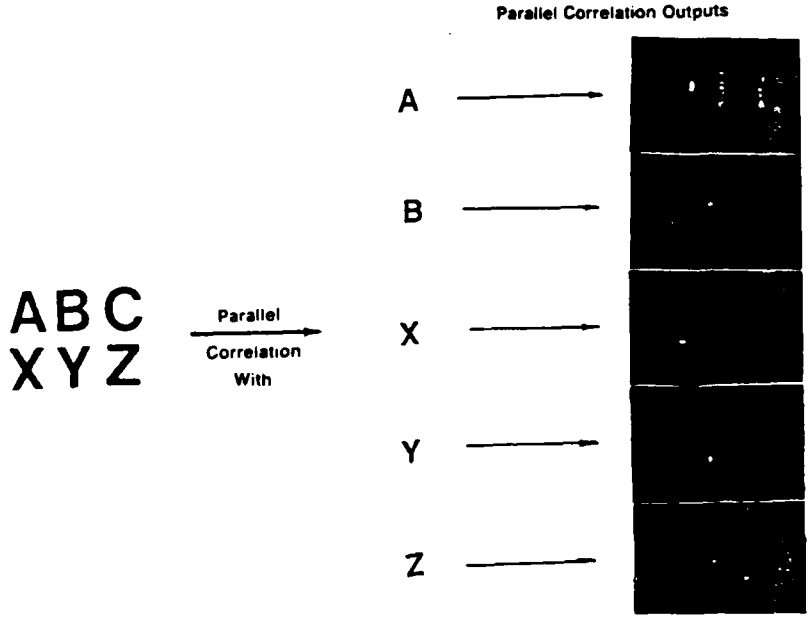

Fig. 3. An experimental demonstration.

4. Experimental demonstration

Instead of using a 2-D phase mask, a 1-D sinusoidal phase grating is used in our experimental demonstration. The phase grating provides first, and second order diffractions. Including zero order beam a total of five diffraction beams is obtained. The spatial frequency of the grating is 20 lines/mm, and diffraction angle α is therefore 1/100 radian. The objects used in our experiments consist of six english characters, as shown in fig. 3. The focal length of L_1 and L_2 are 80 cm and that of L_3 is 10 cm. The distance from lens L_3 to the filter plane was then calculated from eq. (3), to be 20 cm.

With reference to fig. 1, the +1 order reference beam would superimpose the −1 order object beam. If the phase mask does not have a symmetric diffraction pattern, an additional mirror for the reference beam or the object beam may be used to combine the positive orders of reference and object beams. In the case of two-dimensional diffraction, an Amici prism may be used to convert the beams such that the same order of reference and object beams may overlap at the filter plane. However, since the experiment performed was one dimensional, only one mirror is used for the reference beam.

In the construction of the matched filters, one sees that matched filters can be synthesised one at a time with different orders of the reference beams, that include the zero-order. The correlation outputs are observed at different locations simultaneously with respect to the carrier frequencies of the MSFs. An experimental result obtained with this technique is also shown in fig. 3. In this figure, the input scene is applied simultaneously to the filters and the correlation results are shown in the photos. This result illustrates the capability of constructing a mass capacity correlator as we proposed.

5. Conclusion

We have discussed a parallel optical correlator which has a processing capacity of more than 400 times over the conventional single channel correlator. The system will have the same output SNR as a single channel correlator. This proposed technique is rather easy to implement since no mechanical scanner is used for the mass channel correlations. This technique may offer application to rapid mass pattern recognitions.

Acknowledgement

We acknowledge the support of the U.S. Air Force Office of Scientific Research grant AFOSR-86-0264.

References

[1] Vander Lugt, IEEE Trans. Inf. Theory IT-10 (1964) 139.
[2] A.D. Gara, Appl. Optics 18 (1979) 172.
[3] F.T.S. Yu and X.J. Lu, Appl. Optics 23 (1984) 3109.
[4] A. Grumet, U.S. patent 03.779.492 (1972).
[5] H.K. Liu and J.G. Duthie, Appl. Optics 21 (1982) 3278.
[6] D.A. Gregory and H.K. Liu, Appl. Optics 23 (1984) 4560.
[7] H. Dammann and E. Klotz, Optica Acta 24 (1977) 505.
[8] H.K. Liu, U.S. patent 4,188,255 (1980).

SECTION 9

Boolean Logic Gates using MSLM and LCTVs

Implementation of Boolean logic gates using a microchannel spatial light modulator with liquid-crystal televisions

F. T. S. Yu, Q. W. Song, and X. J. Lu

Department of Electrical Engineering, The Pennsylvania State University, University Park, Pennsylvania 16802

Received May 8, 1987; accepted August 2, 1987

A programmable optical system that can perform binary Boolean logic operations with a microchannel spatial light modulator (MSLM) is presented. The MSLM is used as an adder, an inverter, a subtractor, or a buffer. We used three liquid-crystal televisions with a computer as input interfacing devices. Through the use of its feedback loop, the system can consecutively execute a series of logic operations. Experimental results are provided.

Optical Boolean logic gates are the basic elements in a digital optical computer. With advancing techniques, various schemes to perform optical parallel logic gates have been proposed. Some of these implementations utilized different spatial light modulators (SLM's), such as Pockels-readout optical-memory devices,[1,2] twisted nematic liquid-crystal devices,[3] liquid-crystal light valves[4] (LCLV's), liquid-crystal televisions[5] (LCTV's), and magneto-optical devices.[6]

The newly developed microchannel spatial light modulator[7] (MSLM) is a promising, versatile, optically addressed SLM. It offers another means to implement optical parallel Boolean gates. Warde and Thackara[7] demonstrated a method using a MSLM to execute binary logic operations. In their experiment, two input operands must be fed into the system sequentially. Hara *et al.*[8] also presented a scheme that can perform all 16 basic Boolean logic operations. Their system is complicated and consists of three MSLM's and six beam splitters. In addition, the input functions are not programmable.

In this Letter we discuss a system that can execute all 16 basic two-operand Boolean operations with a MSLM and three LCTV's. The MSLM can be used as an adder, a subtractor, an inverter, or a buffer. The LCTV's with a microcomputer are used as programmable input interfacing devices. The basic advantage of the system is the real-time programmable processing capability. By adding a feedback loop to the system one can expand its function to execute Boolean calculations consecutively.

The MSLM is a reflective-type electro-optical SLM. It consists of a photocathode, focusing electrodes, a microchannel plate, a mesh electrode, and an electro-optical (E-O) crystal plate positioned in a sealed vacuum tube. In operation, the write-in light intensity distribution produces an electrical charge distribution on the inner side of the E-O crystal plate. The charge distribution induces an electrical field within the plate. This field in turn modulates the phase retardation between the x and y components of the readout light that makes a double pass through the plate. After it passes through an analyzer, the output intensity can be expressed as[9]

$$I(x, y) = I_o \sin^2[c_1 V_b + c_2 I_w(x, y)], \tag{1}$$

where I_o is the read-out illumination intensity, c_1 is a constant determined by the material property and the cut angle of the crystal plate, c_2 is a parametric constant depending on the bias voltages on the photocathode and all the electrodes, V_b is the bias voltage across the E-O crystal plate, and $I_w(x, y)$ is the intensity of the write-in light. When the bias voltages are properly set, the MSLM can perform a number of optical operations[10,11] in its internal mode processing. These operations include image thresholding, addition and subtraction, contrast reversal, contrast enhancement, edge enhancement, hard-clip thresholding, and gray-level contour extraction. Some of these operations can be utilized to carry out OR, NEGATION, XOR, etc. in Boolean algebraic operations.

In our optical system we use the commercially available LCTV as a programmable object. The working principle of the LCTV has been described well in the literature.[5] The major advantage of the LCTV is that it can be connected directly to a microcomputer for generation of optical patterns.

There are 16 basic operations for two-operand Boolean algebra, as shown in Table 1. For simplicity, we shall consider only the positive logic, for which the high-level intensity represents logic one and the low-level intensity represents logic zero. The sixteen operations can be classified into two categories: (1) Additive operations include F_3, F_5, F_6, F_7, F_8, F_9, F_{10}, F_{11}, F_{12}, and F_{13}. (2) Multiplicative operations include F_1, F_2, F_4, and F_{14}. Note that F_0 and F_{15} can be included in either category.

Figure 1 shows the experimental setup. The microcomputer is used to generate programmable input data arrays into the LCTV's and to control the operation of the optical system. The output data can be detected by a charge-coupled-device (CCD) camera, which either displays the output on a TV monitor for observation or feeds it back into the microcomputer for further execution of the logic operations.

In additive logic operations, the computer writes an operand (image pattern) into LCTV1 and the other operand into LCTV2 and simultaneously sets LCTV3

0146-9592/87/110962-03$2.00/0 © 1987, Optical Society of America

Table 1. Sixteen Possible Functions of Two Binary Variables for Positive Logic

Input		Output															
A	B	F_0	F_1	F_2	F_3	F_4	F_5	F_6	F_7	F_8	F_9	F_{10}	F_{11}	F_{12}	F_{13}	F_{14}	F_{15}
0	0	0	0	0	0	0	0	0	0	1	1	1	1	1	1	1	1
0	1	0	0	0	0	1	1	1	1	0	0	0	0	1	1	1	1
1	0	0	0	1	1	0	0	1	1	0	0	1	1	0	0	1	1
1	1	0	1	0	1	0	1	0	1	0	1	0	1	0	1	0	1
Function name		0	AND	$A\bar{B}$	A	$\bar{A}B$	B	XOR	OR	NOR	NXOR	$\bar{B}$	$A+\bar{B}$	$\bar{A}$	$\bar{A}+B$	NAND	1

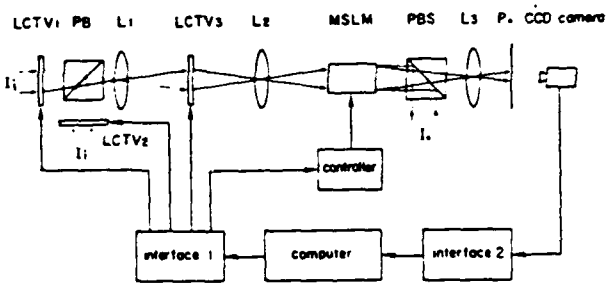

Fig. 1. Schematic diagram of a programmable optical Boolean logic system: I_i, input illumination; PB, beam splitter; L's, imaging lenses; PBS, polarizing beam splitter; I_o, readout illumination; P_o, output plane.

at a uniformly transparent state. Lenses 1 and 2 will image the patterns displayed on LCTV1 and LCTV2 onto the input window of the MSLM. LCTV3 has no effect on this process since it is at a transparent state. To execute OR, the MSLM is operated in the intensity hard-clipping mode. In this mode, the input and output intensities are related by a curve as shown in Fig. 2. Thus only the overlap of the dark parts of both input patterns gives a zero output intensity, while the rest of the result at the output is equal to intensity I_o. In other words, the intensity distribution on the output plane corresponds to the OR operation of the two input operands. If we add a half-wave voltage to the E-O crystal bias voltage V_b, the contrast of the output would be reversed. This yields the NOR of the input operands. In a similar manner, functions F_3, F_5, F_6, F_7, F_8, F_9, F_{10}, F_{11}, F_{12}, and F_{13} can be achieved. To execute XOR, the parameters in Eq. (1) are selected to be $c_1V_b = \pi$ and $c_2I_i = \pi$. Thus we can see that the output intensity would be zero if the write-in intensity were either zero or I_i. On the other hand, if the write-in intensity were $I_i/2$, the output intensity would be I_o. This relationship between input and output intensities is illustrated in Fig. 3, which corresponds to the XOR of the input operands. If we add a half-wave voltage to V_b, the output contrast would be reversed, which corresponds to the NXOR operation.

For the multiplicative operations, the computer would write a first operand into LCTV1 and a second operand into LCTV3, whereas LCTV2 is programmed to be logic zero (i.e., LCTV2 is in opaque stage), and the MSLM is operated in the hard-clipping mode. Thus, when the operand on LCTV1 is imaged onto LCTV3, the intensity distribution immediately behind LCTV3 would be the multiplication of the two input operands. By adding a half-wave voltage to the V_b, we can get the product negation of the inputs. With reference to this basic principle, the functions F_1, F_2, F_4, F_{14} can be achieved with this setup. Functions F_0 and F_{15} can be obtained by operating the MSLM in a saturated mode, so that the output intensity would be zero or I_o, depending on the voltage across the E-O crystal plate regardless of the input operands.

If one uses the feedback loop, the optical system can perform sequential Boolean operations. By utilizing the clock pulses of the computer after each operating cycle, the CCD camera can feed back the output result

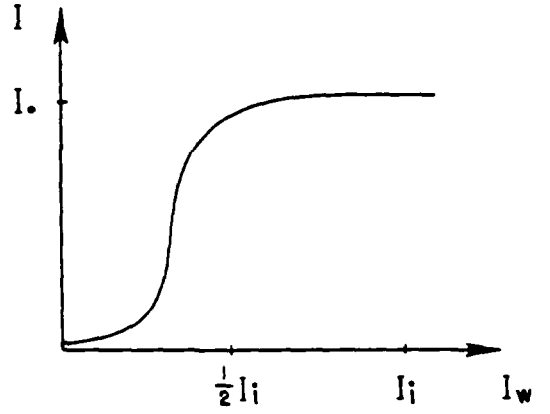

Fig. 2. The input–output intensity relationship of a hard-clipping MSLM.

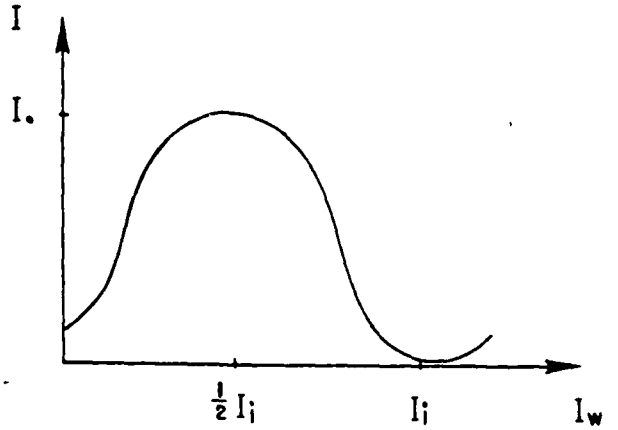

Fig. 3. The input–output intensity relationship of a MSLM for executing XOR.

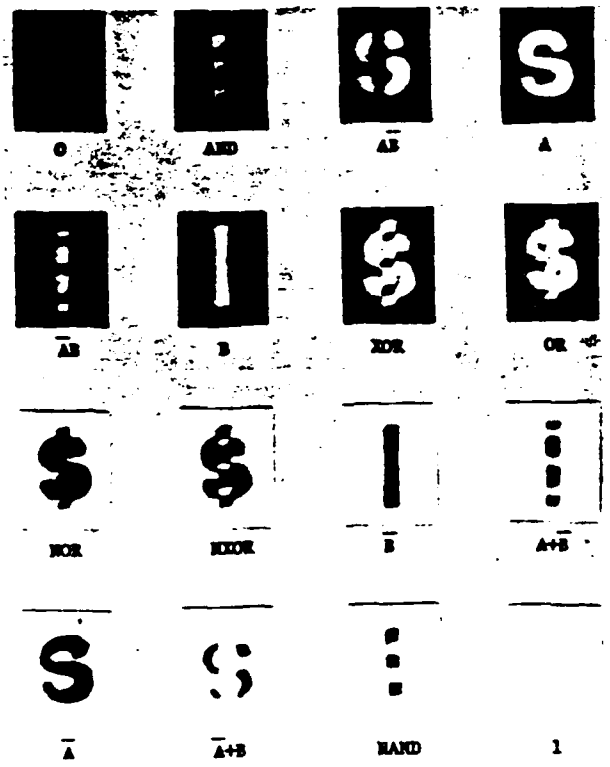

Fig. 4. Experimental results of the 16 Boolean operations.

Fig. 5. A demonstration of a consecutive logic operation.

to the computer. The computer can use this as a new input operand for the next operating cycle.

Finally, for experimental demonstrations, the 16 Boolean operations are shown in Fig. 4. In the experiment, the input illumination is from a white-light point source and the readout illumination is from a He–Ne laser. From these results, we see that the parallel-processing advantage of optics is fully utilized. The speckle noise in the results is due to the high degree of coherence of the readout laser light. The distortion of the output comes mainly from the imperfection of the microchannel plate and the photoelectron imaging system within the MSLM; it also arises from the nonuniformity of the E-O crystal plate. Although the results are not ideal, we believe that they can be significantly improved with an improvement in the MSLM. Further, Fig. 5 shows an experimental result of a consecutive logic operation obtained with this setup. This demonstration indicates that, in principle, the hybrid system can perform a series of consecutive operations. In other words, it can work as a Boolean algebraic calculator.

We have presented an optical system that is capable of performing binary Boolean logic operations with a MSLM and LCTV's. The logic states of the input and output data arrays are represented by light intensity. Combining the merits of the MSLM, the LCTV's, and a computer, the system offers the advantages of optical parallel-processing capability, programmability, and feedback consecutive-processing flexibility. With advances in MSLM performance, the performance of this optical system is expected to improve, resulting in faster response, higher resolution, and less image distortion.

Support from Hamamatsu Photonics KK, which provided the MSLM device, and from the U.S. Air Force Office of Scientific Research under grant AFOSR-86-0264 are acknowledged.

References

1. B. Horwitz and F. Corbett, Opt. Eng. 17, 353 (1978).
2. T. Minemoto, K. Okamoto, and K. Miyamoto, Appl. Opt. 24, 2055 (1985).
3. R. A. Athale and S. H. Lee, Opt. Eng. 18, 513 (1979).
4. M. T. Fatehi, K. C. Wasmundt, and S. A. Collins, Jr., Appl. Opt 20, 2250 (1981).
5. F. T. S. Yu, S. Jutamulia, and D. A. Gregory, "A real-time LCTV XOR-and-XNOR-gate binary image subtraction technique," Appl. Opt. 26, 2738 (1987).
6. F. T. S. Yu, S. Jutamulia, and T. W. Lu, "Optical parallel logic based on magneto-optic spatial light modulator," submitted to Opt. Commun.
7. C. Warde and J. Thackara, Opt. Eng. 22, 695 (1983).
8. T. Hara, N. Mukohzaka, and Y. Suzuki, Proc. Soc. Photo-Opt. Instrum. Eng. 625, 30 (1986).
9. F. T. S. Yu, Q. W. Song, and X. J. Lu, "Operating characteristics and applications of a microchannel spatial light modulator under white-light illumination," submitted to Appl. Opt.
10. C. Warde, Proc. Soc. Photo-Opt. Instrum. Eng. 236, 398 (1980).
11. J. A. McEwan, A. D. Fisher, and J. Lee, in *Digest of Conference on Lasers and Electro-Optics* (Optical Society of America, Washington, D.C., 1985), postdeadline paper PD-1.

SECTION 10

Optical Binary Adder

Optical Binary Adder Using Liquid Crystal Television

Yong Jin and Francis T.S. Yu

Electro-Optics Laboratory

Electrical Engineering Department

The Pennsylvania State University

University Park, PA 16802

Abstract

This paper describes the methods of implementing an optical half-adder and a full adder utilizing programmable liquid crystal televisions (LCTV). The concept of constructing an optical full adder is based upon the realization of an optical read-only-memory (OROM). An experimental demonstration of binary number addition performed by an optical half-adder is given.

I. INTRODUCTION

Prior to our discussion, we note that the optical binary adder, when used in digital optical computing, is a basic part of the central processing unit (CPU). Methods of making an optical half-adder and full adder have been proposed by several investigators in the past few years [1,2]. Having already built a 4-bit half adder, Lohmann and Weigelt have proposed a 1-bit full adder that is based on the spatial filtering technique [1]. In order to implement a 1-bit half-adder, Khan and Nejib [2] have proposed an optical structure that employs liquid crystal switches. In addition to these, we have recently proposed a method that performs XOR logical operations utilizing liquid crystal televisions (LCTV) [3]. The XOR logical operation is in fact a key operation in a binary adder.

The basic difference between a half-adder and a full adder is the carry-transmission. A 1-bit half-adder, however, does not require carry input. If two bits, Ai and Bi, are added together, the half-adder would produce a sum Si, and a carry Ci+1, i.e., $Si=Ai \oplus Bi$, $Ci+1 = Ai \cdot Bi$. In a 1-bit full adder, three inputs, Ci, Ai, and Bi, would also produce a sum and a carry, i.e., $Si = Ai \oplus Bi \oplus Ci$ and $Ci+1 = (Ai \oplus Bi) \cdot Ci + Ai \cdot Bi$. In a n-bit full adder (n>1), the carry is transfered bit by bit from the least significant bit (LSB) to the most significant bit (MSB). We stress that the main difficulty in building an n-bit optical full adder lies within the realization of carry-transmission. To overcome this problem, the optical Read-only-Memory (OROM) is introduced.

In this paper, we propose a multi-channel optical half-adder using LCTVs. This optical half-adder is capable of performing the XOR, AND, NOT, and OR logical operations. An experimental demonstration of the proposed half-adder is provided. Finally, by introducing OROM to the system, we can realize a 2-bit optical full adder.

II AN OPTICAL HALF-ADDER

The logical operations of a half-adder produce a sum Si and a carry Ci+1 such as:

$$Si = Ai \oplus Bi \ , \qquad (1)$$

$$Ci+1 = Ai \cdot Bi \ , \qquad (2)$$

where Ai and Bi are the input bits. Since XOR and AND operations are required in a half-adder, they can easily be implemented with LCTVs as shown in Fig.1. In the optical system, two microcomputers are used in order to produce the image patterns for A and B onto two LCTVs. Two LCTVs perform the XOR operations with the polarization logic in which the logical "0's" are encode on horizontal polarization while the logical "1's" are encoded in vertical polarization. To perform the XOR and AND operations in parallel, it is required that pattern B is written twice (e.g., B2 is the extra copy of B in Fig.1). The sum, S, produced by the LCTVs is directly detected by an analyzer. The intensities of patterns A and B can be combined together to perform the logical operation OR, which is basically performed in the intensity logic. We note that a polarizer set in the contrast reverse mode can be using as a NOT gate. Therefore, an AND gate can be implemented with the optical structure shown in Fig.4. In this structure, the DeMorgan's Theorem is applied, such as,

$$X \cdot Y = \overline{\overline{X} \oplus \overline{Y}}. \qquad (3)$$

In experimental demonstrations, we used four-channel half addition in parallel. We have chosen the following values to reflect the general case.

$$A1 = 0,\ A2 = 1,\ A3 = 1,\ A4 = 0\ ; \qquad (4)$$

$$B1 = 0,\ B2 = 1,\ B3 = 0,\ B4 = 1\ . \qquad (5)$$

Consequently the output data would be,

$$S1 = 0,\ S2 = 0,\ S3 = 1,\ S4 = 1\ ; \qquad (6)$$

$$C1 = 0,\ C2 = 1,\ C3 = 0,\ C4 = 0\ . \qquad (7)$$

The results obtained, which include two input patterns and two output patterns, are shown in Fig.3. Note that the distance between two LCTVs should satisfy the following inequality condition [3]:

$$z < d / \lambda, \qquad (8)$$

where z is the distance between two LCTVs, d is the width of a square resolution cell, and λ is the wavelength of the light source. In our experiment, a He-Ne laser oscillating at λ = 632.8 nm is used. Since the resolution of LCTV d = 370 um, we set the distance between the LCTVs to about 20cm (see Fig.1).

Although, 15x20 pixels were used to represent 1-bit data in our experiment, fewer pixels, as small as one pixel in 1-bit, can be used in this experiment. To reduce the coherent artifact, a white light source can be used in the system [4].

III. AN OPTICAL FULL ADDER

To add the new carry-in to the inputs of A and B at the LSB, the n-bit full-adder should have the capabilities of performing the carry-transmission (between the successive bits from LSB to MSB) and of detecting the overflow errors. For an n-bit full adder, Si and Ci can be obtained by recurrent equations.

$$SSi = Ai \oplus Bi \oplus CCi, \qquad (9)$$

$$CCi+1 = (Ai \oplus Bi)\cdot CCi + Ai\cdot Bi, \qquad (10)$$

where SSi represents the ith sum bit and CCi denotes the ith carry output bit of full adder.

The simplest means of implementing a full adder is to feed the carries bit by bit. This, however, is not an easy task to perform when using an optical processor. Nevertheless, with the addition of an OROM, an optical processor can perform the carry transmission, as proposed in Fig.4 and Fig.5. In other words, the OROM can allows a full adder to perform addition in parallel without feeding carries. We further note that OROM is a digital logic device that can be implemented with any binary logical function.

In a 2-bit full adder, the sum SS and the Cout can be produced by Si and Ci that have been obtained from the output of the improved half-adder. Let us now state the following relations:

$$SS1 = A1 \oplus B1 \oplus Cin = S1, \qquad (12)$$

$$CC2 = \overline{S1}\cdot Cin + A1\cdot B1 = \overline{S1}\cdot Cin + C2, \qquad (13)$$

$$SS2 = S2 \oplus CC2 = S2\cdot\overline{CC2} + \overline{S2}\cdot CC2, \qquad (14)$$

$$Cout = \overline{S1}\cdot S2\cdot Cin + C2\cdot S2 + C3, \qquad (15)$$

where Ai and Bi are the input patterns, Cin is the carry input, Si and Ci are the ith output sum and carry obtained from the improved half-adder,

and Cout is the carry output of the full adder. We stress again that The relations of Eq. (12)-(15) can be implemented with an optical processor using OROM , as shown in Fig.6. The logic diagram for this setup is illustrated in Fig.7.

Overflow error occur whenever the addition of two numbers results in a sum which is too large or too small to be represented by n bits. Consequently, the detection of overflow errors is required for a full adder. This is done by utilizing the well-known rules, for unsigned number,

$$E = Cout, \tag{16}$$

and for signed number,

$$E = Cn \oplus Cn+1, \tag{17}$$

where E=0 and E=1 indicate overflow error and no overflow error respectively.

Thus, in a 2-bit full adder, we would have,

$$E = CC2 \oplus Cout = CC2 \cdot \overline{Cout} + \overline{CC2} \cdot Cout \tag{18}$$

This logical operation may be performed by an optical processor using an OROM, as proposed in Fig.8.

IV. CONCLUSION

We have demonstrated method of building an optical half-adder using a programmable LCTVs. An experimental demonstration shows that a 4-bit half-addition can be obtained. This result shows the general case for optical half-adder. The optical half-adder can be easily extended to perform larger-arrays-number addition, by simply changing the computer

program of the microcomputer. We note that no extra coding procedure is required in the half-adder, since the number was automatically encoded by the LCTV. To extend a half-adder to perform a full adder operation, we introduce an OROM for carry transmission and overflow error detection. An optical architecture of 2-bit full adder using OROM is also proposed in this paper.

V. ACKNOWLEDGMENT

We acknowledge the support of the U.S. Air Force Office of Scientific Research grant AFOSR-86-0264.

Figure Catalog

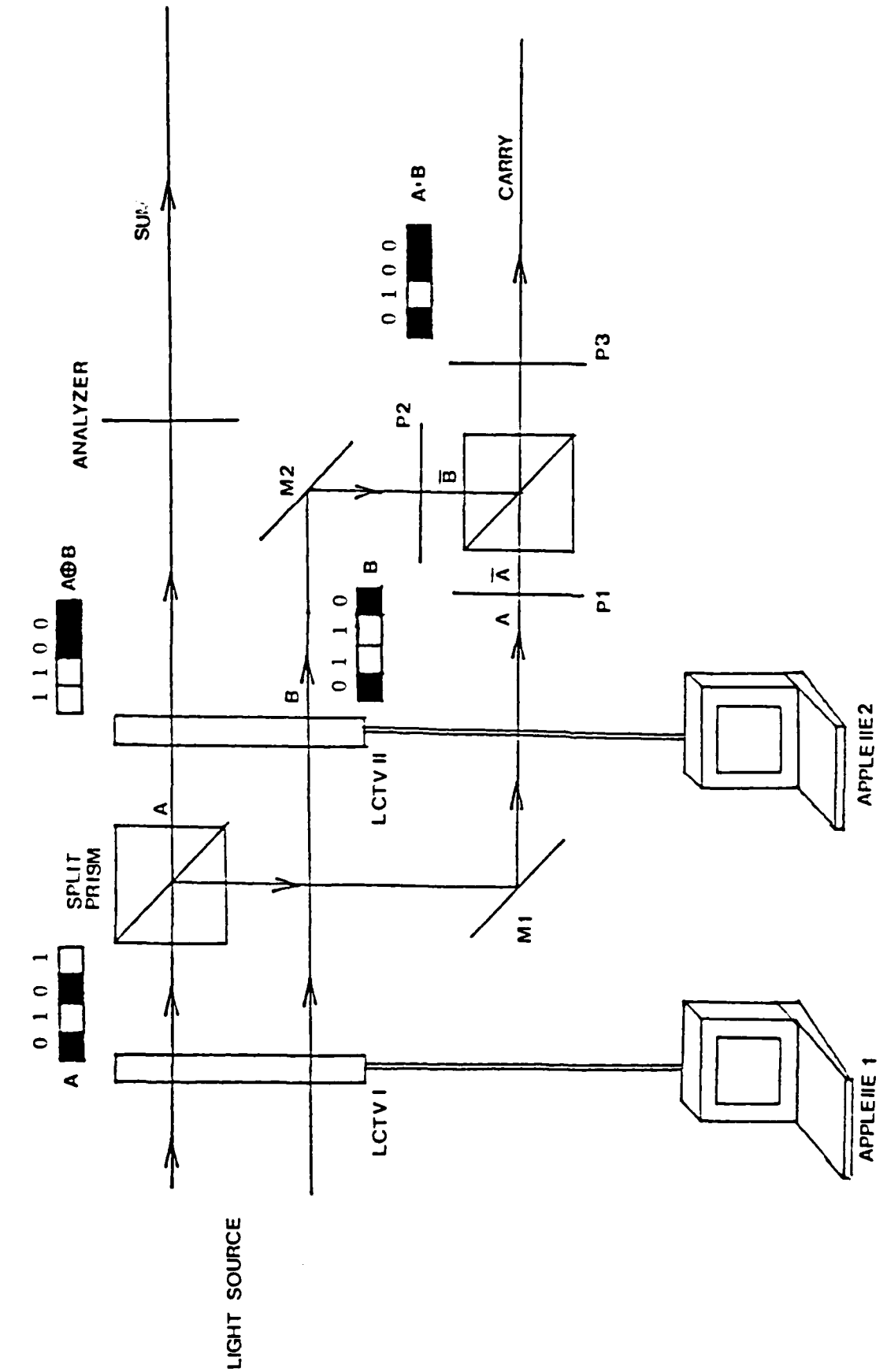
LIGHT SOURCE
A
0 1 0 1
SPLIT PRISM
A
LCTV I
APPLE IIE 1
M1
A
P1
Ā
P2
B̄
M2
B
0 1 1 0
B
LCTV II
APPLE IIE 2
1 1 0 0
A⊕B
ANALYZER
SUM
0 1 0 0
A·B
CARRY
P3

Fig. 1

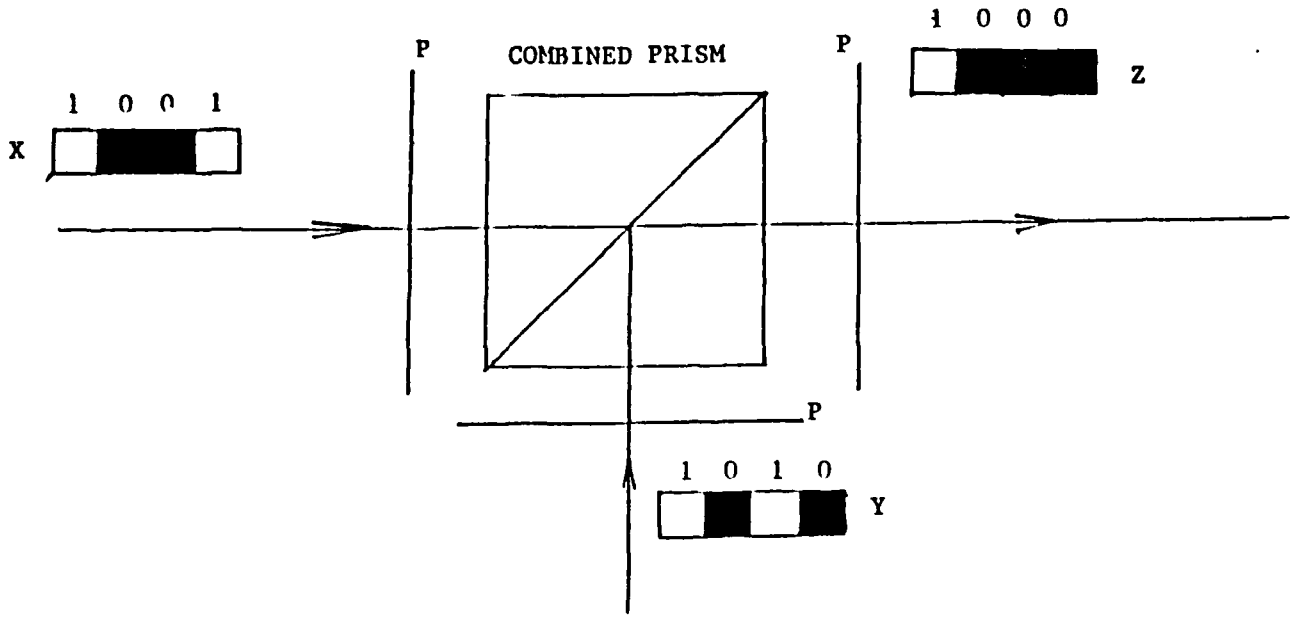

Fig. 2

A

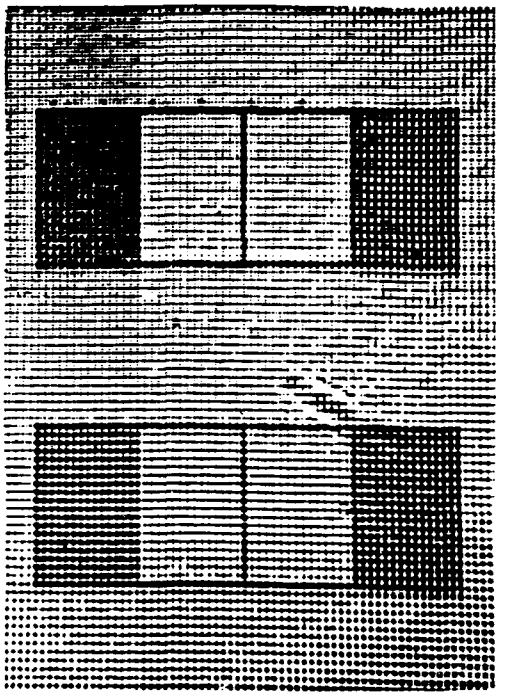

B

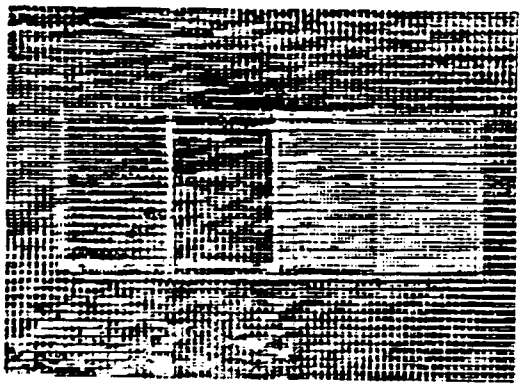

S

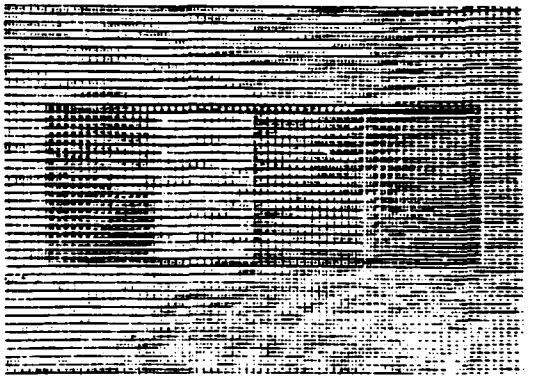

C

Fig. 3

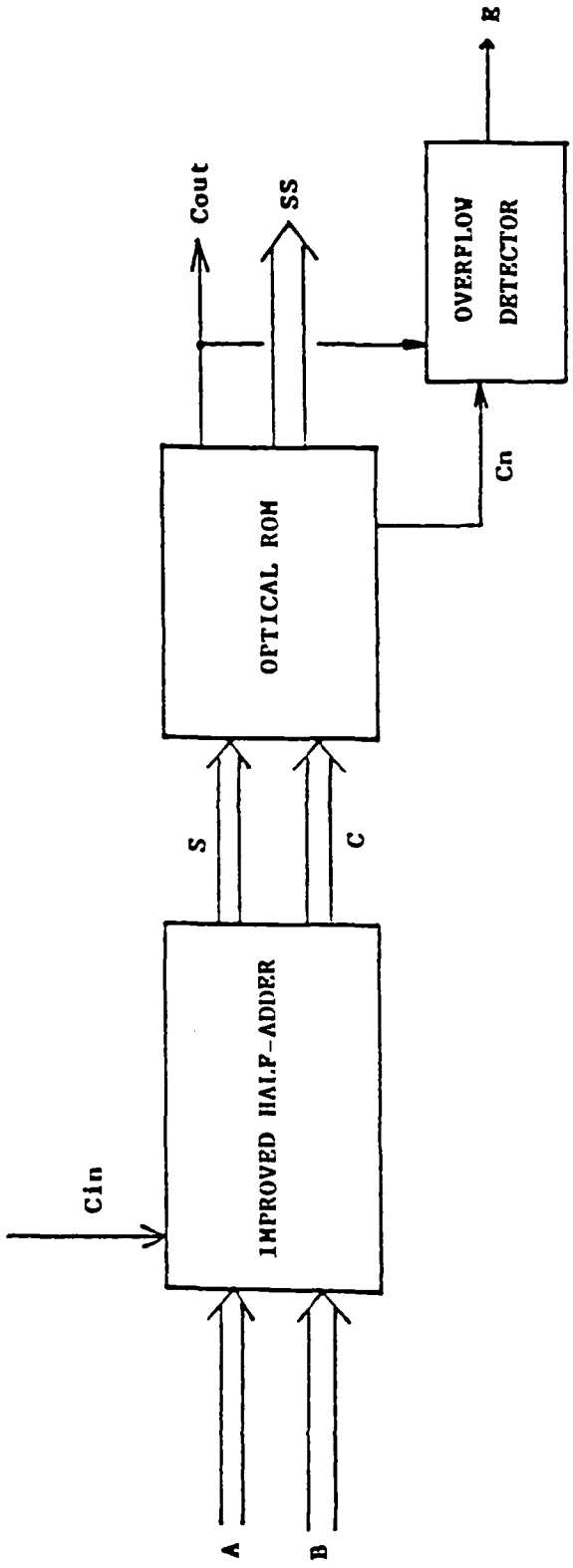
A
B
Cin
IMPROVED HALF-ADDER
S
C
OPTICAL ROM
Cn
Cout
SS
OVERFLOW DETECTOR
E

Fig. 4

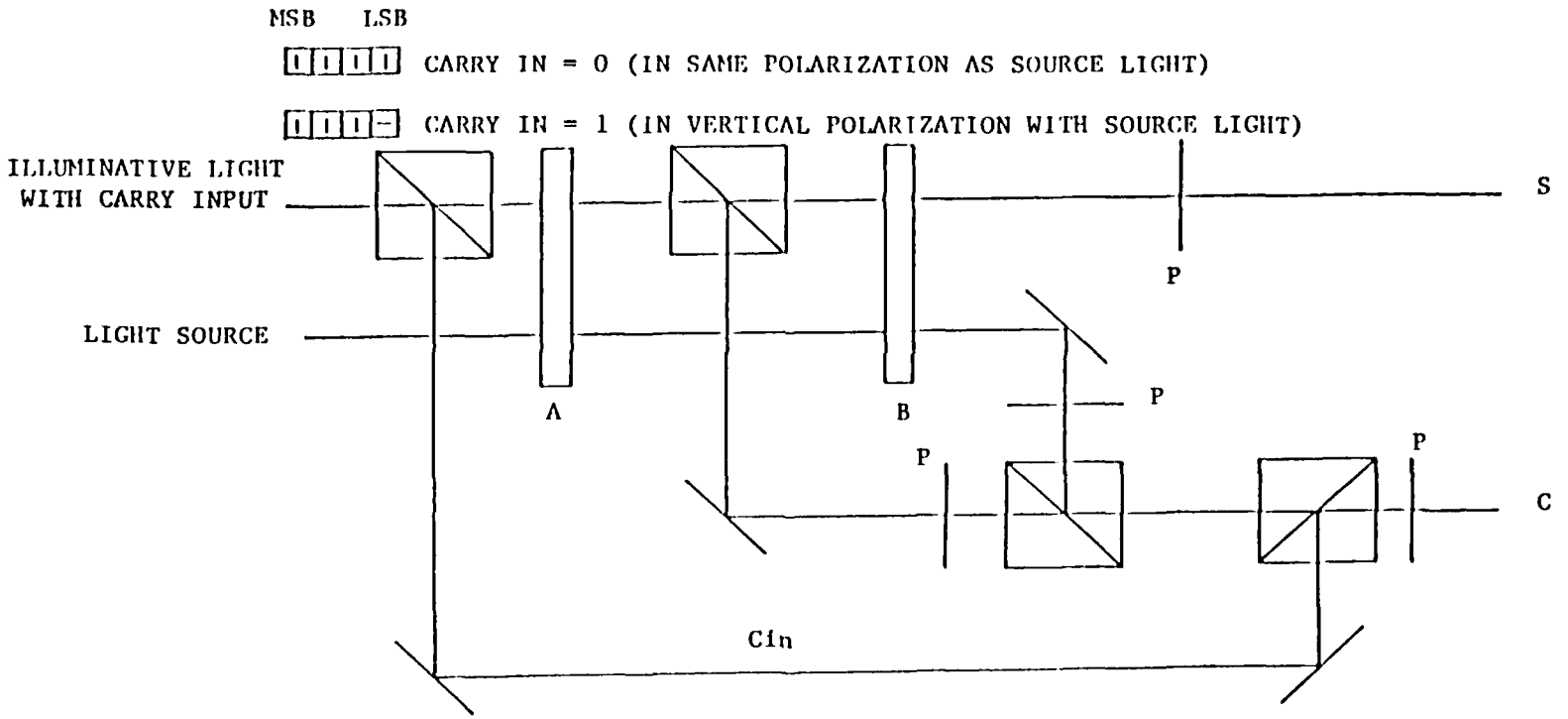
MSB LSB
1 1 1 1 CARRY IN = 0 (IN SAME POLARIZATION AS SOURCE LIGHT)
1 1 1 - CARRY IN = 1 (IN VERTICAL POLARIZATION WITH SOURCE LIGHT)
ILLUMINATIVE LIGHT WITH CARRY INPUT
LIGHT SOURCE
A
B
P
P
P
P
S
C
Cin

Fig.5

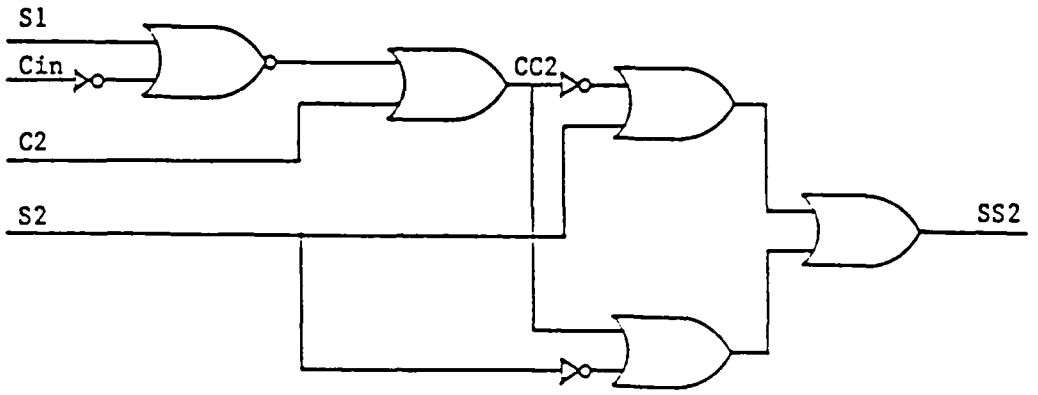

(a)

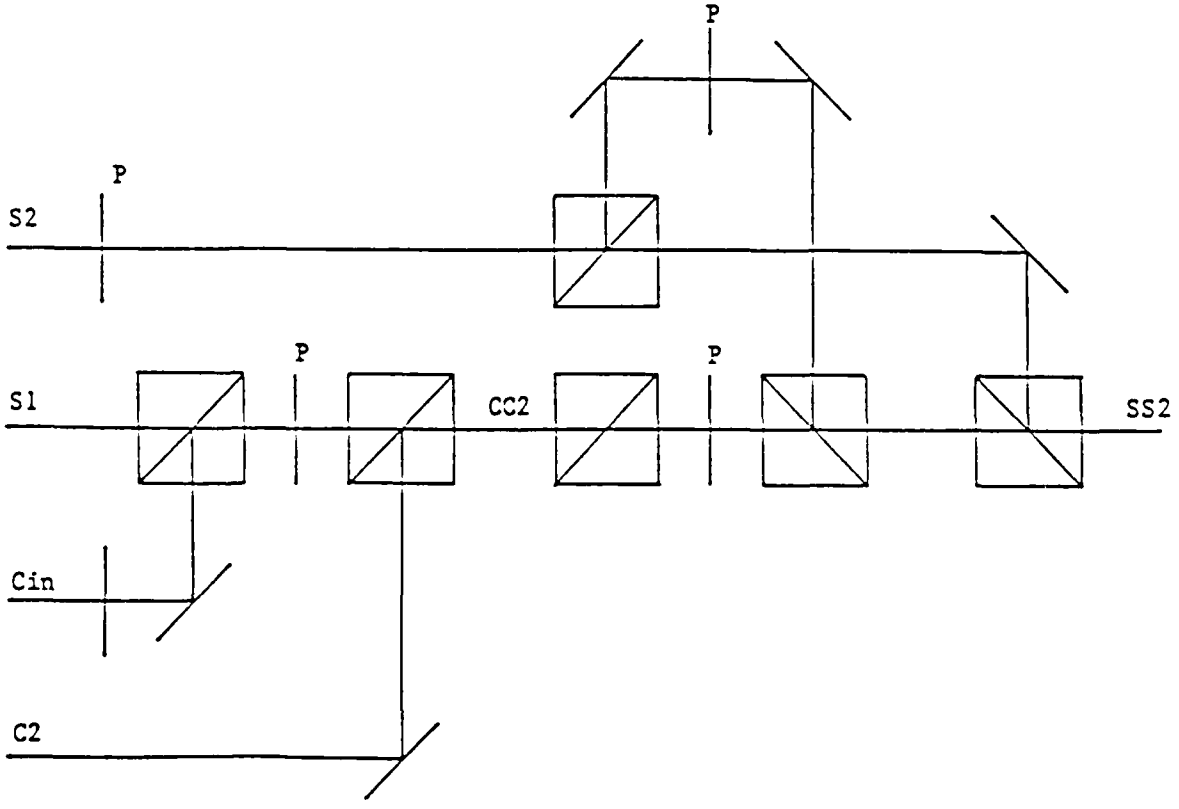

(b)

Fig. 6

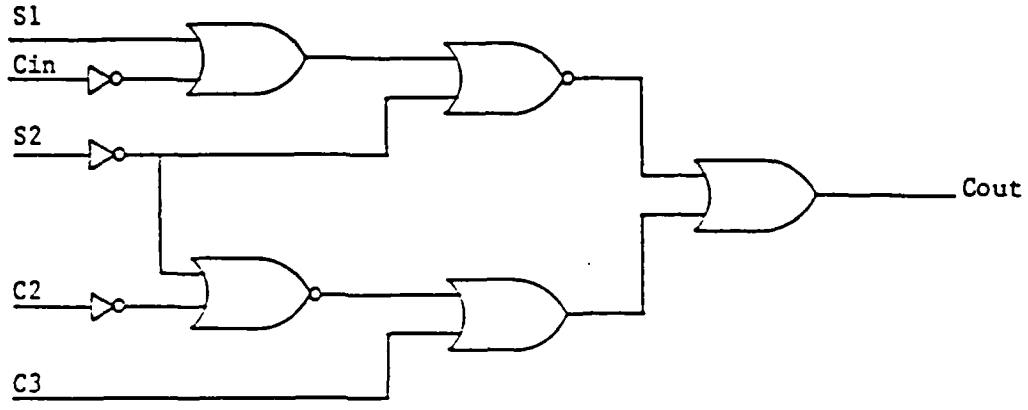

(a)

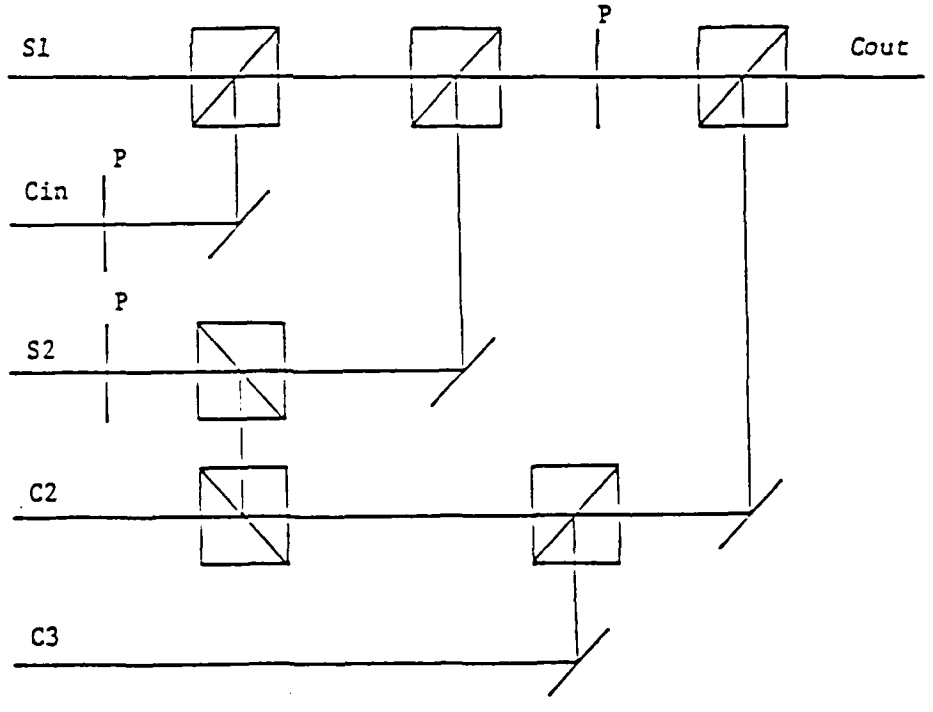

(b)

Fig. 7

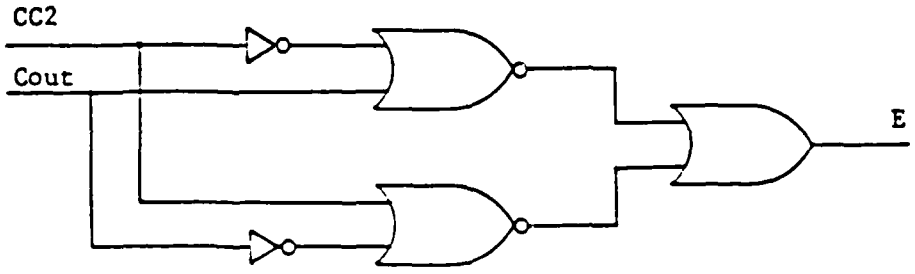

(a)

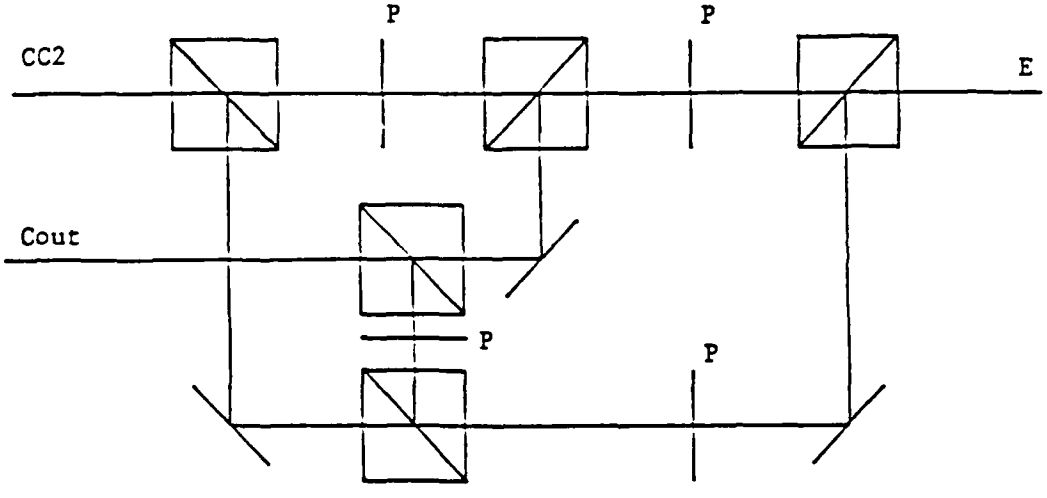

(b)

Fig. 2

SECTION 11

Digital-Optical Matrix Multiplication

DIGITAL OPTICAL ARCHITECTURES FOR MULTIPLE MATRIX MULTIPLICATION

Francis T.S. Yu, Taiwei Lu and Miao-Fu Cao
Department of Electrical Engineering
Pennsylvania State University
University Park,PA16802

ABSTRACT

Two optical architectures utilizing a binary number algorithm for multiple matrix multiplication are presented. An inner-product technique is utilized in one of the architectures, so that multiple matrix multiplication can be performed in parallel. For the other architecture, systolic array processing along with the inner-product method are used. This technique would alliviate the bottleneck effect that is due to the electro-optic interfacing and the complexity of the high order matrix operations. We show that both architectures can offer high accuracy and high speed processing capabilities.

I. Introduction

Optical matrix multiplication is one of the prominent areas in optical computing. In early 1970's, Lee et al.[1] proposed a method to perform multiple matrix multiplication using the Fourier transform property of lenses. Another architecture was later developed by Nakano et al.[2]. They utilized a linear array of LED's along with a combination of spherical lenses and cylindrical lenses to perform triple matrix multiplication. Some efforts have also been made to carry out high speed matrix-matrix and triple matrix multiplication [3-4].

We shall however in this paper describe a method for multiple binary number multiplication. The essential merit of this proposed method is that the multiplications and summations of digits are performed in parallel.

We shall discuss two optical architectures for multiple matrix multiplication. The first architecture employs the inner-product method to carry out Multiple Matrix Multiplication (MMM) for which high accuracy and high speed operations can be achieved. The second architecture combines the inner-product method with the systolic array engagement technique. This inner-product-systolic technique is capable of large matrix multiplication and can also be applied to linear and bilinear transformations. Several preliminary experimental demonstrations of these proposed techniques are provided.

of these proposed techniques are provided.

II. System Description

1) Multiple Binary Number Multiplication

In most electronic computers the binary number multiplication is performed sequentially. The operation of the multiplication of three binary numbers by a computer is carried out as follows:

The three binary numbers are

a = 111 ;

b = 110 ;

c = 011 .

'b' is multiplied by the least significant bit (LSB) of 'a'; 'b' is shifted one bit to the left, multiplied by the second bit of 'a'; 'b' is shifted left again, multiplied by the most significant bit (MSB) of 'a'; then a summation is taken over the three multiplication results and the intermediate result 'ab' is obtained:

```
        1 0 1     x 0
      1 0 1       x 1
  +   1 0 1       x 1
-------------------------
    1 1 1 1 0
```

ab = a x b = 101 x 110 = 11110 .

The same procedure is repeated between the intermediate result 'ab' and 'c' to produce the result abc.

```
      1 1 1 1 0   x 1
    1 1 1 1 0     x 1
  + 1 1 1 1 0     x 0
  -----------------
    1 0 1 1 0 1 0
```

abc = ab x c = 11110 x 011 = 1011010 .

However the three binary number multiplication can be performed in parallel using an optical system as shown in Figure 1(a). In the optical system, 'a' is encoded on a 1-D spatial light modulator (SLM), b and c are pre-shifted and encoded on two 2-D SLM's. The digit '1' is represented by the transparent spots on masks, whereas '0' and blank are opaque. The three masks are placed at planes X1, X2 and X4 respectively. The intermediate product ab is obtained at plane X3 and the final result abc is at the plane X5. Notice that the results are in mixed binary form to avoid carries. It is easy for a computer to convert mixed binary numbers to binary numbers[6]. Figure 1(b) shows the optical implementation for triple binary number multiplication. Both the binary number multiplication and the matrix multiplication involve many multiplication and addition operations. In the system, the multiplications are performed by the transmittances of the SLM's, and the additions are carried out by focusing the light into a point. An incoherent collimated light is incident on plane X1; the cylindrical lens CL1 at plane X1 expands each bit of 'a' horizontally to illuminate SLM2 such that the multiplications take place; the spherical lens SL1 focuses the light vertically on plane X3 to perform the

summation. A cylindrical lens CL2 at X3 expands each bit of the intermediate product ab to be incident on the corresponding column of SLM3. Spherical lens SL2 performs summations vertically again. The final result is detected at plane X5 using the CCD detector.

2) Multiple Matrix Multiplication (MMM)

An architecture for vector-matrix-matrix multiplication is first described. The vector-matrix-matrix multiplication can be written as

$$[x1\ x2]\begin{vmatrix} y11 & y12 \\ y21 & y22 \end{vmatrix}\begin{vmatrix} z11 & z12 \\ z21 & z22 \end{vmatrix} = [x1y11+x2y21\ \ x1y12+x2y22]\begin{vmatrix} z11 & z12 \\ z21 & z22 \end{vmatrix}$$

$$=[u1\ u2]\begin{vmatrix} z11 & z12 \\ z21 & z22 \end{vmatrix} \quad (1a)$$

$$=[u1z11+u2z21\ \ u1z12+u2z22] \quad (1b)$$

$$=[v1\ v2], \quad (1c)$$

where $u1=x1y11+x2y21;$ (2a)

$u2=x1y12+x2y22;$ (2b)

$v1=u1z11+u2z21;$ (2c)

$v2=u1z21+u2z22.$ (2d)

The architecture of vector-matrix-matrix multiplication is shown in Fig.2(a). The vector [x] is encoded on SLM1, and two matrices [Y] and [Z] are on SLM2 and SLM3 respectively. Notice that each element of vector [X] and matrices [Y] and [Z] is in the binary form described in Fig.1(a). All the multiplications for [X] x [Y] are carried out between plane X1 and X2 and all the

summations are performed between plane X2 and X3. The same procedures are repeated between X3 and X4, X4 and X5 to perform [U] x [Z].

We can also perform the multiple matrix multiplication by using this architecture. The first matrix

$$[X]=\begin{vmatrix} x11 & x12 \\ x21 & x22 \end{vmatrix}$$

is decomposed into two vectors X1=[x11 x12] and X2=[x21 x22]. The computer shifts the vectors into SLM1 sequentially. At the output plane the CCD detector detects each corresponding vector of the output matrix [V] sequentially as shown in Fig.2(b).

However, to make full use of the parallel processing capability of the optical system, an improved optical architecture to perform MMM in parallel is proposed. As is seen in Figs.3(a) and (b), the image on plane x3 can be considered as the one dimensional Fourier transform of the input signal on plane X1, by ignoring the existence of SLM2. To separate the two vectors [u11 u12] and [u21 u22] at the focus plane X3, two sinusoidal gratings with different frequences f1 and f2 are inserted immediately behind the two input vectors [x11 x12] and [x21 x22]. The two frequences are carefully chosen to get an appropriate separation distance h between vectors [u11 u12] and [u21 u22] on the X3 plane. In a similar manner, two sinusoidal gratings are placed behind the two vectors [u11 u12] and [u21 u22] at plane X3. Two separated vectors [v11 v12] and [v21 v22] are obtained at the output plane X5 as shown in Fig.3(b).

We have discussed the optical system for parallel MMM utilizing the inner-product method. However, in some applications such as bilinear transformation, the input signals are entered sequentially and the transformation matrix is large. The large size devices are not currently available. So we introduce another hybrid optical system which combines the systolic array engagement method with the inner-product method. This system can overcome the bottleneck effect due to the electro-optic interfacing. It is also easy to decompose the large matrices using this system. The optical system is controlled by a microcomputer. The matrices are shifted onto the SLM's (e.g. Magneto Optical SLM's (MOSLM's) or Liquid Crystal Televisions (LCTV's)) step by step, as shown in Fig.4. Here each matrix is arranged in a systolic array form. Each element of the matrices is encoded in the binary form shown in Fig.1(a). The CCD detector performs time integration of the output signal. For 2x2 matrices multiplication, the output matrix is obtained after four steps.

III. Experiment Demonstration

Several preliminary experiments are carried out based on the proposed optical architectures. The first one is a triple binary number multiplier, as shown in Fig.1 and Fig.5. A white light source, two cylindrical lenses with focal length 10mm and two spherical lenses each with focal length 100mm are used in the setup. Several masks with aperture size 2mm are used instead of

SLM's to prove the usefulness of the architecture. Figure 5(a) shows the three masks representing a = 101, b = 110, c = 011 respectively. Figure 5(c) shows the output signal in a mixed binary form (abc = 0122210) displayed on an oscilloscope. After passing through a thresholding circuit the output result is quantized and sent into a computer. The computer further converts the final result into binary form abc = 1011010, as shown in Fig 5(d).

The second experiment is for vector-matrix-matrix multiplication. The three masks in Fig.6(a) represent the vector [X]=[01000 00011] and two matrices

$$[Y]=\begin{vmatrix}00100 & 00001\\ 00011 & 00010\end{vmatrix} \qquad [Z]=\begin{vmatrix}10000 & 00010\\ 01000 & 00110\end{vmatrix}.$$

Figure.6(c) shows the horizontally expanded output signals in mixed binary forms displayed on a scope,

[V] = [0001121001100 0001331011000].

The final results in binary forms are shown in Fig.6(d),

[V] = [0010001001100 0011011011000].

The last experiment is a triple matrix multiplication based on the architecture described in Fig.2(b). The three matrices are

$$[X]=\begin{vmatrix}00100 & 01000\\ 00010 & 00011\end{vmatrix};\ [Y]=\begin{vmatrix}00100 & 00001\\ 00011 & 00010\end{vmatrix};\ [Z]=\begin{vmatrix}10000 & 00010\\ 01000 & 00110\end{vmatrix}.$$

Figure 7(c) shows the horizontally expanded output matrix [V] in mixed binary forms:

$$[V]=\begin{vmatrix}0001121001100 & 0001331011000\\ 0000010132000 & 0000101102000\end{vmatrix}.$$

After the output data is detected by the CCD camera, it passes through a thresholding circuit and is fed into a microcomputer. The computer finally converts it into binary form as shown in Fig. 7(d):

$$[V] = \begin{vmatrix} 0010001001100 & 0011011011000 \\ 0000011100000 & 0000101110000 \end{vmatrix}.$$

IX. Conclusion

We have presented a technique that can perform multiple binary number multiplication in parallel. Based on this technique two optical architectures for multiple matrix multiplication are developed. Since the matrices are in binary or mixed binary form and the processing is performed in parallel, these systems have the capability to perform high accuracy and high speed multiple matrix multiplication. Several preliminary experiments using photographic masks have been carried out. Future research will involve the hybrid optical system using real-time SLM's. The optical system will be controlled by a microcomputer. These architectures can also be applied to linear and bilinear transformations (The application to bilinear transformation will be discussed in a forthcoming paper).

Acknowledgement

We wish to acknowledge the support of U.S. Air Force of Scientific Research grant AFOSR-86-0264.

References

[1] R.A. Heinz, J.O. Artman and S.H. Lee, "Matrix Multiplication by Optical Methods," Appl. Opt. 9,2161(1970).

[2] H. Nakano and K. Hotate, "Real-time Processing of the Multiple Matrix Product Using an Incoherent Optical System," Appl. Opt. 24, 4238(1985).

[3] R.A. Athale and J.N. Lee, "Optical System for Efficient Triple-Matrix-Product Processing," Opt. Lett. 8, 590(1983).

[4] D. Psaltis, D. Casasent and M. Carlotto, "Iterative Color-Multiplexed, Electro-Optical processor," Opt. Lett. 4,348(1979).

[5] F.T.S. Yu, M.F. Cao and J.E. Ludman, "Microcomputer-Based Programmable Optical Signal Processor," Opt. Eng. 25,846(1986).

[6] R.P. Bocker, H.J. Caulfield and K.Bromley, "Rapid Unbiased Bipolar Incoherent Calculator Cube," Appl. Opt. 22, 804(1983).

[7] F.T.S. Yu, M.F. Cao and T. lu, "A Hybrid Optical System for Linear Transformation Processing," SPIE Vol.698, 276(1986).

AD-A190 076 STUDY OF MICROCOMPUTER-BASED REAL-TIME PROGRAMMABLE OPTICAL SIGNAL PROCES..(U) PENNSYLVANIA STATE UNIV UNIVERSITY PARK DEPT OF ELECTRICAL EN.. F T YU

2/2

UNCLASSIFIED 18 NOV 87 AFOSR-TR-87-1802 AFOSR-86-0264 F/G 12/6 NL

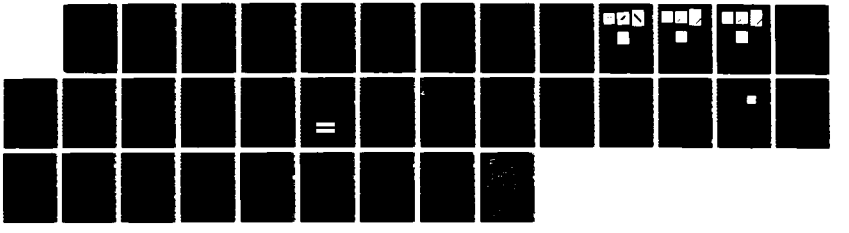

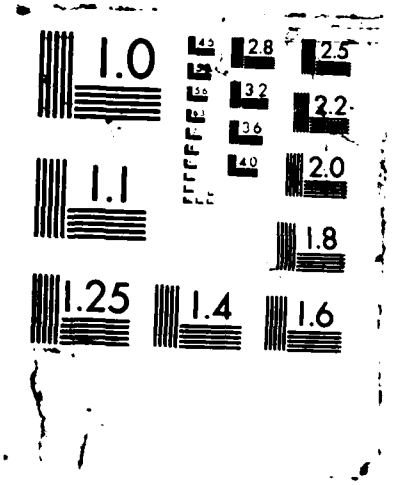
1.0
1.1
1.25
1.4
1.6
1.8
2.0
2.2
2.5
2.8
3.2
3.6
4.0

Figure Captions

Fig. 1: Optical system for triple binary number multiplication: a) the basic architecture, b) the optical implementation, c) top view of the system, d) side view of the system.

Fig. 2: Architecture for vector-matrix-matrix multiplication.

Fig. 3: a) Optical system implementation of MMM. b) Architecture for MMM.

Fig. 4: Architecture for MMM utilizing the systolic-inner product method.

Fig. 5: a) Three masks for triple binary number multiplication. b) Output signals detected on plane X5. c) Result displayed on an oscilloscope in mixed binary form. d) Final result in binary form.

Fig. 6: a) Three masks for vector-matrix-matrix multiplication. b) Output signals detected on plane X5. c) Output vector [v1 v2] displayed on an oscilloscope in mixed binary form. d) Final output vector [v1 v2] in binary form.

Fig. 7: a) Three masks for MMM. b) Output signals detected on plane X5. c) Output matrix [V] in mixed binary form. d) Final output matrix [V] in binary form.

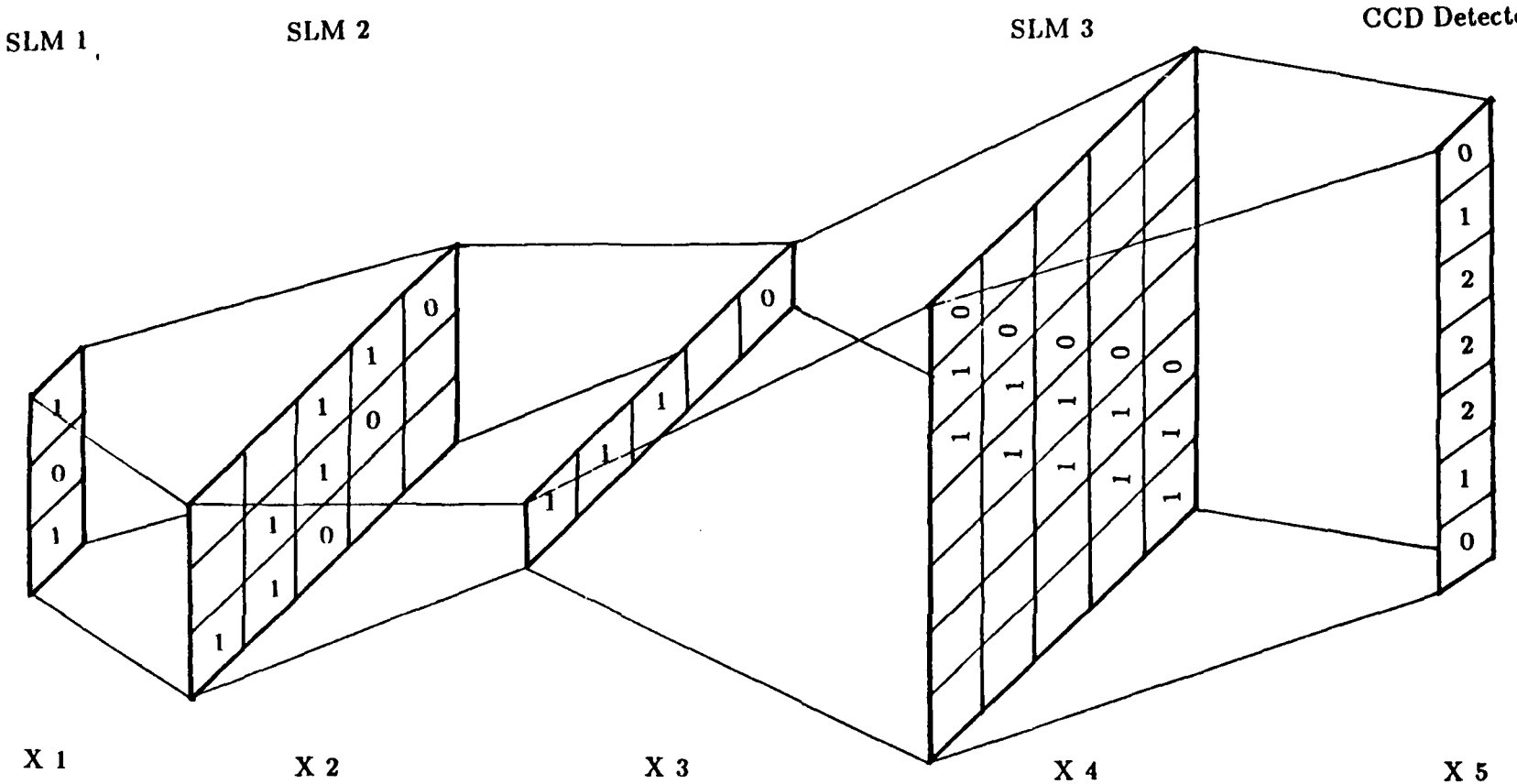

(a)

Fig. 1

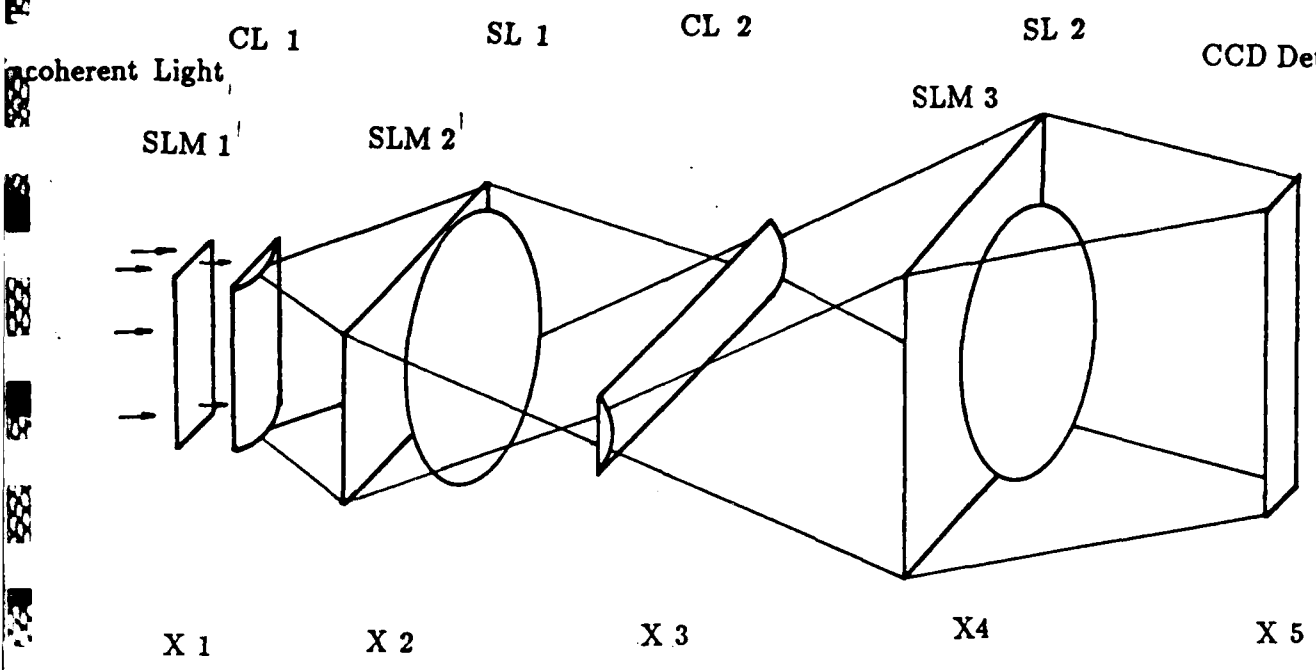
CL 1
SL 1
CL 2
SL 2
CCD Detector
coherent Light
SLM 3
SLM 1
SLM 2
X 1
X 2
X 3
X4
X 5

(b)

Fig. 1

Incoherent Light

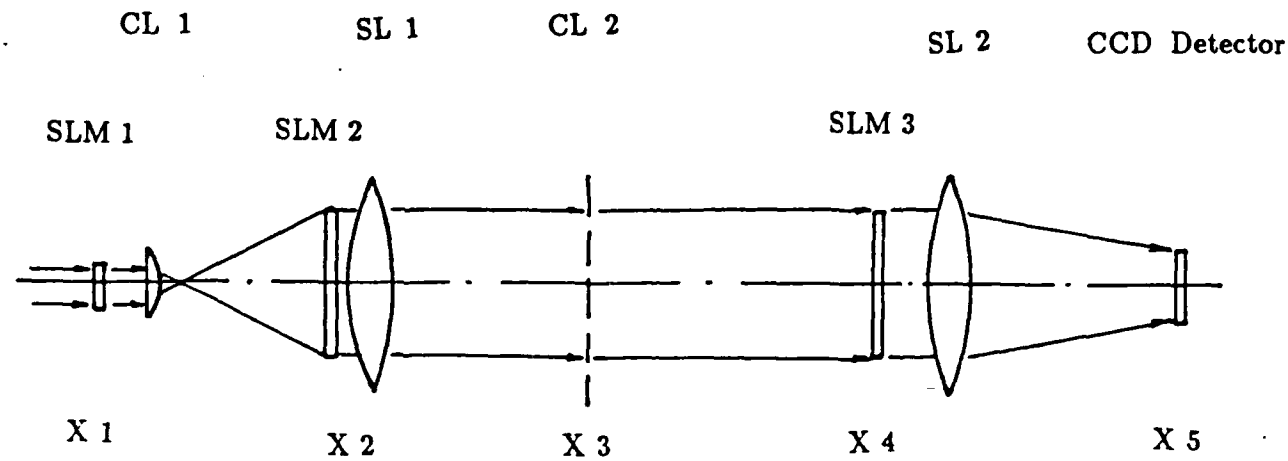

(c)

Incoherent Light

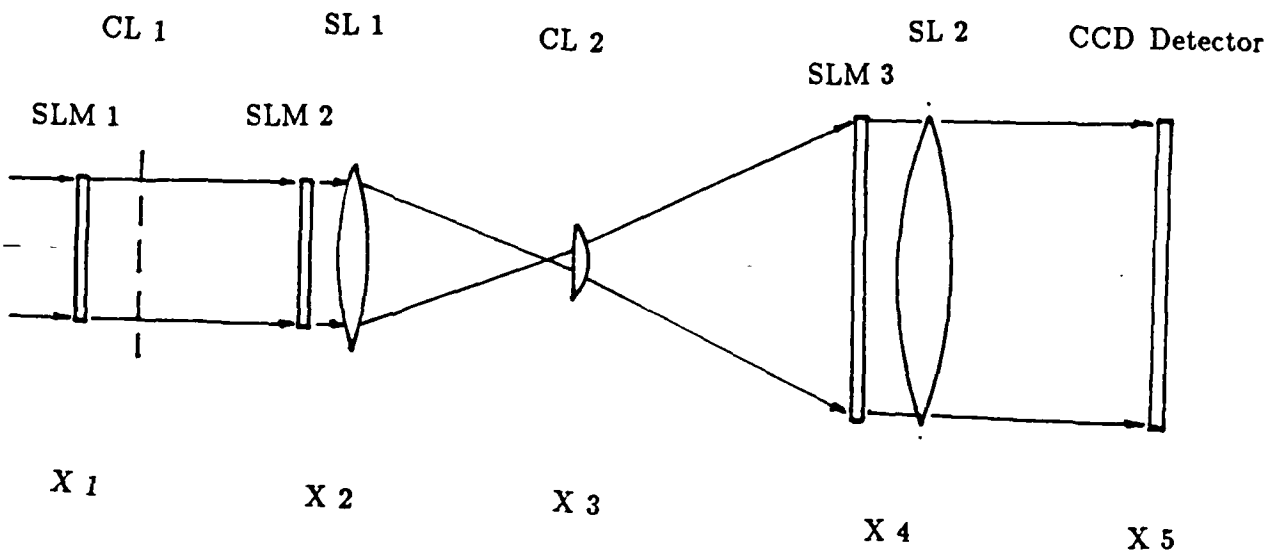

(d)

Fig. 1

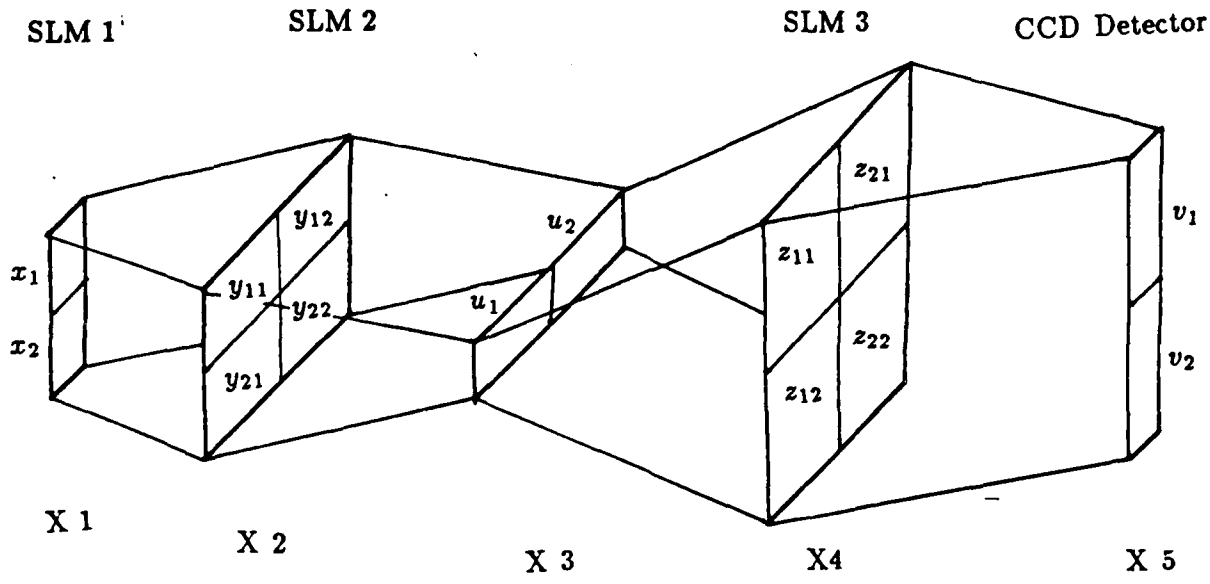
SLM 1
SLM 2
SLM 3
CCD Detector
x_1
x_2
y_{12}
y_{11}
y_{22}
y_{21}
u_2
u_1
z_{21}
z_{11}
z_{22}
z_{12}
v_1
v_2
X 1
X 2
X 3
X4
X 5

(a)

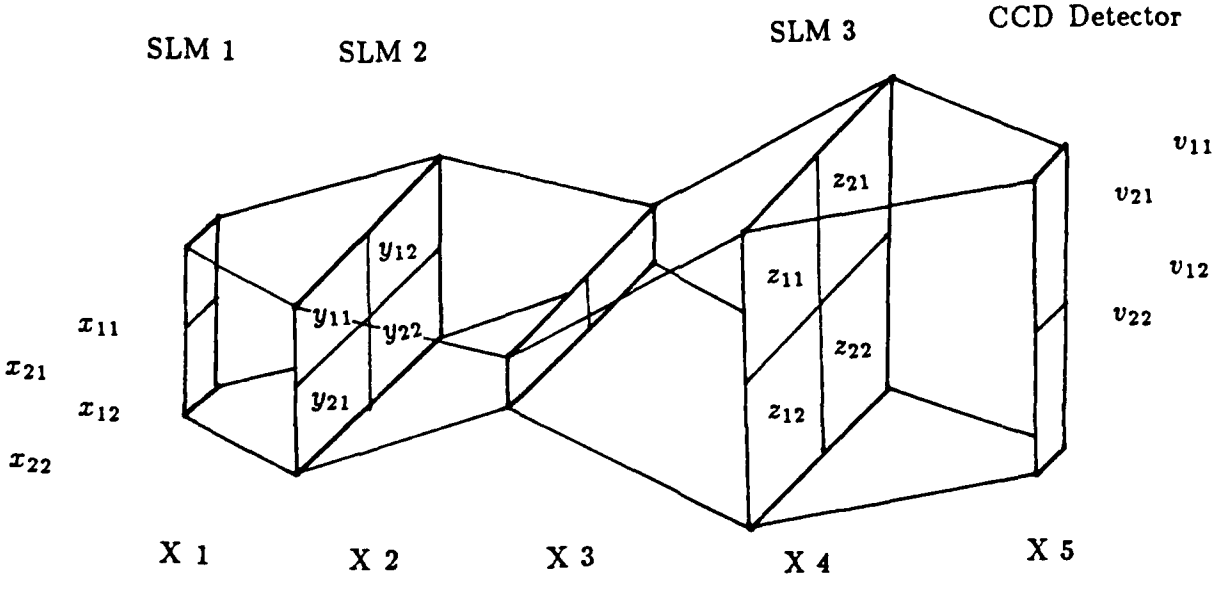
SLM 1
SLM 2
SLM 3
CCD Detector
x_{11}
x_{21}
x_{12}
x_{22}
y_{12}
y_{11}
y_{22}
y_{21}
z_{21}
z_{11}
z_{22}
z_{12}
v_{11}
v_{21}
v_{12}
v_{22}
X 1
X 2
X 3
X 4
X 5

(b)

Fig. 2

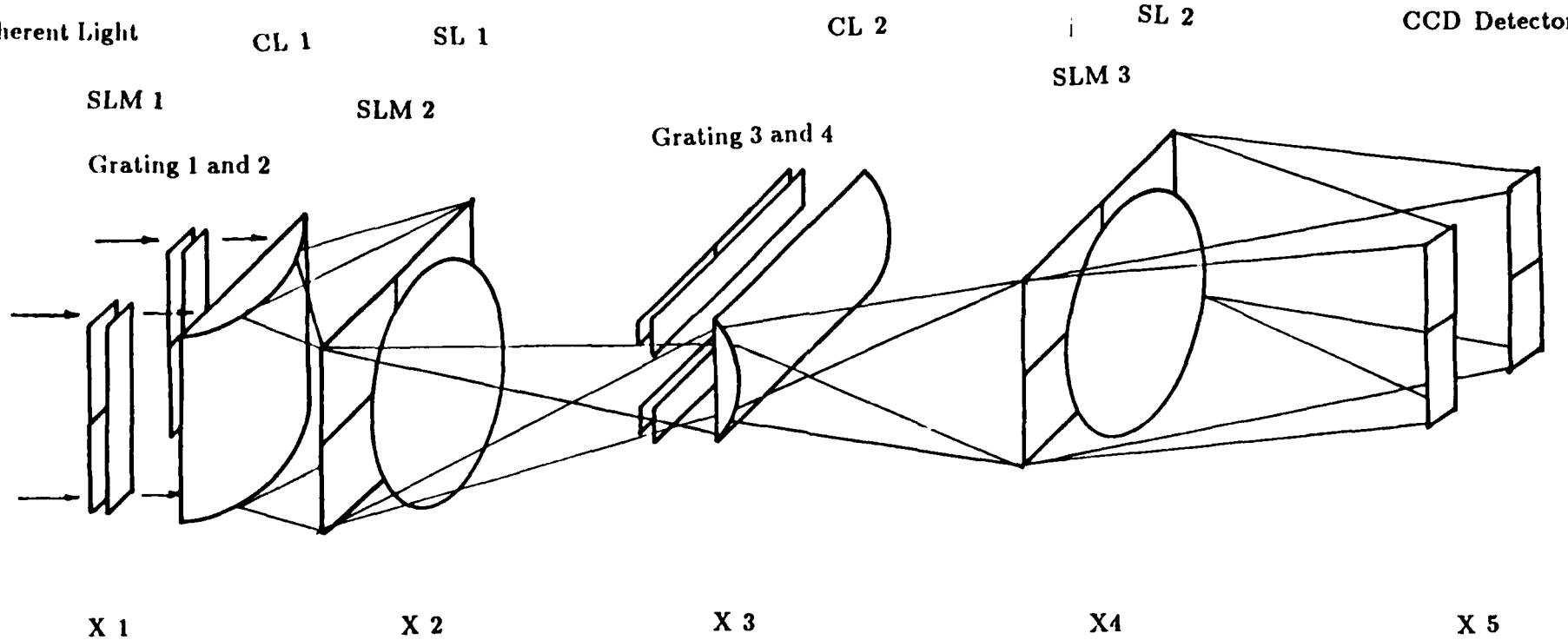
ncoherent Light
CL 1
SL 1
CL 2
SL 2
CCD Detector
SLM 1
SLM 2
SLM 3
Grating 1 and 2
Grating 3 and 4
X 1
X 2
X 3
X4
X 5

(a)

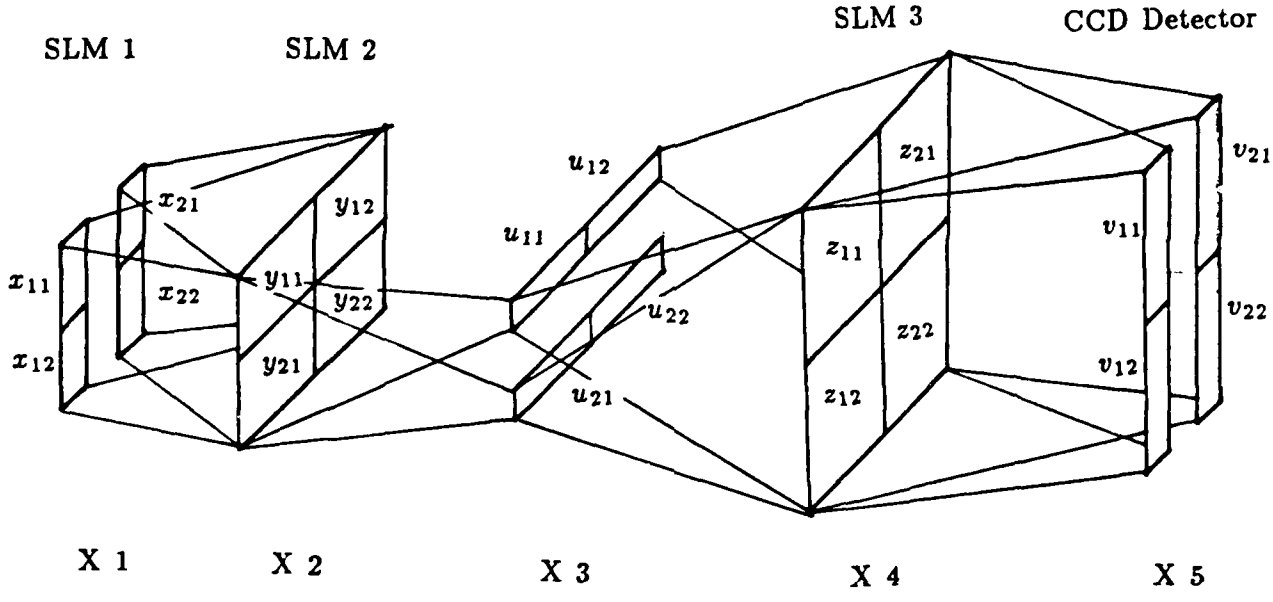
SLM 1
SLM 2
SLM 3
CCD Detector
x_{11}
x_{12}
x_{21}
x_{22}
y_{11}
y_{12}
y_{21}
y_{22}
u_{11}
u_{12}
u_{21}
u_{22}
z_{11}
z_{12}
z_{21}
z_{22}
v_{11}
v_{12}
v_{21}
v_{22}
X 1
X 2
X 3
X 4
X 5

(b)

Fig. 3

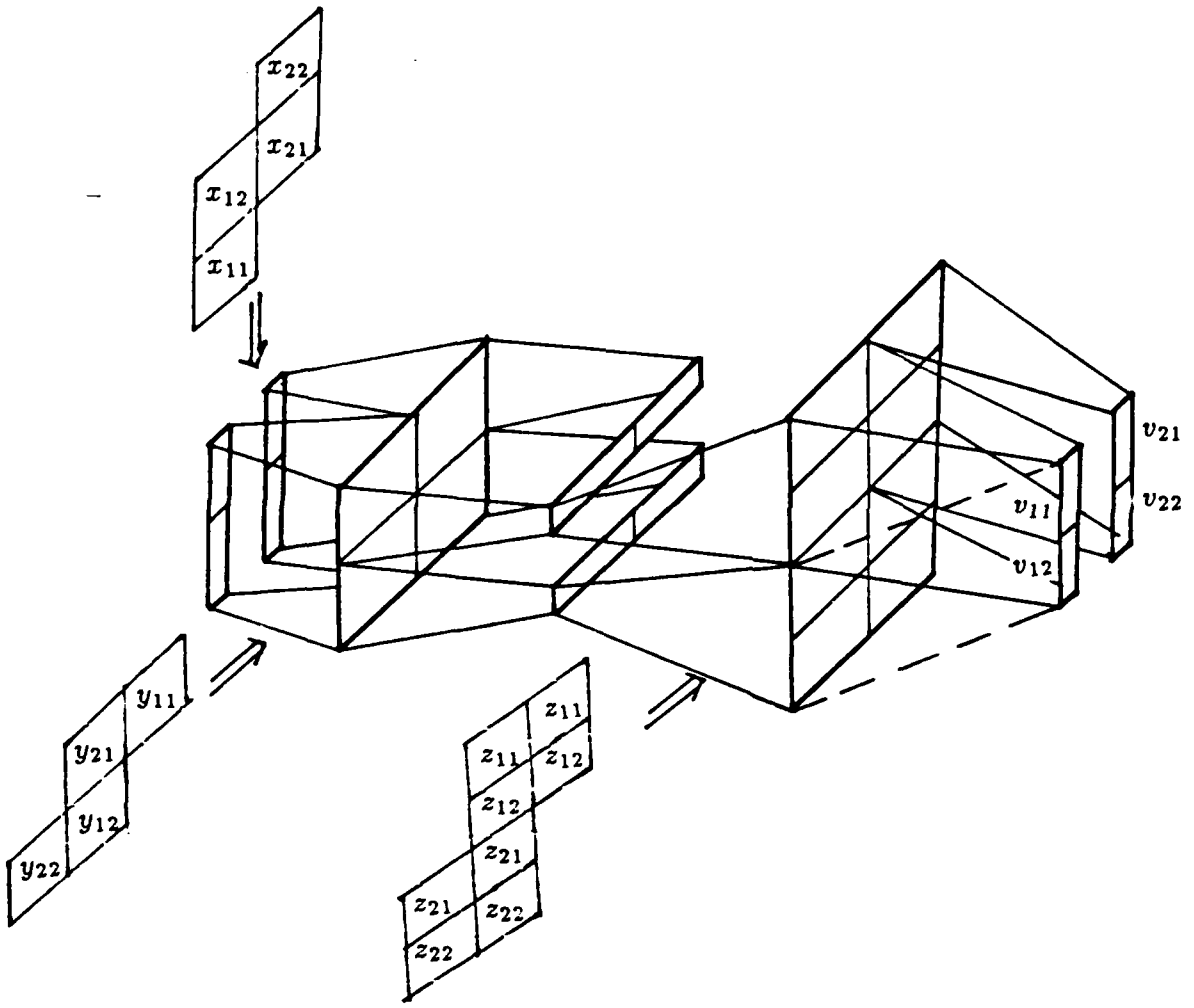
x_{22}
x_{21}
x_{12}
x_{11}
v_{21}
v_{22}
v_{11}
v_{12}
y_{11}
y_{21}
y_{12}
y_{22}
z_{11}
z_{11} z_{12}
z_{12}
z_{21}
z_{21} z_{22}
z_{22}

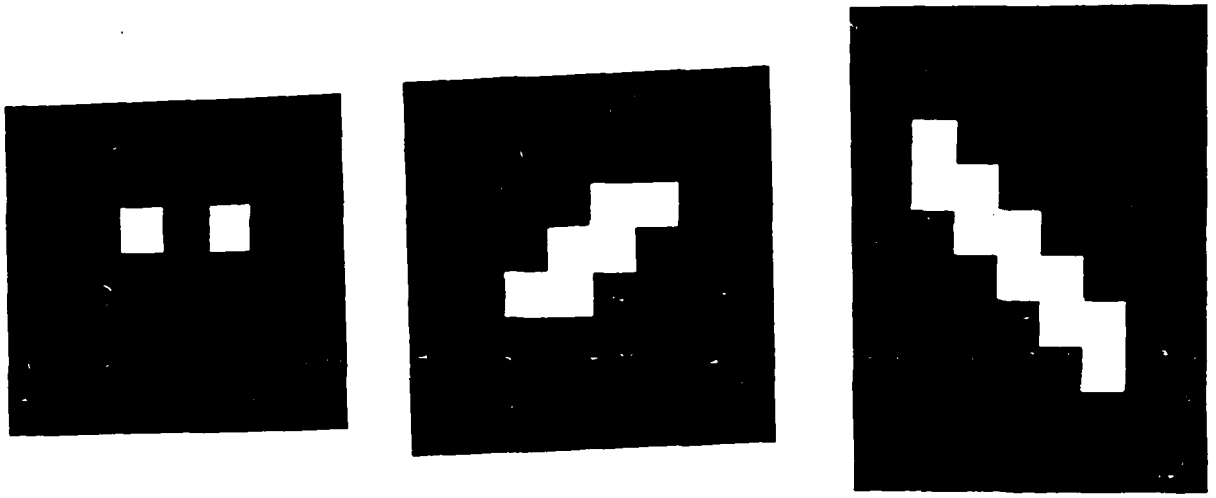

(a)

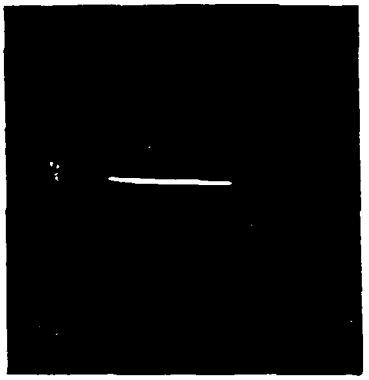

(b)

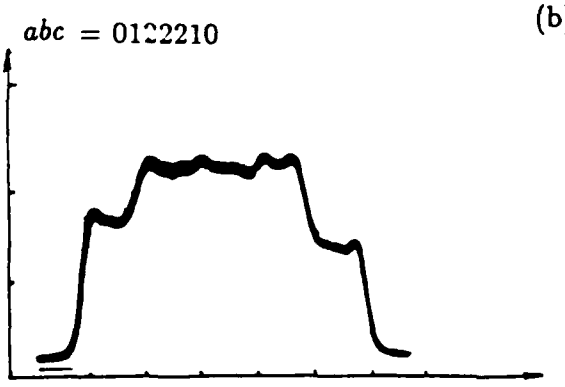

(c)

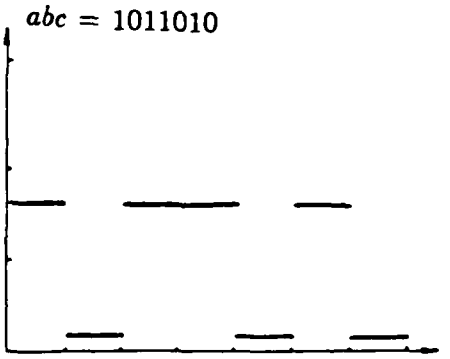

(d)

Fig. (5)

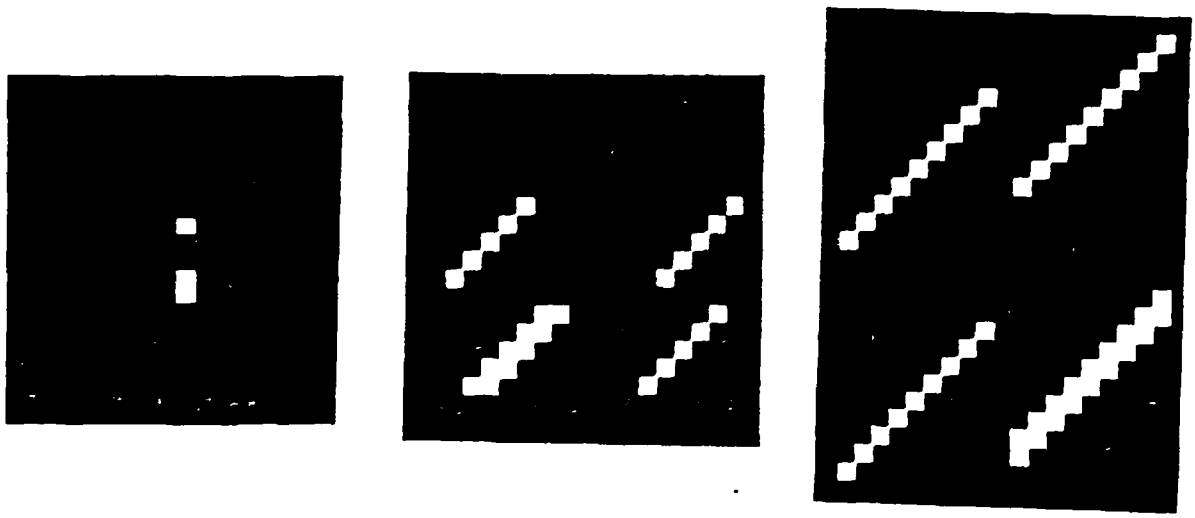

(a)

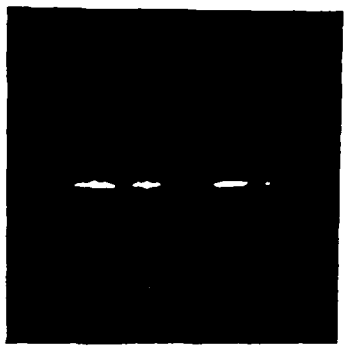

(b)

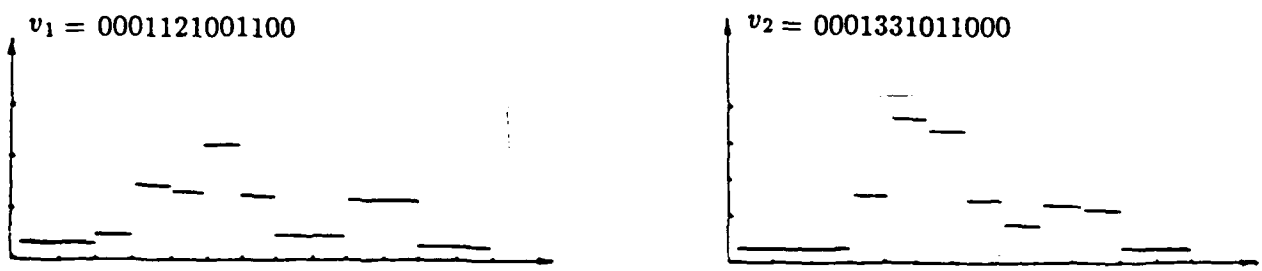
v_1 = 0001121001100
v_2 = 0001331011000

(c)

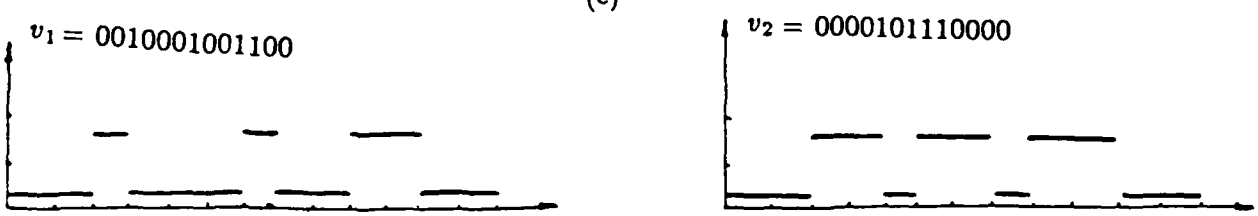
v_1 = 0010001001100
v_2 = 0000101110000

(d)

Fig. (6)

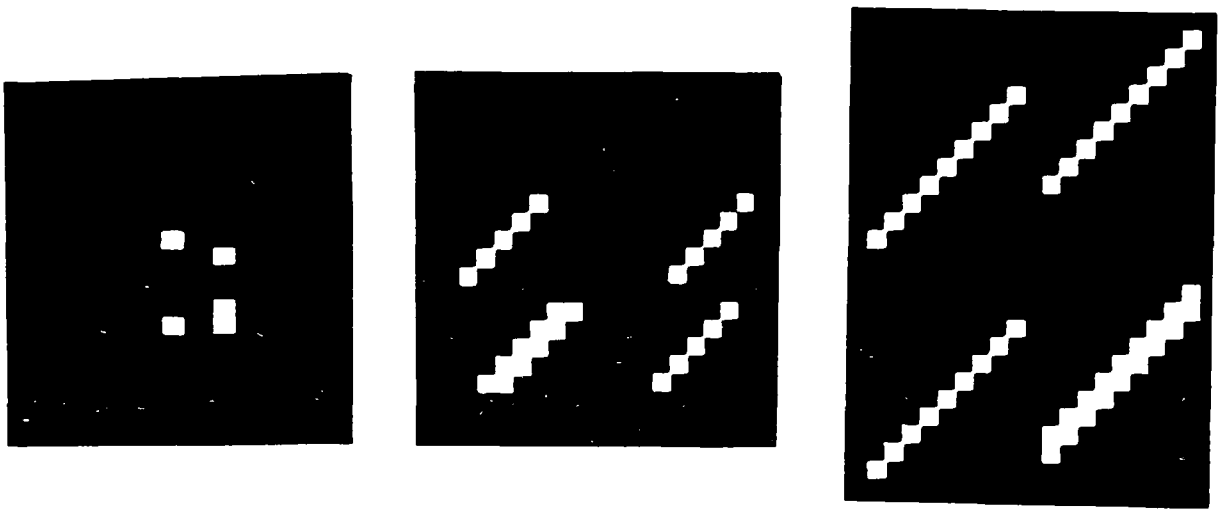

(a)

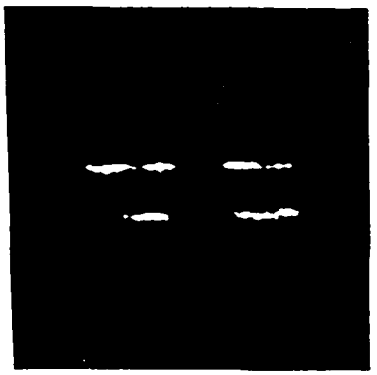

(b)

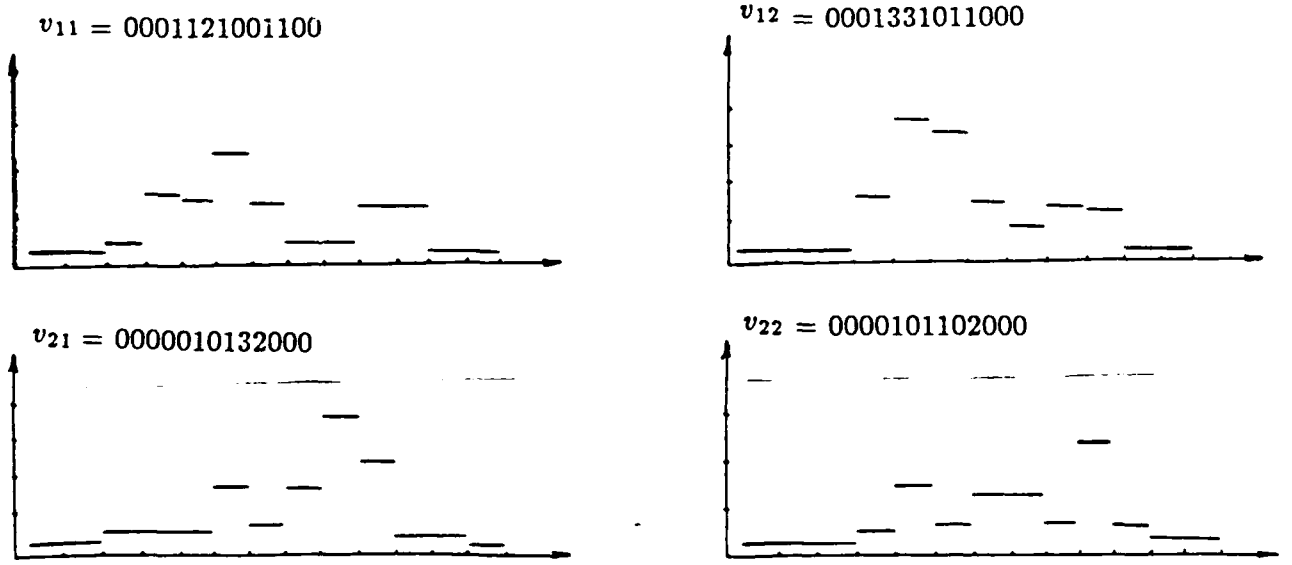
v_{11} = 0001121001100
v_{12} = 0001331011000
v_{21} = 0000010132000
v_{22} = 0000101102000

(c)

Fig. (7)

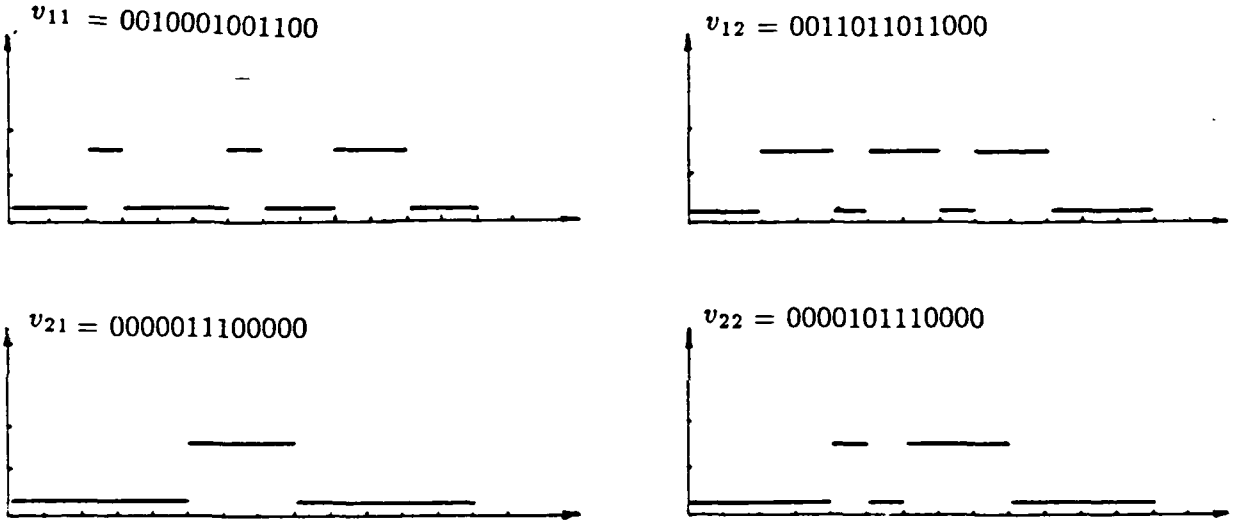
v_{11} = 0010001001100
v_{12} = 0011011011000
v_{21} = 0000011100000
v_{22} = 0000101110000

(d)

Fig. (7)

SECTION 12

Optical Perfect Shuffle

Optical Perfect Shuffle Using Spatial Filtering

Q.W. Song F.T.S. Yu,

Electrical Engineering Department

The Pennsylvania State University

University Park, PA 16802 USA

One of the inherent advantages of the optical computer is its noninteractive interconnecting capability. The optical perfect shuffle (PS) which forms the basis of such an interconnection network is a useful concept in optical computer architecture. Recently, proposals of optical PS have been made by Goodman *et al* [1] and Marchic [2] for the application to VLSI systems and single-mode optical fibers, respectively. More recently, Lohmann *et al* have implemented the optical PS with the use of four prisms [3]. In this letter, we shall demonstrate that two sets of data can be shuffled using an optical spatial filter. An experimental demonstratioin is also provided.

Originally, the term PS is referred to a method of shuffling cards. As demonstrated in Fig. 1, the upper half of data are removed and then interlaced with the lower half. We note that this shuffling of data can be quickly achieved by optical spatial filtering [4]. Examples of PS applications to FFT and sorting algorithms have been discussed by Stone [5] and Parker [6].

The optical system to perform PS is depicted in Fig. 2. Two sets of data are designated by $s_1(x,y)$ and $s_2(x,y)$, which are seperated by a distance 2β at the input plane P_1. With coherent illumination, the complex light distribution at the spatial frequency plane P_2 can be described as

$$E(p,q) = S_1(p,q)e^{-i\beta q} + S_2(p,q)e^{i\beta q}, \tag{1}$$

where $S_1(p,q)$ and $S_2(p,q)$ are the Fourier spectra of the input data $s_1(x,y)$ and $s_2(x,y)$, respectively. To implement perfect shuffle, we would place a sinusoidal grating in the Fourier plane P_2. We assume that the grating function is

$$H(q) = \frac{1}{2}\{1 + cos[(\beta + \Delta\beta)q]\}, \tag{2}$$

where $\Delta\beta$ is a small displacement constant. Thus, the output intensity distribution on P_3 can be shown as

$$I(x,y) = \frac{1}{2}|s_1(x, y-\beta)|^2 + \frac{1}{2}|s_2(x, y+\beta)|^2 + \frac{1}{4}|s_1(x, y-\Delta\beta) + s_2(x, y+\Delta\beta)|^2 + \frac{1}{4}|s_1(x, y-2\beta-\Delta\beta)|^2 + \frac{1}{4}|s_2(x, y+2\beta+\Delta\beta)|^2. \tag{3}$$

From the third term of Eq. (3), we see that $s_1(x,y)$ and $s_2(x,y)$ are slightly shifted on opposite directions along the Y axis. If the incremental shift $\Delta\beta$ is equal to the separation between the processing data, then s_1 and s_2 would be perfectly interlaced. Thus, the two sets of input data would be perfectly shuffled.

In our experiment, we used two sets of English letters as imput data for demonstration. Figure 3(a) shows the input data. Figure 3(b) gives the output shuffled data, obtained with the proposed technique. We note that if two optical filtering systems are cascaded in tandem, the PS operation can be applied to a 2-D data array, such that one shuffles horizontally and the other vertically,.

References

[1] J.W. Goodman, J.F. Leonberger, S.Y. Kung, and R.A. Athale, "Optical Interconnections for VLSI systems," Proc. IEEE 72, 850 (1984).

[2] M.E. Marchic, "Combinatorial Star Couplers for Single-Mode Optical Fibers," FOC/LAN 84, pp.175-179.

[3] A.W. Lohmann, W. Stork, and G. Stucke, "Optical Perfect Shuffle," Appl. Opt., 25, 1530 (1986).

[4] F.T.S. Yu,*Optical Information Processing* (John Wiley & Sons INc., New York, 1983).

[5] H.S. Stone, "Parallel Processing with the Perfect Shuffle," IEEE Trans. Comput. $C-20$ (Feb. 1971).

[6] D. S. Parker, Jr., "Notes on Shuffle/Exchange Type Switching Networks," IEEE Trans. Comput. $C-29$ (Mar. 1980).

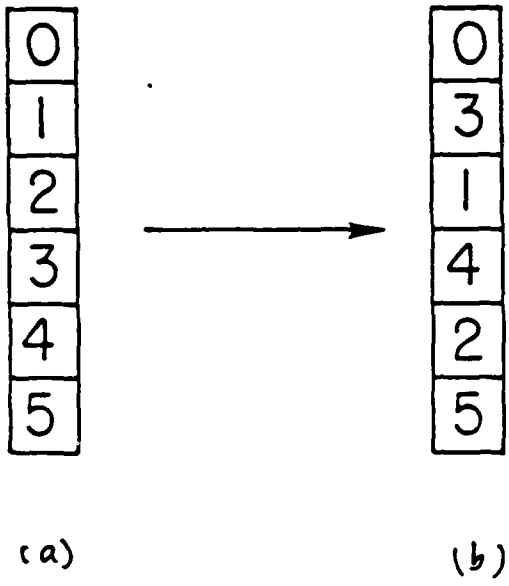

Figure 1. A demonstration of PS permutation. (a) Input data. (b) The shuffled version. The small boxes represent processing elements.

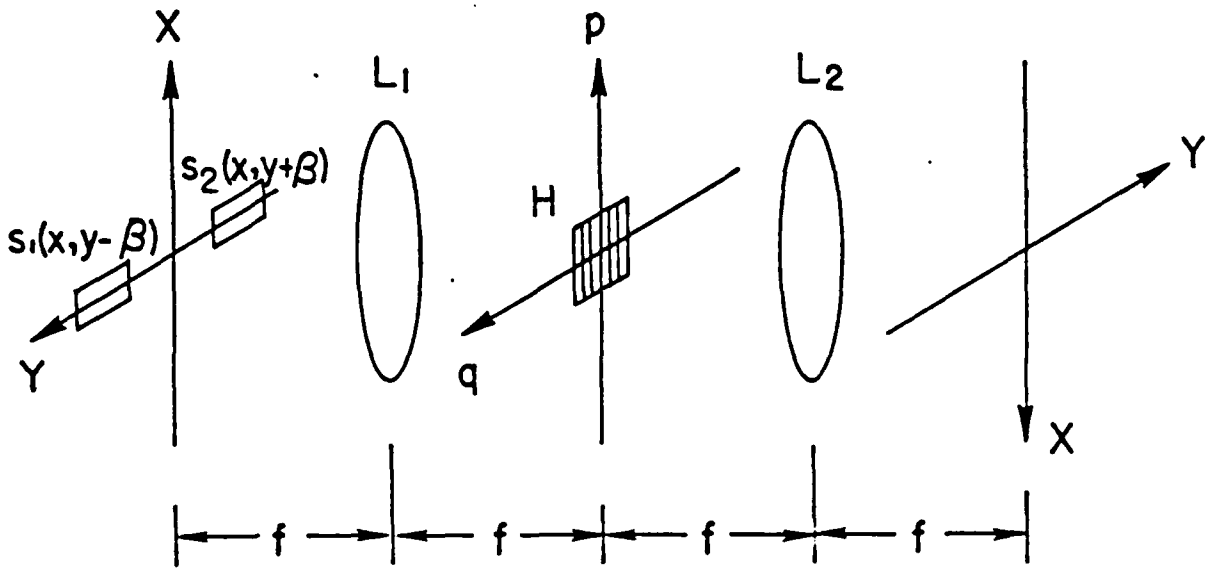

Figure 2. An optical PS system: s_1 and s_2, input data; Ls, lenses; H, Filtering grating.

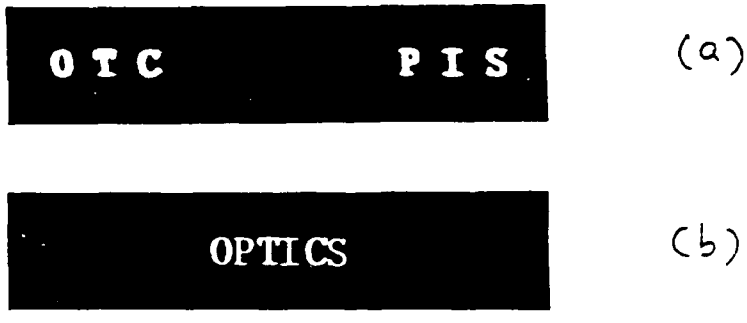

Figure 3. Experimental result of the PS. (a) Input data. (b) The shuffled version.

SECTION 13

Hybrid Optical Computing

Hybrid Optical Computing

Francis T. S. Yu

A high accuracy, high data rate, electro-optical architecture

Light weight and pocket size, the optical signal processor can perform a myriad of complicated processing operations. It success is primary due to the profound diffraction phenomena of coherent light. The essential merit of an optical signal processor must be the capability of processing the signal in complex amplitude, parallelism, large capacity, high speed and wavelength diversity. Several processing operations have proven to be more efficient with optical techniques than with their electronic counterparts. These operations are: Fourier transformers, convolution and correlation operations, spectrum analysis, and others. However, optical signal processors are very inflexible compared with electronic computers. The major advantage of an electronic computer must be the flexibility, programmability and easy accessability. The question is "Can we exploit the efficient operation of the optics and the flexibility of the electronic computer to come up with a more realistic, but not futuristic, electro-optical (EO) architecture to meet our computational needs?" The answer to this question is, "yes."

First, let me point out that the earlier development of electronic computer was based on state-of-the-art technology available at that time. It was a very realistic approach that we should adopt for the development of our electro-optical computer. Second, the current optical signal processor can be regarded as a highly efficient processing system, for example a high performance vehicle. However, without human intervention, the vehicle cannot perform properly. In order for an optical signal processor to function efficiently, we introduce an electronic computer to lend a hand. The intervention of an electronic computer is not for data processing. Rather, its purpose is to control the electro-optical devices so data can be primarily processed by the optical processor. Thus, high accuracy and high data rate processing can be achieved by the electro-optical computer.

Digital-Optical computing

Credit for the first optical architecture proposed to carry out matrix-vector multiplication must be given to J. W. Goodman. They used a light emitting diode (LED) to generate a time sequence vector and with a binary mask to control the variable openings representing a matrix format to perform matrix-vector multiplication. A similar LED, but with higher accuracy optical architecture for matrix-vector operation, was later developed by others. They utilized a linear array of LED to generate an input vector and array of acousto-optic cells to represent a matrix formulation of vector-matrix multiplication. To avoid the interfacing difficulties, still others introduced a systolic array processing concept for optical matrix-matrix multiplication.

However, the analog nature of the optical processing techniques limits the accuracy of the operations. To alleviate this problem, digital representation was introduced. Multiplying two numbers on a digit-by-digit basis, a numerical multiplication technique was demonstrated that can be performed with optical convolution operations. Next, the concept of implementing a real-time convolution-based multiplication was introduced, the idea being an outer product technique with correlation matrices. There are a number of architectures proposed to exploit the parallelism of optics which can be found in a survey paper by R. A. Athale. (See Read more about it).

Matrix-Matrix multiplication

To exploit the parallelism of optical processing, an electro-optical (EO) processor is shown in Fig. 1. This EO architecture utilizes an outer product technique for matrix-matrix multiplication.

Figure 2 shows the outer product computation. When the row and column electrodes of a two-dimensional (programmable) electro-optic spatial light modulator (SLM), is addressed by two binary vectors a and b, such as

Copy available to DTIC does not permit fully legible reproduction

$\bar{a} = [1\ 0\ 1]$, and $\bar{b} = [0\ 1\ 1]$

the corresponding outer product would be

$$c = \bar{a}^{T}\bar{b} = \begin{bmatrix}1\\0\\1\end{bmatrix}[0\ 1\ 1] = \begin{bmatrix}0&1&1\\0&0&0\\0&1&1\end{bmatrix}.$$

It is clear now, that a matrix-matrix multiplication can be computed by successive outer product operations, as can be seen in the following illustration.

$$\begin{bmatrix}a_{11}&a_{12}&a_{13}\\a_{21}&a_{22}&a_{23}\\a_{31}&a_{32}&a_{33}\end{bmatrix}\begin{bmatrix}b_{11}&b_{12}&b_{13}\\b_{21}&b_{22}&b_{23}\\b_{31}&b_{32}&b_{33}\end{bmatrix}$$

$$= \begin{bmatrix}a_{11}\\a_{21}\\a_{31}\end{bmatrix}[b_{11}\ b_{12}\ b_{13}] + \begin{bmatrix}a_{12}\\a_{22}\\a_{32}\end{bmatrix}[b_{21}\ b_{22}\ b_{23}] + \begin{bmatrix}a_{13}\\a_{23}\\a_{33}\end{bmatrix}[b_{31}\ b_{32}\ b_{33}]$$

Such computations can also be used to carry out the multiplication of two arbitrary matrices by appropriate decomposition and summing.

Since a multiplication between two single bits is equivalent to a logic operation AND, an outer product operation can be carried out with a Magneto-Optic (MO) SLM. In other words, the row and column electrodes of the MOSLM can be addressed with two binary vectors a and b, and the outer product C can be directly evaluated.

With reference to the EO architecture of Fig. 1, the grating in the Fourier plane diffracts the outer products of AB, from the MOSLM, to form an elementary 2 × 2 matrix at the origin of the output plane. As an example, a 2 × 2 elementary matrix $C = AB$ representation of a 16 × 16 extended binary matrix is seen in the experimental result shown in Fig. 3. Thus, a higher order matrix multiplication can be obtained by decomposing the matrices into a number of elementary 2 × 2 matrices and then performing the basic matrix multiplication optically.

Symbolic Logic Processing

Basic optical logic array processing has been reported recently.[10] Thus, a programmable optical symbolic logic processor can be constructed as shown in Fig. 4. A collimated light is used to illuminate three cascaded SLMs. The product of their generated patterns is then imaged onto a charge coupled device (CCD) area detector. The output CCD data are then fed to electronic "OR" circuits, before being stored in a high speed memory subsystem.

As an example, a binary input pattern A is subdivided into N × N small regions called "logic cells." To perform the logic operation, the value a_{ij} (0 or 1) of each ijth cell are encoded with binary patterns, as shown in the top row of Fig. 5 (a). We then utilize a 2 × 2 pixel of the SLM for each logic cell. The other binary input pattern B is encoded in a similar manner, as shown in the bottom row of Fig. 5(a). These encoded binary patters can be generated with a microcomputer memory subsystem. The encoded patterns of A and B are then written into the SLM1 and SLM2, respectively. Since SLM1 and SLM2 are closely cascaded, the combination states of a_{ij} and b_{ij} are represented by the patterns shown in Fig. 5(b). A logic operation in one channel is also represented by a 2 × 2 pixel pattern of the SLM3. $(\alpha,\beta,\gamma,\delta)$ represents the switching states (0 or 1) of the pixels of a logic mask as shown in Fig. 5(c). Thus, the combinations of these 2 × 2 pixel logic cells would provide a total of 16 logic gates.

A CCD area detector is used to transform the optical signal from every pixel (after the light passes through the cascaded SLM) into arrays of electrical signals. The four pixel signals of a logic cell can be combined with a Transistor Transistor Logic (TTL) "OR" gate. Thus, a logic operation resulting from a logic cell can be expressed as

$$c_{i,j} = \alpha(a_{i,j}b_{i,j}) + \beta(a_{i,j}\bar{b}_{i,j}) + \gamma(\bar{a}_{i,j}b_{i,j}) + \delta(\bar{a}_{i,j}\bar{b}_{i,j}),$$

where ~~and~~ + stand for ~~complement and~~ logic "OR" operation~~, respectively~~.

The spatial representations of the sixteen logic gates and the resulting patterns are shown in Fig. 6. Since the final result of c_{ij} is represented by an electrical signal, it can be directly stored in the memory subsystem, which can be used in the next cycle of operation.

It should be noted that the combinations of the 16 logic functions are the fundamentals of the arithmetic operations of a digital computer. It is obvious that the proposed technique has the ability to perform the arithmetic operation of two input patterns.

Discrete Linear Transformations

A discrete linear transformation (DLT) system represented in Fig. 7 can be characterized by an impulse response h_{mn}. The input-output relationship of such a system can be summarized by the following equation:

$$g_m = \sum_{n=1}^{n} f_n h_{m,n}, \quad m = 1,2\ldots,m.$$

Since the output g_m and input f_n can be considered as vectors, the above equation can be represented in matrix form, that is

$$\begin{bmatrix} g_0 \\ g_1 \\ g_2 \\ \vdots \\ g_{m-1} \end{bmatrix} = \begin{bmatrix} h_{0,0} & h_{0,1} & h_{0,2} & \cdots & h_{0,n-1} \\ h_{1,0} & h_{1,1,2} & h_{1,2} & \cdots & \cdots \\ h_{2,0} & h_{2,1} & h_{2,2} & \cdots & \cdots \\ \vdots & \vdots & \vdots & \ddots & \vdots \\ h_{m-1,0} & \cdots & \cdots & \cdots & h_{m-1,n-1} \end{bmatrix} \begin{bmatrix} f_1 \\ f_2 \\ f_3 \\ \vdots \\ f_{n-1} \end{bmatrix}$$

or abbreviated as,

$$[g_m] = [h_{m,n}][f_n],$$

where $[h_{m,n}]$ is known as a transform matrix. Thus, the different DLTs would have different transform matrices. We shall now illustrate a few frequently used DLTs:

Discrete Fourier Transform (DFT)

The DFT is defined by

$$F_m = \frac{1}{N} \sum_{n=0}^{n-1} f_n \exp\left[\frac{-i2\pi}{N} mn\right], \quad 0 \le m \le n-1,$$

where $h_{m,n} = \exp\left[\frac{-i2\pi mn}{N}\right]$ is also known as the transform kernel. To implement the DFT transformation in an electro-optical processor, we shall present the complex transform matrix in real elements. The corresponding real transform matrices can be written as

$$R_e[h_{m,n}] = \cos\left[\frac{2\pi mn}{N}\right],$$

and

$$Im[h_{m,n}] = \sin\left[\frac{2\pi mn}{N}\right],$$

which are the well-known discrete cosine transform (DCT) and discrete sine transformation (DST).

Discrete Hilbert transform (DHT)

It is well-known that the relationship between the real and imaginary parts of an analytic signal can be described by the Hilbert transformation. The elements of a discrete Hilbert transform (DHT) matrix can be written as

$$h_{m,n} = \begin{cases} \frac{2}{\pi} \times \frac{\sin^2[\pi(m-n)/2]}{(m-n)}, & m-n \neq 0, \\ 0, & m-n = 0. \end{cases}$$

Discrete Chirp-Z transform (DCZT)

Another frequently used linear transformation is Chirp-Z transform, which can be used to compute the DFT coefficients. The elements of the DCZT transform matrix can be written as

$$h_{m,n} = \exp[i\pi(m-n)^2/N]$$

We note that this type of shift-invariant transformation, as well as other types of DLTs, can be implemented by an electro-optical processor with a systolic array processing technique.

Since the discrete linear transformation can be viewed as the result from a matrix-vector multiplication, the systolic array processing architecture can be used for the implementation of DLT. Thus, by combining the systolic array processing technique and the two's complement representation, a DLT can be performed with an electro-optical processor as shown in Fig. 8. This technique has a high accuracy and low error rate processing capability and it is compatible with other digital processors.

An example of DLT using the systolic array processing technique is illustrated in Fig. 9. In Fig. 9(a), a three-sample points discrete cosine transform (DCT) matrix is encoded in the two's complement form, and multiplied with an input vector using the systolic array method. A discrete sine transformation (DST), carried out by the systolic array method, is shown in Fig. 9(b). Thus, by combining DCT and DST of Figs. 9(a) and 9(b), a discrete Fourier transform can be obtained.

Copy available to DTIC does not permit fully legible reproduction

Concluding Remarks

Since MOSLM can be addressed in patial parallel mode, the whole frame pattern on MOSLM can be switched in a very rapid manner, for example 6.4 μs for a 64 × 64 MOSLM; 51.2 μs for a 512 × 512 MOSLM). By utilizing a high speed memory subsystem (the technology is available) with a specially designed interfacing circuit, a relatively slow microcomputer can be used to manipulate the parallel operation of the MOSLMs. This is known as a single instruction multiple data (SIMD) operation. In addition, with the introduction of a microcomputer into the system, a man-machine communication link is also provided. To generate the systolic array formats rapidly, a table look up structure is suggested. After the time integrating CCD detector, a high speed analog to digital converter (ADC) and a serial-parallel deformater would be used. Thus, by exploiting the programmability of the computer, various linear algebraic operations can be performed with this hybrid optical architecture.

Finally, by exploiting the efficient operation of opics and the programmability of electronic computer, it is the author's belief that hybrid optical architecture would be the logical approach toward modern optical computing. However, much remains to be done in the development of electro-optical devices before the hybrid optical computing can become a widespread practical reality. We hope this article will stimulate interested readers to produce more imaginative hybrid opucal computing applications in the future.

Read more about it

- J. W. Goodman, A. R. Dias, and L. M. Woody, "Fully parallel, high speed incoherent optical method for performing discrete Fourier transforms," *Opt. Lett.*, vol. 2, no. 1, 1978.
- D. Casasent and M. Carlotto, "Multidimensional adaptive radar array processing using an iterative optical matrix-vector processor," *Opt. Eng.*, vol. 21, 1982.
- H. J. Caulfield and W. T. Rhodes, "Acousto-optic matrix-vector multiplication," *J. Opt. Soc. Am.*, vol. 71, 1981.
- R. A. Athale, W. C. Collins, and P. D. Stilwell, "high accuracy matrix multiplication with outer product opucal processor," *Appl. Opt.* vol. 22, 1983.
- P. S. Guilfoyle, "Systolic acousto-optic binary convolver," *Opt. Eng.* vol. 23, 1984.
- D. Psaltis, D. Casasent, D. Neft, and M. Carlotto, "Accurate numerical computation by optical convolution," *SPIE*, vol. 232, 1980.
- R. A. Athale and W. C. Collins, "Optical matrix-matrix multiplier based on outer product decomposition," *Appl. Opt.*, vol. 21, 1982.
- R. A. Athale, "Optical matrix algebraic processors: a survey," 10th International Optical Computing Conference, 1983.
- F.T.S. Yu, M. F. Cao and, J. E. Ludman, "Microcomputer-based programmable optical signal processor," *Opt. Eng.* vol. 25, 1986.
- J. Tanida and Y. Ichioka, "Optical logic array processor," Proc. 10th IOCC, 1983.

About the author

Francis T. S. Yu is an Evan Pugh Professor of Electrical Engineering at the Pennsylvania State University. He is an active researcher in modern optical signal processing and optical computing. He is a Fellow of IEEE, OSA, and SPIE. □

Fig. 1. An Electro-Optical Processor.

Fig. 2. An Outer Product Computation.

Fig. 3. Matrix Multiplication.

Fig. 4. An Electro-Optical Symbolic Logic Processor.

Fig. 5. (a) Encoded Input Patterns.
(b) Product of the Input Patterns.
(c) A Logic Mask.

Fig. 6. Representation of the Sixteen Logic Functions.

Fig. 7. Discrete Linear Transform.

Fig. 8. An Electro-Optical DLT Processor.

Fig. 9. Systolic Array DLT Matrix Representation.
(a) Discrete Cosine Transform.
(b) Discrete Sine Transform.

TABLE I

ADC — analog to digital converter

CCD — charge coupled device

DCT — discrete cosine transformation

DCZT — discrete chirp - z transformation

DFT — discrete Fourier Transformation

DHT — discrete Hilbert Transformation

DLT — discrete linear transformation

DST — discrete sine transformation

EO — electro-optical

LED — light emitting diode

MO — magneto-optic

MOSLM — magneto-optic spatial light modulator

SIMD — single instruction multiple data

SLM — spatial light modulator

TTL — transistor-transistor logic

Copy available to DTIC does not permit fully legible reproduction

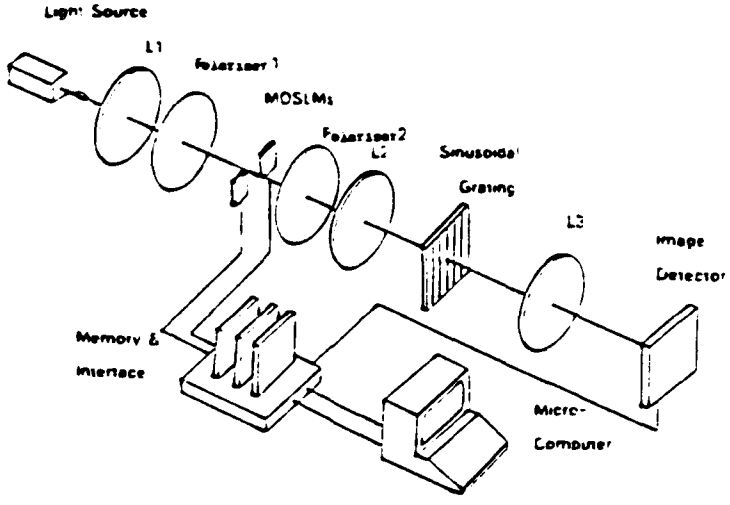

Fig. 1

$$\bar{\varepsilon} = [1\ 0\ 1]$$

$$\bar{\varepsilon} = [0\ 1\ 1]$$

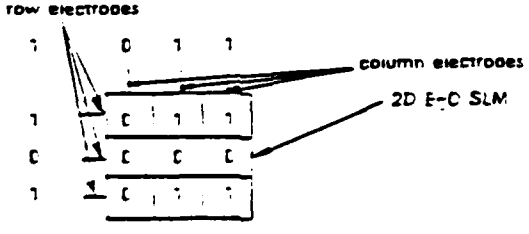

$$C = \bar{\varepsilon}^T \bar{\varepsilon} = \begin{bmatrix} 1 \\ 0 \\ 1 \end{bmatrix} \cdot [0\ 1\ 1] = \begin{bmatrix} 0 & 1 & 1 \\ 0 & 0 & 0 \\ 0 & 1 & 1 \end{bmatrix}$$

Fig. 2

Copy available to DTIC does not permit fully legible reproduction

$$A = \begin{pmatrix} 16.75 & 22.50 \\ 22.50 & 56.50 \end{pmatrix} \qquad B = \begin{pmatrix} 50.25 & 53.25 \\ 51.50 & 10.25 \end{pmatrix}$$

$$C = A\,B = \begin{pmatrix} 2000.4375 & 1122.5625 \\ 4040.375 & 1777.25 \end{pmatrix}$$

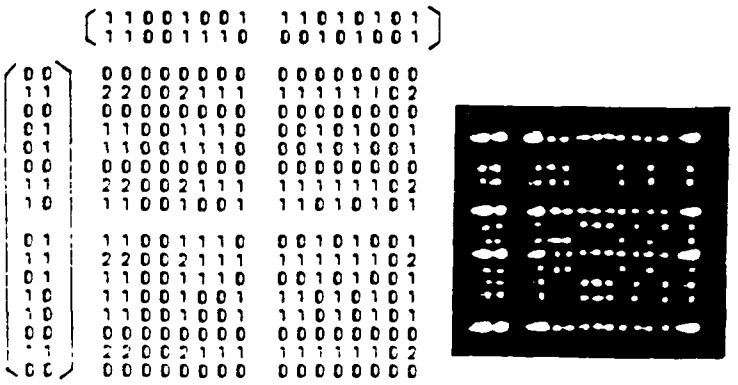

Fig. 3

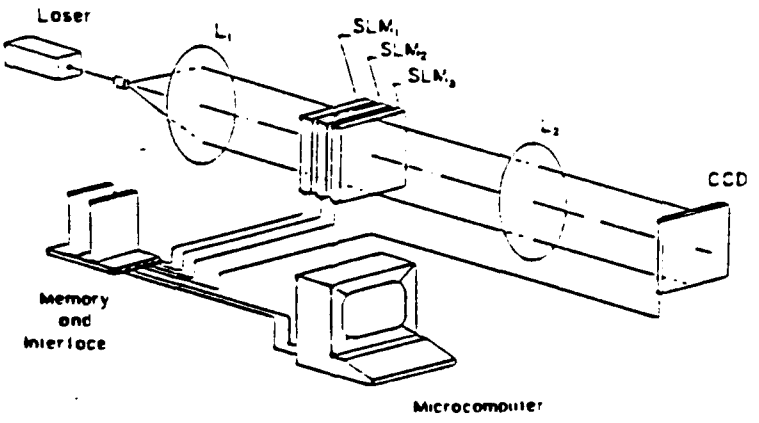

Fig. 4

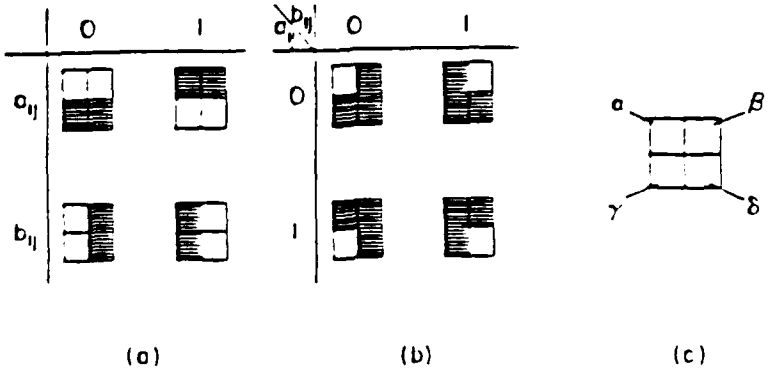

Fig. 5

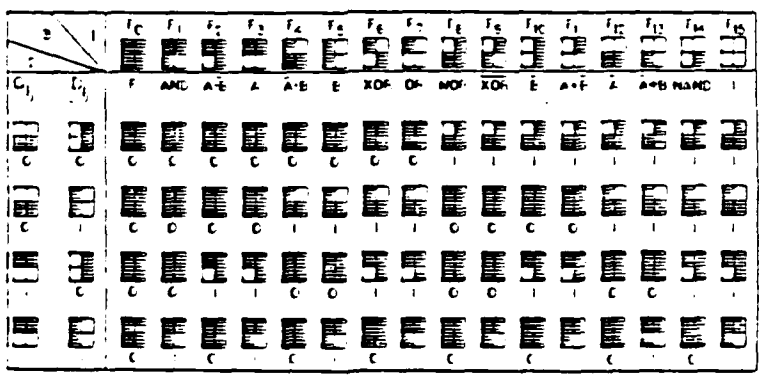

NOTE: 1- CONTROL PATTERNS
2- INPUT PATTERNS
3- OUTPUT PATTERNS

Fig. 6


f_{n+k}
$h_{m,n}$
$g_{m;k}$

Fig. 7

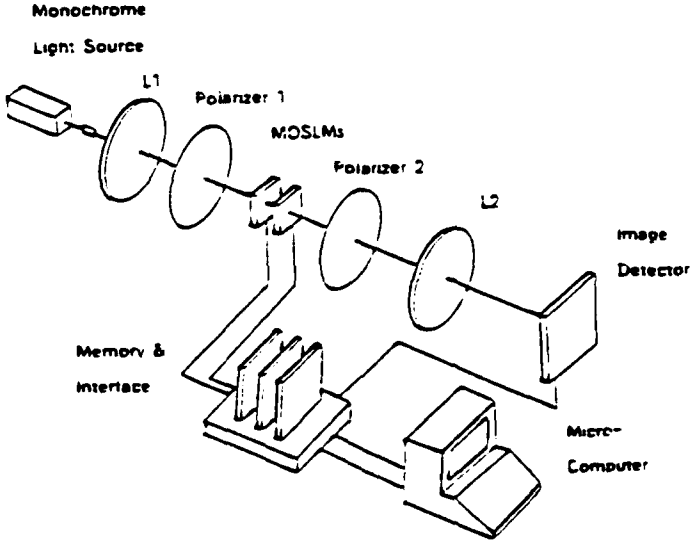
Monochrome
Light Source
L1
Polarizer 1
MOSLMs
Polarizer 2
L2
Image
Detector
Memory &
Interface
Micro-
Computer

Fig. 8

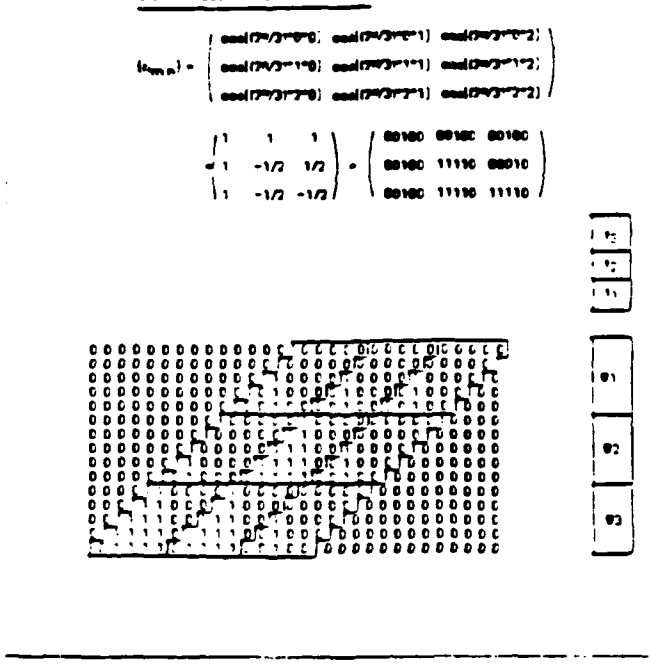
Discrete Cosine Transform (DCT)
1 1 1
1 -1/2 1/2
1 -1/2 -1/2
00100 00100 00100
00100 11110 00010
00100 11110 11110

(a)

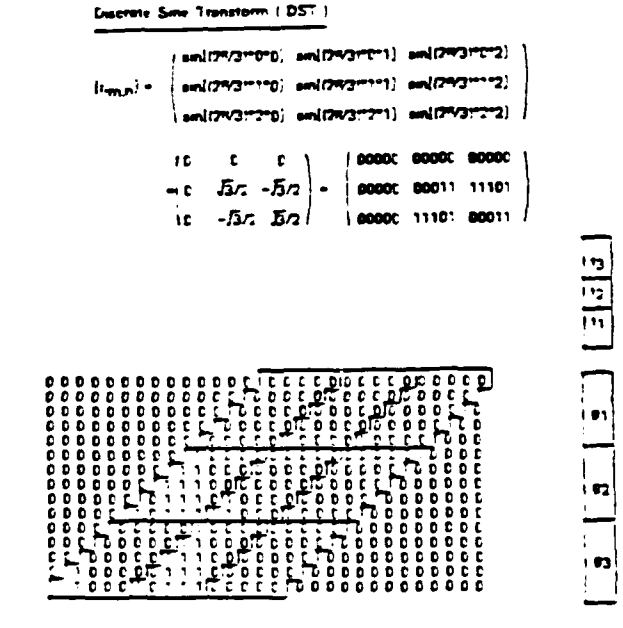
Discrete Sine Transform (DST)
0 0 0
0 √3/2 -√3/2
0 -√3/2 √3/2
00000 00000 00000
00000 00011 11101
00000 11101 00011

(b)

Fig. 9

SECTION 14

Concluding Remarks

14. Concluding Remarks

Optical signal processor can perform a myriad of complicated processing operations. Its success is primarily due to the profound diffraction phenomena of coherent light. The essential merit of an optical signal processor must be the capability of processing the signal in complex amplitude, parallelism, large capacity, high speed nad wavelength diversity. Several processing operations have proven to be more efficient with optical techniques than with their electronic counterparts. These operations are: Fourier transformers, convolution and correlation operations, spectrum analysis, and others. However, optical signal processors are very inflexible compared with electronic computers. The major advantage of an electronic computer must be the flexibility, programmability and easy accessability. The question is "Can we exploit the efficient operation of the optics and the flexibility of the electronic computer to come up with a more realistic, but not futuristic, electro-otpcial (EO) architecture to meet our computational needs?" The answer to this question is, "yes."

First, let us point out that the earlier development of the electronic computer was based on state-of-the-art technology available at that time. It was a very realistic approach that we should adopt for the development of our electro-optical computer. Second, the current optical signal processor can be regarded as a highly efficient processing system, for example a high performance vehicle. However, without human intervention, the vehicle cannot perform properly. In order for an optical signal processor to function efficiently, we introduce an electronic computer to lend a hand. The intervention of an electronic computer is not for data processing. Rather, its purpose is to control the electro-optical devices so data can be primarily processed by the optical processor. Thus, high

accuracy and high data can be primarily processed by the optical processor. Thus, high accuracy and high data rate processing can be achieved by the electro-optical computer.

It is, however, our believe that hybrid optical processing (e.g., microcomputer based optical processing) would be the logical approach toward modern optical computing. However, much remains to be done in the development of electro-optical devices before the hybrid optical computing can become a practical reality. Nevertheless, I believe that hybrid optical signal processing is at the threshold of widespread application. I hope that this report will serve the basic foundation, already established in part, to lead the interested readers to produce more imaginative hybrid-optical processing and computing applications.

Section 15

List of Publications Supported by this AFOSR Grant

15. List of Publications Supported by this AFOSR Grant

1. F.T.S. Yu, M.F. Cao and T. Lu, "A Hybrid Optical System for Linear Transformation Processing," SPIE, Vol. 698, August 1986.

2. F.T.S. Yu, S. Jutamulia and T. W. Lin, "Real-Time Polychromatic Signal Detection using a Color Liquid Crystal Television," Opt. Eng., Vol. 26, pp. 453-460, May 1987.

3. F.T.S. Yu, S. Jutamulia, "Implementation of Systolic Substitution Logic using Optical Associative Memories," Appl. Opt. Vol. 26, pp. 2293-2294, June 1987.

4. F.T.S. Yu, S. Jutamulia and T. Lu, "Optical Parallel Logic Based on Magneto-Optic Spatial Light Modulator," Opt. Commu.," Vol. 63, pp. 225-239, August 1987.

5. S. Jutamulia, T. W. Lin and F.T.S. Yu, "Microcomputer-Based Programmable Real-Time Incoherent Correlator," Opt. Commun., Vol. 64, pp. 115-119, October 1987.

6. F.T.S. Yu, X. J. Lu, Y. Suzuki and M. Wu, "Microchannel Spatial Light Modulator with White-Light Processing," Opt. Commun., Vol. 63, pp. 371-374, September 1987.

7. F.T.S. Yu and Q. H. Zhou, "A Multichannel Optical Correlator," Opt. Commun, Vol. 64, pp. 111-114, October 1987.

8. F.T.S. Yu, Q. W. Song and X. J. Lu, "Implementation on Boolean Logic Gates using a Microchannel Spatial Light Modulator with LCTVs," Opt. Lett., Vol. 12, pp. 962-964, November 1987.

9. Y. Jing and F.T.S. Yu, "Optical Binary Adder using Liquid Crystal Television," Opt. Commun. (In Press).

10. F.T.S. Yu, C. Zhang and S. Jutamulia, "Experimental Applications of One-Step Holographic Associative Memories to Symbolic Substituion, Optical Engineering (In Press).

11. F.T.S. Yu and M. F. Cao, "Digital Optical Matrix Multiplication Based-on a Systolic Outer-Product Method," Opt. Eng. (In Press).

12. F.T.S. Yu, T. Lu and M. F. Cao, "Digital Optical Architectures for Multiple Matrix Multiplication," Opt. Commun., (In Press).

13. Q. W. Song and F.T.S. Yu, "Optical Perfect Shuffle using Spatial Filtering," Appl. Opt., (In Press).

14. F.T.S. Yu, "Hybrid Optical Computing," IEEE Potential (In Press).

15. F.T.S. Yu, "Partially Coherent Processing," Encyclopedia of Physics and Science and Technology, Vol. 10, Academic Press, 1987.

16. F.T.S. Yu, S. Jutamulia, T. Lu, Q. Song, and D. Gregory, "Implementation of Optical Parallel Logic using Magneto-Optic Spatial Light Modulator," 14th Congress of ICO, pp. 25-26, August 1987.

17. M. F. Cao, "Real-Time Electro-Optical Pattern Recognition and Optical Computing," a Ph.D. thesis, The Pennsylvania State University, May 1987.

18. F.T.S. Yu, "Hybrid Optical Computing, Architecture and Design," 14th Congress of ICO, pp. 243-244, August 1987.

END
DATE
FILMED
4-88
DTIC